

THE SPREAD OF MYXOMATOSIS IN BELGIUM:

A MODEL-BASED RECONSTRUCTION

Aantal woorden: 20339

Kobe Coorevits

Stamnummer: 01205753

Promotor: Prof. dr. Bernard De Baets

Copromotor: Dr. Ir. Jan Baetens

Masterproef voorgelegd voor het behalen van de graad Master of Science in de bio-ingenieurswetenschappen: landbouwkunde

Academiejaar: 2016 - 2017



Deze pagina is niet beschikbaar omdat ze persoonsgegevens bevat.
Universiteitsbibliotheek Gent, 2021.

This page is not available because it contains personal information.
Ghent University, Library, 2021.

Dankwoord

Het heeft een paar maand langer geduurd dan gepland, maar uiteindelijk is het zover. Het is moeilijk te bevatten dat dit het laatste labuur zal zijn dat ik verricht als student bio-ingenieurswetenschappen. Ik heb genoten van de vrijheid die het studentenleven rijk is, vrienden gemaakt voor het leven en vooral enorm veel bijgeleerd. Natuurlijk waren er ook minder leuke kantjes, zoals de stress, als ik (alweer) te laat begon met te studeren, of wanneer een deadline net iets sneller dan verwacht voor de deur stond.

Het heeft mij bloed, zweet en een paar zenuwzinkingen gekost, maar deze kers op de taart is nu toch afgeraakt. Zonder hulp was dit echter nooit mogelijk geweest. Vooraleerst wil ik dus Dr. Jan Baetens bedanken voor de intensieve samenwerking met intellectuele discussies. Daarnaast wil ik hem ook bedanken voor zijn geduld als hij mij voor de vierde keer iets moest uitleggen, en de liters rode inkt, die hij voor mij heeft doen vloeien. Daarnaast wil ik ook Prof. De Baets bedanken voor zijn kritische geest, die er voor gezorgd heeft dat ik met mijn voeten stevig op de grond bleef staan. Natuurlijk mag ik ook mijn mede-thesisstudenten, en bij verdere uitbreiding alle medewerkers van de vakgroep, niet vergeten, wiens gezelschap het werken veel aangenamer maakten. Tenslotte wil ik mijn ouders en mijn zussen bedanken, die mij regelmatig van spijs, drank en troostende woorden hebben voorzien in deze barre tijden.

Samenvatting

Een arts uit Frankrijk had in de jaren 1950' een grote populatie konijnen op zijn landgoed, wat niet naar zijn zin was. Zoekend naar een manier om van de diertjes af geraken, kwam hij te weten dat myxomatose, een dierenziekte, succesvol was gebleken om konijnenpopulaties onder controle te houden in Australië. Deze waren daar geïntroduceerd voor de jacht, door Britse kolonisten, waarna ze, door hun bovenmaats reproductief vermogen, uitgegroeid waren tot een enorm ecologisch en economisch probleem. Dit wetende, liet de arts een paar konijnen, genfecteerd met myxomatose, los. Dit was voldoende om van zijn konijnenprobleem verlost te zijn, maar had catastrofale gevolgen voor de wilde konijnenpopulaties in Europa. De ziekte verspreidde zich ook naar België. Het toenmalig Ministerie van Landbouw heeft in een document, genaamd het Bulletin Sanitaire genoteerd waar en wanneer er ziektehaarden van myxomatose gevonden waren in België. In deze thesis baseren we ons op dit document om de introductie van myxomatose in België te reconstrueren met een ruimtelijk expliciet ziektemodel. Ter ondersteuning daarbij zullen een sensitiviteitsanalyse en een literatuurstudie worden uitgevoerd.

Uit de literatuurstudie werd nuttige kennis verworven over de eigenschappen van myxomatose en de populatiedynamica van konijnen. Daarnaast werden de beschikbare ziektemodellen uitgebreid besproken. Dan werd de data geanalyseerd, waaruit bleek dat myxomatose vanuit vijf uitbraken België is binnengedren. Vervolgens werd het verloop van de epidemie gereconstrueerd. Nadat we hadden bevestigd dat het ruimtelijk expliciet model een ziektegolf kan simuleren, werd er een sensitiviteitsanalyse op toegepast, waardoor we konden bepalen welke parameters van het model het belangrijkste zijn voor de verspreiding van de ziekte. Er werd ook aangetoond dat er informatie kan gewonnen worden uit een ruimtelijke gevoeligheidsanalyse, die in een niet-ruimtelijke verborgen blijft. Gesterkt door de hierbij gewonnen kennis en de informatie uit de literatuurstudie, waren we in staat parameters te infereren, die in het model in staat stelden een ziektegolf te produceren die in voldoende mate op die uit de data lijkt, waarmee de onderzoeksvraag beantwoord werd.

Summary

In the 1950s, a French physician wanted to get rid of the rabbits on his estate. He found out that a disease, called myxomatosis, had been successful at controlling rabbits in Australia. They had become an ecological and economical problem, due to their notorious reproductive capacity, after they had been introduced for hunting purposes. Having learned this, the physician inoculated a few rabbits with myxomatosis and released them. This got rid of his problem, and the majority of the European rabbit population. During its spread across the continent in the following years, myxomatosis also entered Belgium. The Ministry of Agriculture kept reports on its spread in a document called the Bulletin Sanitaire, which contains the number of nidi that were reported and their location for every two weeks. In this thesis, based on the data of the Bulletin Sanitaire, we reconstruct the introduction of myxomatosis in Belgium with a spatially explicit model, backed up by a profound sensitivity analysis and a thorough literature review.

From the literature review, we were able to obtain useful knowledge on the properties of myxomatosis, the population dynamics of rabbits, as well as getting a review of different epidemic models. After that, we analysed the data from the Bulletin Sanitaire, from which we learned that myxomatosis entered Belgium in five different outbreaks. We also reconstructed the progress of the epidemic. After confirming that the spatially explicit model can simulate an epidemic wave, we performed a sensitivity analysis on it, from which we were able to identify the parameters that are the most important for the progress of the epidemic wave. We also showed that a spatial sensitivity analysis can discover information that is hidden in a non-spatial sensitivity analysis. Aided by the knowledge gathered by the sensitivity analyses and the literature review, we were able to infer parameters for the spatially explicit model that enabled it to simulate an epidemic wave that resembles the data in a general sense, answering the research question.

Contents

Dankwoord	i
Nederlandse samenvatting	iii
Summary	v
Contents	ix
Symbols	xi
Abbreviations	xiii
List of Figures	xiii
List of Tables	xvi
1 Introduction and Problem Statement	1
1.1 Introduction	1
1.2 Research objectives	1
2 Epizootics in Rabbits	3
2.1 Introduction to epizootics	3
2.1.1 What are epizootics?	3
2.1.2 Importance of epizootic diseases	3
2.2 The European rabbit	4
2.2.1 Biology	4
2.2.2 Geographic range and habitat	5
2.2.3 Importance of rabbits	5
2.3 History of the European rabbit	7
2.3.1 Domestication of the European rabbit	7
2.3.2 Introduction of rabbits into Australia	8
2.4 Myxomatosis	9
2.4.1 Symptoms and disease progression	9
2.4.2 Disease transmission and virulence	10
2.5 Introduction of myxomatosis in the European rabbit	10
2.5.1 Introduction of myxomatosis in Australia	10

2.5.2	Introduction in Europe	10
2.5.3	Impact of myxomatosis	12
2.5.4	Evolution of myxomatosis	12
2.6	Rabbit haemorrhagic disease	13
2.6.1	Symptoms and disease progression	13
2.6.2	History and impact of RHD	14
2.6.3	RHDV2	14
3	Modelling Epidemical Diseases	15
3.1	General principles	15
3.2	Foundational epidemic models	16
3.2.1	Contagious diseases	16
3.2.2	Vector-borne diseases	18
3.2.3	Discrete-time models	19
3.2.4	Stochastic models	20
3.3	Spatial models	21
3.3.1	Reaction-diffusion models	21
3.3.2	Agent-based complex systems	24
4	The 1953-1954 Myxomatosis Epidemic in Belgium	29
4.1	The dataset	29
4.1.1	The Bulletin Sanitaire	29
4.1.2	Data exploration	29
4.1.3	Epidemic progress	32
4.2	Myxomatosis and land cover	36
4.2.1	Overall analysis	36
4.2.2	Investigating the link between land cover and myxomatosis spread	38
4.2.3	Hypothesis tests	39
5	A Spatially Explicit Model for the 1953-1954 Outbreak of Myxomatosis in Belgium	43
5.1	The spatially explicit myxomatosis model	43
5.1.1	The non-spatial model	43
5.1.2	A spatially explicit model for myxomatosis	44
5.2	Preliminary sensitivity analysis	46
5.2.1	Disease mortality	47
5.2.2	Disease duration	48
5.2.3	Reproductive rate	48
5.2.4	Natural mortality	49
5.2.5	Short range transmission rate	49
5.2.6	Long range transmission rate	50
6	Sensitivity Analysis of the Spatially Explicit Myxomatosis Model	57
6.1	Local sensitivity analysis	57
6.2	Global sensitivity analysis	58
6.2.1	Morris screening	58

6.2.2	The Sobol' method	58
6.2.3	Calculating Sobol' indices in practice	61
6.3	Global sensitivity analysis of the myxomatosis model	62
6.3.1	Selecting the model output	62
6.3.2	Input selection and sampling procedure	63
6.3.3	Homogeneous land cover	64
6.3.4	Heterogeneous land cover	71
6.3.5	Conclusion	73
6.4	Spatial sensitivity analysis	73
6.4.1	Method and input selection	73
6.4.2	Results and conclusions	74
7	The Myxomatosis model in practice: Simulating the 1953-1954 outbreak.	77
7.1	Model calibration	77
7.1.1	From Bayesian inference to approximate Bayesian computation	77
7.1.2	Applying ABC to the myxomatosis model	78
7.1.3	Results of the ABC procedure	79
7.1.4	Model validation	81
7.1.5	Conclusions	83
7.2	Scenario analysis	84
7.2.1	Revisiting the forest area	84
7.2.2	Rabbit haemorrhagic disease	85
7.2.3	Chytridiomycosis	86
8	Conclusion	93
	Bibliography	95

Symbols

c_i	a polygon with index i
C_M	case mortality
D	diffusion coefficient
$E(Y)$	expected number of offspring
k	number of parameters used for the sensitivity analysis
K	carrying capacity
m	natural mortality
\mathcal{N}	neighbourhood
O_{ij}	fraction of the circumference of c_i shared with c_j
r	reproductive rate
R_0	basic reproductive number
s	probability that another individual is susceptible
S_i	first order Sobol' index
S_{Ti}	total order Sobol' index
$V(y)$	variance of y
$w(\tau)$	generation-time distribution
α	death rate due to the disease
β	transmission rate
β_{ij}	pairwise transmission rate
$\bar{\beta}$	long range transmission rate: homogeneous land cover
$\bar{\beta}_i$	long range transmission rate: heterogeneous land cover
$\underline{\beta}$	short range transmission rate: homogeneous land cover
$\underline{\beta}_i$	short range transmission rate: heterogeneous land cover
$\beta(\tau)$	infectiousness over time
γ	removal rate
Δt	length of the time step
ϵ	reciprocal of the survival time
ζ	feeding rate
θ	fraction of retained samples
λ	dispersal rate
μ	death rate of the pathogen
ν	rate at which infected individuals become resistant
σ	transition rate from latent to infective
∇^2	Laplacian

Abbreviations

ABC	approximate Bayesian computation
ACS	agent-based complex system
CA	cellular automaton
CML	coupled-map lattice
EE	elementary effect
GSA	global sensitivity analysis
HDMR	high dimensional model representation
IBM	individual-based model
LHS	latin hypercube sampling
Lu	Lausanne strain
MYXV	myxoma virus
OAT	one-at-a-time
PDE	partial differential equation
RHD	rabbit haemorrhagic disease
RHDV	rabbit haemorrhagic disease virus
RHDV2	rabbit haemorrhagic disease virus-2
SIR	susceptible-infected-recovered
SLS	standard laboratory strain

List of Figures

2.1	Distribution of rabbit burrows in Coto del Rey	6
2.2	Symptoms of myxomatosis	9
2.3	Spread of myxomatosis in Australia	11
3.1	Effect of coinfection on a SIR-system	18
3.2	Simulation of a measles epidemic with a discrete SIR-model	20
3.3	SARS transmission tree	22
3.4	Simulated introduction of Rabies in England	23
3.5	Mosquito time-step of an IBM	25
3.6	Human time-step of an IBM	25
3.7	Simulation result of a malaria IBM	26
3.8	Transition probabilities of the Rabies CA	27
3.9	Simulation result of the rabies CA	28
4.1	nidi of myxomatosis in the 1953-1954 epidemic	30
4.2	Relative number of towns with at least one nidus.	31
4.3	Map of the cumulative nidi: wild rabbits	31
4.4	Map of the cumulative nidi: domesticated rabbits	32
4.5	Total area enclosed in the epidemic wave.	33
4.6	The outbreak in Antwerp	34
4.7	Epidemic wavefronts during the first three months.	35
4.8	The CORINE map with the 6 land cover classes.	36
4.9	Histogram of the land cover of Belgium according to the CORINE-map.	37
4.10	Relative surface areas for the infected towns and the infection hulls.	37
4.11	Evolution of the relative land cover classes	38
4.12	Relative land cover area in the outbreaks and Belgium	39
4.13	Marginal histograms of the different relative land covers.	40
4.14	Test results for the non-parametric statistics	41
5.1	A cell of the grid and its five neighbouring cells.	46
5.2	SIR-plot for the benchmark	47
5.3	Map of epidemic wave for the benchmark	48
5.4	Effect of changing C_M	49
5.5	Effect of changing ϵ	50

5.6	Effect of changing r	51
5.7	Effect of changing m	52
5.8	Effect of changing $\underline{\beta}$: SIR plot	53
5.9	Effect of changing $\underline{\beta}$: epidemic wave	54
5.10	Effect of changing $\overline{\beta}$: SIR plot	55
5.11	Effect of changing $\overline{\beta}$: epidemic wave	56
6.1	Illustration of the morris method	59
6.2	Generating the parameter matrices	61
6.3	Example convex hull	63
6.4	Results: susceptible rabbits	65
6.5	Results: infected rabbits	66
6.6	Results: rabbits that died from the disease	67
6.7	Results: areas with at least one infected rabbit	68
6.8	Results: area where at least one rabbit died from the disease	69
6.9	Results: area where at least 10 percent of the population is infected	70
6.10	Results: susceptible rabbits: heterogeneous land cover	71
6.11	Results: infected rabbits: heterogeneous land cover	72
6.12	Sensitivity maps for the infected rabbits $t = 50$ d.	74
6.13	Sensitivity maps for the infected rabbits $t = 100$ d.	75
6.14	The variance maps	76
7.1	First procedure: marginal posterior distributions	80
7.2	First procedure: two-dimensional posterior distribution	81
7.3	Second procedure: marginal posterior distributions	81
7.4	Second procedure: two-dimensional posteriors	82
7.5	Comparison of the simulations and the data: infected area	82
7.6	The disease dynamics of the three scenarios	83
7.7	Comparison of the simulations and the data: autumn	84
7.8	Comparison of the simulations and the data: winter	85
7.9	Comparison of the simulations and the data: spring	86
7.10	Comparison of the simulations and the data: summer	87
7.11	Scenario with slower disease transmission in forest: maps	88
7.12	Comparison of the disease dynamics of the RHD scenario and the slower disease spread in forest areas	89
7.13	Scenario of RHD: maps	90
7.14	Scenario of chytridiomycosis: maps	91

List of Tables

2.1	Strains of different virulences in MYXV	13
4.1	Results from the Cramér-Von Mises test for normality.	39
5.1	Benchmark parameter values	47
6.1	Sampled parameter ranges for System (5.6)	64
7.1	Parameter values for the calibration.	79
7.2	The parameter values for the simulations.	82

CHAPTER 1

Introduction and Problem Statement

1.1 Introduction

In the 1950s, a French physician wanted to get rid of the rabbits on his estate. He had learned that, in the previous year, a disease called myxomatosis had been successful at controlling rabbit pests in Australia. The herbivores had become an ineradicable problem when a nobleman introduced some game at his estate, hoping to establish a population for the hunt. His order of five hares, seventy-two partridges and some sparrows also included twelve grey rabbits, which, after introduction, promptly became an ecological and economical disaster due to the species' notorious reproductive capacity. Knowing this, the physician inoculated a few rabbits he caught with a strain of myxomatosis and released them. This proved to be a successful way to solve his rabbit problem. So successful in fact, that he also got rid of the majority of the European rabbit population in the years that followed. This caused major problems for their natural predators, and for the rabbit farms, who now had to vaccinate their rabbits. The disease also entered Belgium, where the Ministry of Agriculture kept reports on its spread. This document, called the Bulletin Sanitaire, contains the location and number of nidi they found for every two weeks.

1.2 Research objectives

The primary objective of this dissertation, is to use the data from the Bulletin Sanitaire to reconstruct the spread of myxomatosis in Belgium using an epidemic model. The secondary objective is to perform a sensitivity analysis on said model, which is often overlooked for spatio-temporal models. To do this we will first perform a literature study about the history and biology of the European rabbit, myxomatosis, and the different epidemic models that are available. Using this knowledge, we will analyse the data of the Bulletin sanitaire. After that we will explain the details of an existing spatio-temporal epidemic model. Following on that we will perform an extensive sensitivity analysis, to gain knowledge on the model behaviour and the relations between its outputs and parameters. This will enable us to perform a calibration using the analysed data, after which we will examine whether the calibrated model is able to reconstruct an epidemic and simulate some scenarios.

It may seem strange, to investigate an epidemic that happened more than fifty years ago. However, modelling this event may further understanding of the processes governing the introduction of novel pathogens into an animal population. These events have become inevitable in the globalized society we live in today and although myxomatosis does not pose a threat for humans, there are other animal diseases that do so, e.g. rabies and the black plague. Besides, there is a huge amount of information available about the disease dynamics, virulence and history of myxomatosis, which can help us model the disease in a more accurate way.

CHAPTER 2

Epizootics in Rabbits

In this chapter we will provide some general information about epizootics, after which we will proceed to discuss the biology, history and importance of the European rabbit (*Oryctolagus cuniculus*). After that we will discuss the two most important diseases in rabbits and their respective histories: myxomatosis and rabbit haemorrhagic disease.

2.1 Introduction to epizootics

2.1.1 What are epizootics?

To assess the impact of myxomatosis on rabbits, it is important that some terms are explained in relation to animal diseases. An animal disease is typically enzootic, meaning that it occurs in a population at a regular, predictable or expected rate. An epizootic, the equivalent of an epidemic for animals, occurs when there is an unexpected and irregular increase in the number of cases for a specific population, place and time [111]. The term outbreak, which is often associated with epizootics, has a different meaning. Outbreaks of botulism, for instance, occur annually in waterfowl with predictable regularity and are as such not epizootic [111]. An important term associated with epizootic diseases and their importance for human healthcare is a zoonose. This is a disease that can be transferred from vertebrates to humans [102].

2.1.2 Importance of epizootic diseases

The study of epizootic diseases is of great importance for human healthcare as of all pathogens infecting humans, 61% are zoonotic [102]. Some have caused widespread panic when they emerged as epizootics, for example, the crisis following the development of Creutzfeldt-Jakob disease in humans that had eaten meat of cattle infected with bovine spongiform encephalopathy [49]. Other well-known zoonotic diseases are rabies, which is present in several mammals, the bubonic plague, transferred to humans from rats with flea bites, toxoplasmosis, which can damage the embryo in pregnant women [58] and the influenza strain H5N1, also referred to as the bird flu [102]. Epizootics can also emerge when a foreign pathogen enters a native host species that is not adapted to it. If this happens in native species from an ecosystem, it can cause enormous damage. The introduction

of chytridiomycosis in Australia, for instance, caused big drops in amphibian populations and led some species to the brink of extinction [10]. An important example for Europe is the accidental introduction of myxomatosis and rabbit haemorrhagic disease in rabbits. A beneficial aspect of diseases that can develop to epizootics is their potential for controlling vertebrates in areas where they do not belong [96]. For this purpose the same pair of diseases has been used to control rabbits in Australia (see Section 2.4 and 2.6).

2.2 The European rabbit

2.2.1 Biology

The European rabbit (*Oryctolagus cuniculus*) is a small mammal, a rabbit species that belongs to the lagomorph (*lagomorpha*) order together with hares, e. g., the brown hare (*Lepus europaeus*), and pikas (*Ochotona sp.*), small animals resembling guinea pigs. They share a trait with the rodent order (*Rodentia*), i.e., they both have gnawing incisors that never stop growing. A key difference between these families is the presence of two additional peg-like teeth next to the upper incisors of lagomorphs. Still, they are often misclassified as rodents [16, 71]. Lagomorphs consist of two families: the leporids (*Leporidae*), containing the rabbits and hares, and the pikas (*Ochotonidae*). The difference between hares and rabbits can be confusing as they look very similar. The clearest way to distinguish them is by investigating their reproductive behaviour. The young of rabbits are called kittens or sometimes pups and are altricial, meaning they need the care of their parents at birth to survive as they are born naked, and with closed eyes. The young of hares, called leverets, are born precocial, meaning they are open-eyed, fully furred and do not need much care from their parents [71]. All lagomorphs are herbivores, feeding on grasses, leaves, bark, seeds and roots. To get the most out of this low-quality diet they pass their meals through their digestive tract twice, using a process called coprophagy, which essentially means that they eat their own feces. They are hindgut fermentors, implying that they use micro-organisms in their hindgut to digest compounds that their own enzymes cannot break down. For that purpose, their guts are large, especially their caecum and appendix, where most of the fermentation processes take place [16, 71]. Most hares and rabbits are solitary animals, but the European rabbit is an exception. It is one of the two social leporid species that live in burrows, the other being the pygmy rabbit (*Brachylagus idahoensis*) [71]. These underground tunnel networks, called warrens, can occupy up to two acres of land [16]. They are territorial animals, active at dusk, that live and forage in colonies of up to 20 adults, but most groups contain three to five males and three to seven females [16, 71]. European rabbits can breed throughout the year if conditions are favourable, which is uncommon among leporids. Yet, there are seasonal peaks of high and low reproductive activity [71]. They are induced ovulators, so the stimulus of courtship and copulation is required to ovulate. After a gestation period of about 31 days [16], the females give birth to about four–five young at a time [109], which leave the warren in less than a month. A female can produce several (3–8) nests a year of which 70% are born between April and June [109], resulting in about 14 to 28 young per female per year. Females reach sexual maturity in 3.5 months, males around four months and they can live up to nine years [71] but the average life expectancy of adult rabbits is about 1.5 years [23]. Estimates of how many rabbits survive until their first reproductive season differ from 3 to 14 % [109] to 20 % [68].

2.2.2 Geographic range and habitat

The European rabbit is now found around the globe due to human intervention (see Section 2.3), but its natural range used to be limited. It is the last species remaining of the *Oryctolagus* genus which used to be present as different species across Europe. After the glaciations in the pleistocene era, they got confined to the Iberian peninsula in south-western Europe, some parts of northern Africa and southern France [15, 27, 71, 104]. All lagomorphs have two fundamental requirements to survive in their environment: they need places for shelter and places to eat, preferably in close proximity to one another, forming a mosaic of open patches and shrubs. Shelter provides both protection from predators and a way to keep themselves warm or cool. European rabbits also prefer soft soil to dig their burrows. In open areas, like grassland, they are more susceptible to predation from birds of prey, while in scrubland, they are more susceptible to predation by mammals [70, 71]. The habitat type has a big influence on how rabbits cohabit, their population density and the transmission of diseases [70, 108]. Lombardi et al., (2003) [70] conducted a study in Spain in three habitats: scrubland, with dense vegetative cover but low food availability, grassland, with low cover with high forage abundance and an intermediate habitat, the ecotone [70]. The highest rabbit densities are present in the ecotone habitat, followed by grassland, while the number of burrows are the highest in the ecotone, followed by the scrubland. Burrows are distributed randomly in the latter, while they are aggregated in the other two habitats (see Figure 2.1). There is no significant difference in mortality due to predation between the three habitats, while mortality due to disease was only present in habitats with an aggregation of burrows. There is a significant link between aggregation and mortality due to contagious diseases, like myxomatosis and RHD [70].

For the rabbits' dietary requirements, the plant species composition of a given area is less important than the general availability of edible plants throughout the year. This dietary flexibility is partly accountable for the success of the European rabbit in areas that do not have a single plant species in common [62, 71]. Rabbits show a high tolerance for dehydration, according to [47]. They can survive for two months on dry pastures in summer without drinking water, losing up to 48% of their body weight in water in the process [47]. This enables them to survive the dry environment of the Australian outback and Iberian peninsula [16, 47].

2.2.3 Importance of rabbits

In their natural ranges, lagomorphs are often important for the ecosystem. They are not exclusively a good food source for predators, given that their grazing behaviour keeps the natural vegetation in a traditional state. Across the Iberian peninsula, European rabbits are considered a keystone species [27], a species that has a disproportionately large effect on an ecosystem and whose loss would cause significant changes in other species' populations and ecosystem processes [71]. Their grazing behaviour creates an open scrubland with open areas and tight shrubs, essentially an ideal rabbit habitat. Several animal species seek shelter in their empty burrows, and at least 72 plant species' seeds are dispersed by rabbit pellets [27, 71]. There are forty predators present on the Iberian peninsula that prey on the European rabbit. This list contains four reptiles, 19 birds of prey and 17 mammals of which several specialize in rabbits as their primary food source. For example, the diet of the critically endangered Iberian lynx (*Lynx pardinus*) consists of 80% rabbit.

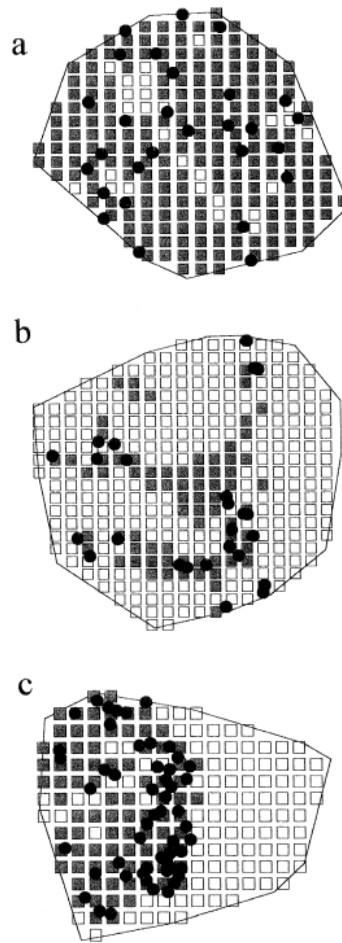


Figure 2.1: Vegetative cover and distribution of rabbit burrows (circles) at Coto del Rey, Spain, in a) scrubland, b) grassland, and c) an ecotone. Squares represent 50-by-50 metres areas of open land (white) and scrubland (dark) [70].

The decline of rabbit populations due to the introduction of myxomatosis and rabbit haemorrhagic disease (RHD) (See sections 2.4 and 2.6), in addition to the destruction of natural habitat, is believed to be the main cause of this species' decline, and several others, including the Spanish imperial eagle (*Aquila heliaca*) [27, 71]. The European rabbit is the only lagomorph species to have been domesticated (see Section 2.3.1). They are kept as pets all over the world. In the United States, estimates suggest that there are about five million pet rabbits living in about two million homes. They are generally easy to care for as pets [71]. Domestic rabbits are also bred for shows. Breeder organizations recognize more than 50 breeds worldwide [71]. However, the importance of rabbits is not limited to being a source of entertainment or aesthetic pleasure. Rabbits and hares have been an important food source throughout history [27]. There is evidence that our ancestors turned to hares and rabbits as a source of meat whenever larger game or easier to capture animals like shellfish and turtles' populations declined [26]. While they may be small, populations recover quickly from hunting due to their high reproductive rate. Their meat is high in protein and low in cholesterol and fat, which makes it a healthy choice of meat. The consumption and production of domesticated rabbits for their meat has increased to about 857 million rabbits a year of which

most are reared in China, Italy and France. Rabbits and hares are also hunted for sport in many countries [27, 71, 104]. After meat, fur is the most prominent rabbit product. It is a cheaper alternative to more expensive mammal furs. Rabbit skins from meat production are not suitable as furs for clothing, however, the hair can still be processed into felt and the skins can be turned into glue or fertilizer. The fur from long-haired angora rabbits is in a completely different category and is used in luxurious clothing because of its fineness and luster [71].

Domestic rabbits have been used since the early 1800s as subjects for scientific experiments that have led to several important discoveries, such as the discovery of the Graffian follicle and the first embryo transplantation. They are easy to obtain and docile to handle and the prominent veins in their ears make it easy to draw blood [16, 71]. Their short gestation periods are an advantage for studies related to reproduction. Rabbits display or can be induced to display some of the same diseases and genetic abnormalities occurring in humans, including diabetes, tuberculosis and cancers, making them good test animals for those diseases [13, 71].

On the other hand, there are also many problems associated with rabbits, the European rabbit in particular. They are notorious for having caused enormous ecological and economical damage, since their rapid reproduction and big appetite can put a lot of pressure on an unprepared ecosystem (see Section 2.3.2). In several countries, the introduction of rabbits has caused other animals that depend on local plants to disappear since these were eaten by the rabbits. In some cases, they can cause local predator populations to increase due to the increased availability of prey. This can reduce the number of other prey animals as the pressure from predators becomes higher. This is called hyperpredation [11, 71]. Where rabbit numbers are too high, overgrazing can cause the death of plants that are keeping the soil stable with their root systems, which leads to severe erosion problems. Their selective grazing behaviour of native plant species can cause introduced plants to increase in numbers [62]. In agriculture and forestry, they cause losses due to their feeding on field crops and pasture and the ring-barking of young woody plants during the winter [27, 71]. In addition, European rabbits have caused damage by tunnelling underneath the foundation of buildings and ancient sites [27, 71]. Lagomorphs carry a variety of diseases, some of which can be contracted by humans. Tularemia, caused by the bacterium *Francisella tularensis*, is a dangerous infectious disease. Humans are infected through tick bites, handling diseased animals or eating their uncooked meat. Some species of cottontails and hares are also known to be susceptible to the bubonic plague caused by the bacterium *Yersinia pestis* [71].

2.3 History of the European rabbit

2.3.1 Domestication of the European rabbit

The domestication of the European rabbit, the only domesticated lagomorph, started in the Roman period. Romans kept rabbits, deer, hares and birds in leporia, enclosed spaces several acres in size [26, 71]. Rabbits were hunted within leporia with muzzled ferrets, who chased the animals out of their enclosures so people could catch them wielding nets, a technique still used to this day [70]. They did not domesticate rabbits, but were responsible for spreading the animals throughout Europe since rabbits could easily dig under the walls surrounding leporia and escape into the environment. As humans urbanised the landscape, life for rabbits became easier due to the increase in food and the decline of predators, thus helping them establish successfully through Europe

[26, 71]. Medieval French monks are credited with domesticating rabbits between 500 and 1000 CE. They had a taste for foetal rabbits, called *laurices* which they collected right after birth. Because of the close monitoring of the pregnant females, they were put in more enclosed spaces than the *leporia*. So they forced the rabbits to breed and give birth on the ground in high-walled courtyards [26, 71]. Ironically, during the Middle Ages rabbits were considered rare animals, prized for their meat, fur and hides. Because of their high value, maintaining and controlling warrens was a privilege for the king and nobility. Around 1100, with the decline of beavers, bears and other fur-bearing animals, land-owners started setting aside and carefully maintaining pieces of land for keeping rabbits. Predators were eliminated, food was supplied and sometimes holes were dug to facilitate their burrowing. Here, the selection for bigger size started as big females were left to breed while smaller females and old males were caught for food and fur. Gradually, hutches to contain rabbits were introduced, and, by about 1600, breeders were selecting for different fur colours to provide variety for customers. The angora and lop-eared rabbits appeared in the 1700s and it was not until the 1800s that the Belgian hare (Flemish giant) appeared. Only after the 1800s it was allowed for non-aristocratic people to keep rabbits and hunt them, so both rural and urban people started keeping them in classic backyard hutches for food [26, 71].

2.3.2 Introduction of rabbits into Australia

The European rabbit has been introduced in many countries including New-Zealand, Australia and parts of south-America. Of these, the introduction in Australia is best known for its disastrous impact on endemic wildlife and agriculture [62]. Before the animal evolved into a pest, domestic rabbits had been present for a long time in Australia after English settlers had arrived in Sidney in 1788. Many domestic rabbits were released by acclimatization societies which basically meant that they wanted to make Australia more like Great-Britain. However, when wild rabbits from Great-Britain were imported in 1859 and 1870 in Victoria and South-Australia, they started to reproduce rapidly and in no time huge numbers spread across Australia. Under favourable conditions, they moved about 125 kilometers per year, up to 300 along riverways. By 1910, despite attempts at shooting and poisoning, and the introduction of predators like cats (*Felis catus*) and foxes (*Vulpes vulpes*), rabbits had spread from Winchelsea in south eastern Australia, over 3000 km west to the Indian ocean, and more than 2000 km north to the tropic of Capricorn. Rabbits were described as a grey blanket covering Australia. Even the famous rabbit-proof fences could not stop their invasion [56, 71, 96].

As mentioned in Section 2.2.2, European rabbits are well adapted to the Mediterranean climate, which is similar to the climate of southern Australia. Burrows of several native marsupials such as wombats (*Vombatus ursinus*), rat-kangaroos (*Potoroidae*) and the bilby (*Macrotis lagotis*) provided shelter. The rabbits also arrived with few parasites or diseases. Some natural predators were present, but extensive control measures on these to protect sheep and cattle potentially reduced their effect on rabbits. The greatest ally of the rabbit invasion was the change in land cover from shrubs and trees to grasses and annual herbs to feed cattle. This created a perfect grazing environment for rabbits. Their browsing and grazing substantially modified the landscape by preventing the regeneration of trees and shrubs, and encouraging weed invasion and soil erosion. Rabbits were and still remain the most destructive vertebrate pest in Australia causing massive agricultural losses and ecological damage. It was not until the introduction of myxomatosis that the problem got under control (see Section 2.5) [56, 71, 96].

2.4 Myxomatosis

2.4.1 Symptoms and disease progression

The myxoma virus or MYXV is a poxvirus naturally found in two American rabbit species (*Sylvilagus brasiliensis* and *Sylvilagus bachmani*) in which it causes a small, localised fibroma. Yet, in European rabbits, the virus causes myxomatosis, a serious disease, which is mostly lethal [34, 56]. Rabbits that get infected by virulent strains of the myxoma virus develop symptoms after approximately 4 days, which include conjunctivitis and an elevated rectal temperature. After 6 days anogenital swelling is present and secondary lesions appear on the face and ears of the animal. After 8 to 10 days rabbits with the acute form of the disease have developed the typical swollen head and face, swollen, droopy ears, serous and later mucopurulent secretion from the eyes and nose, and several cutaneous swellings, sometimes called tumours or myxomas, ranging from a few millimeters to several centimeters in diameter. The animals have difficulties breathing in this stage. The anogenital region is swollen and oedematous. In males, the scrotum and testes are extremely swollen (see Figure 2.2). The virus is similar to HIV because it also actively destroys the immune system. Death occurs typically between 8 and 12 days after infection due to secondary infections [34, 56, 96].

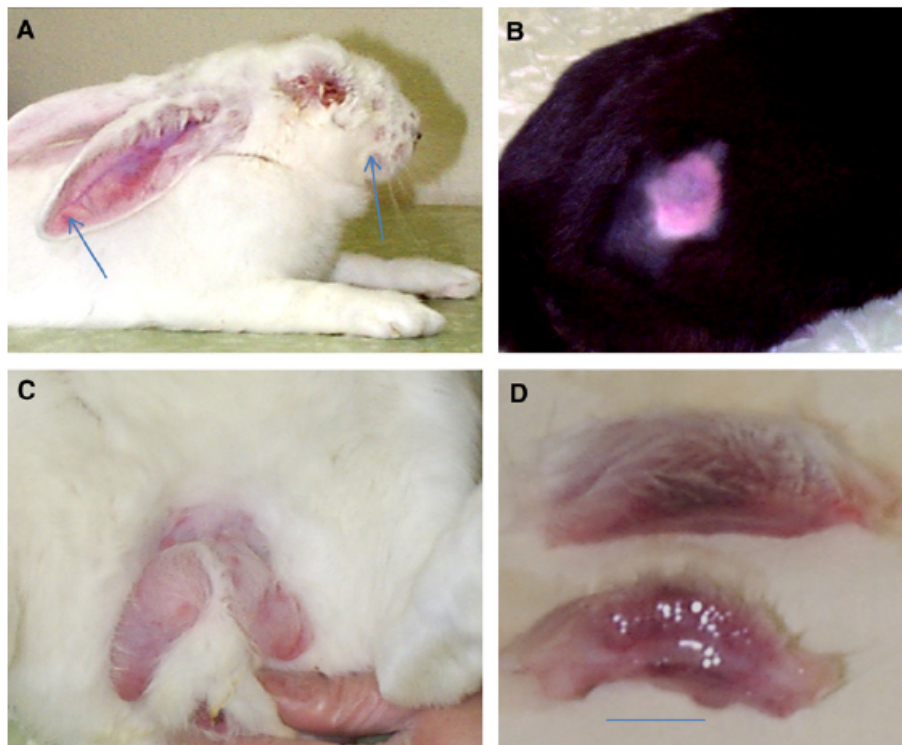


Figure 2.2: Myxomatosis in the European rabbit: (A) laboratory rabbit, with swollen head, closed eyelids and lesions on head and ear (arrows), (B) primary lesion after inoculating a laboratory rabbit about 10 days after infection (image Dr S. M. Best), (C) Oedema of scrotum 10 days after infection, and (D) cut section of primary lesion 10 days after infection (scale bar = 1 cm) [56]

2.4.2 Disease transmission and virulence

The virus is mostly transmitted by biting arthropods, like mosquitoes and fleas. The virus adheres to their mouthparts when they probe through the virus-rich epidermis of the fibromas and lesions. The virus can then be released passively into a new host when the arthropod takes its next blood meal. This enables the spread between different populations since the virus can stay alive in the parasite even when no rabbits are present [34, 56]. The secreted mucus also contains a lot of virus particles and enables the direct transmission between individuals by the respiratory route which is responsible for close-range transmission between colony members [17]. The disease is most severe in young rabbits and peaks during summer [71].

2.5 Introduction of myxomatosis in the European rabbit

2.5.1 Introduction of myxomatosis in Australia

An interesting aspect of the introduction of myxomatosis in the European rabbit is that it allows to examine what happens when a novel pathogen gets grip of a completely naive mammalian host species. Because of the short generation time of rabbits and their vast numbers in Australia, the coevolution of the host and its parasite could be studied in real time. The use of myxomatosis as a biological control agent has been suggested as early as 1919 and some early laboratory trials were done, but no field releases were permitted [34, 56]. In the 1930s, investigations were undertaken to determine the potential of MYXV. Although the virus reduced the populations in enclosure experiments, it did not spread well in field trials. Only when native stickfast fleas (*Echidnophaga sp.*) were present in the absence of European foxes (*Vulpes vulpes*), which removed sick rabbits, local spread did occur [17]. Mosquitoes do not appear to have been present in sufficient numbers to act as significant vectors in these trials, as they were conducted in dry country. However, laboratory trials had demonstrated the potential of both mosquitoes and flies to transmit the disease [17]. The conclusion from these trials was that MYXV was unlikely a good agent for rabbit control, except maybe in areas with lots of vectors and no predators [17]. This shows how difficult it can be to predict the impact of an emerging novel disease [56]. As rabbit numbers had increased significantly in the 1940s, further trials were undertaken near the Murray valley in northern Victoria and southern New South Wales to assess the role of mosquito vectors [90]. The virus spread only with low efficacy and seemingly disappeared, even in high density rabbit populations. However, the virus persisted in the environment and in December 1950 it finally emerged in its epizootic form (See Figure 2.3). Its emergence was driven by large irruptions of mosquitoes along the flood plains of the Murray-Darling basin and the massive numbers of susceptible rabbits present there [90]. The virus strain that was released here is referred to as the Standard Laboratory strain (SLS). It was derived from an European rabbit in Brazil, and subsequently supplied to researchers in the USA [33, 56].

2.5.2 Introduction in Europe

In the summer of 1952, a French physician, being tired of the damage to his garden, inoculated two wild rabbits at his estate about 70 km west of Paris with a strain of MYXV he obtained at a

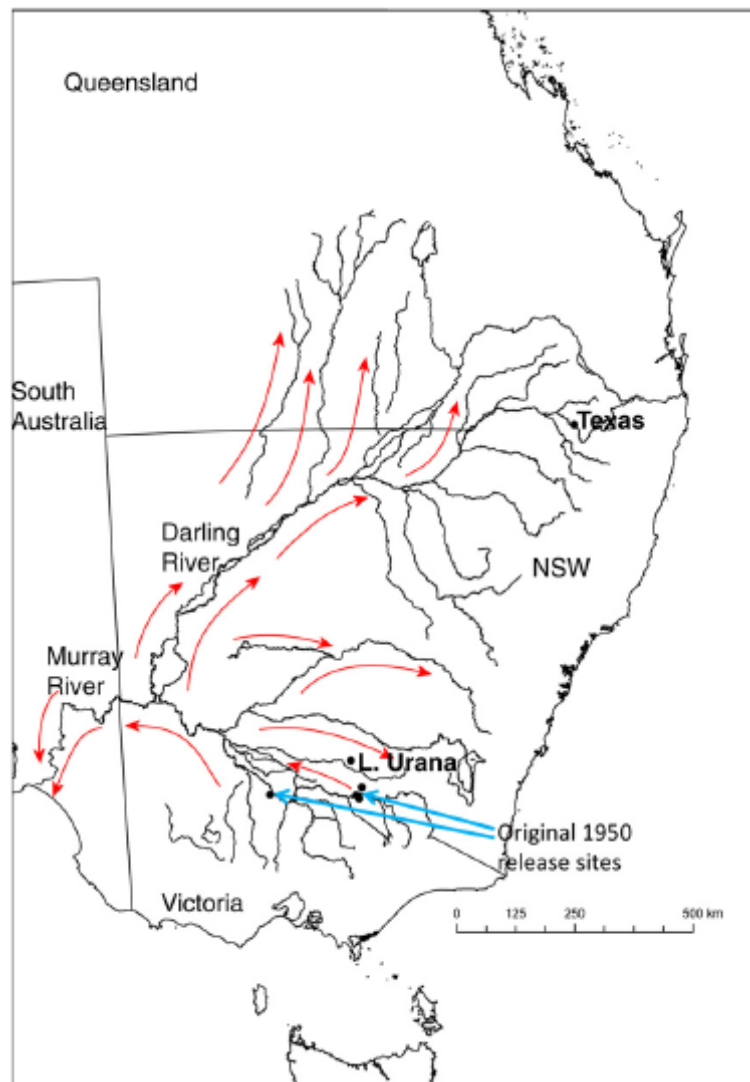


Figure 2.3: Spread of myxoma virus in the summer of 1950/51 after introduction in south-eastern Australia showing the rivers of the Murray-Darling basin. Approximate spread of the virus along the river basin is shown by the red arrows [34, 56, 90].

lab in Lausanne, Switzerland. This strain of MYXV is referred to as the Lausanne strain or Lu [33]. It has a similar case fatality as the SLS (see Section 2.5.1), as in lab test 100% of infected rabbits die after 10-12 days. Despite attempts to stop the spread of the disease over the next 10 years, all areas in Europe inhabited by rabbits got infected. The Lu strain also spread into the commercial and backyard rabbit industries, where it was partially controlled by vaccination and quarantine measures [34, 77]. From continental Europe, MYXV was introduced into Britain in 1953 where the virus also became enzootic, despite attempts at containing it [56]. Whereas in Australia the main vectors were mosquitoes, the European rabbit flea *Spilopsyllus cuniculi*, a parasite that can only reproduce on the European rabbit [71], was a major vector. In comparison to the more seasonal mosquitoes this meant in Europe the disease could also spread in the winter [56].

2.5.3 Impact of myxomatosis

In Australia, the virus first caused an enormous drop in rabbit populations. However, it became less virulent in the following years, as rabbit populations became less susceptible (see Section 2.5.4) [56]. This is often referred to as an example of failed biological control, but this is an oversimplification. The first epidemic wave reduced the population by approximately 90% [56]. The drop in rabbit numbers in 1950 provided ecological breathing space, allowed a rapid regeneration of plant species and an increase in agricultural productivity [34]. Although rabbit numbers increased again the years after the release and again became a significant environmental problem, myxomatosis continued to control the population and increased the effectiveness of conventional control measures, like poisoning and habitat destruction [110]. In addition, predators like cats (*Felis catus*), foxes (*Vulpes vulpes*) and dingos (*Canis familiaris dingo*) could keep populations under control after they had substantially been reduced [110]. After the introduction of RHD (See Section 2.6) the influence of myxomatosis on rabbit populations has become unclear [56].

In Europe, the impact on the rabbit populations was catastrophic. In France it has been estimated that the population was reduced by 90 to 98% and in Britain it has been estimated that more than 99% of the population was eliminated [104]. The rabbit occupied several sociological and ecological functions. In forestry and farming it was a serious pest, but it was also a major source for recreational hunting (See Section 2.2.3). Across the Iberian peninsula, rabbits are a keystone species and the losses caused by myxomatosis, hunting and subsequent RHD infections have caused several predator populations, like the European lynx (*Lynx pardinus*) and the Spanish imperial eagle (*Aquila adalberti*) to decline [34, 71]. Rabbit grazing is crucial to maintaining the ecosystem of the Iberian peninsula (See Section 2.2.3). In addition rabbit production costs increased due to vaccination and quarantine measures, as well as ongoing production losses [56].

2.5.4 Evolution of myxomatosis

In the decades following the introduction of myxomatosis in Australia, it became less effective at controlling the population [4, 71] because of two reasons. The first one is that the rabbits that survived the epidemic had a more resistant genotype and passed their resistance genes down to their offspring, which in turn were less susceptible to the disease [4, 71, 96]. The second reason is that the virus became less virulent during the next decade [34]. During the years after the introduction, several types of the virus with high virulence, intermediate and low virulence were

present [4, 34]. High virulence is associated with high mortality in laboratory rabbits (>90%), with lots of lesions on the skin and short survival times (about 11 days). Intermediate virulence is associated with intermediate to high mortality (50 – 90%), still lots of lesions and intermediate survival times in laboratory rabbits (14 – 26 days), whereas in low virulence strains most animals recovered and few lesions were present [4, 34]. Table 2.1 shows that selection favours intermediate strains. The latter still have high mortalities and lead to many virus-rich lesions, which makes it easier for parasites to draw blood and spread the virus. However, disease duration is notably longer, allowing a bigger time frame for the disease to spread before the rabbits die [4].

Table 2.1: Comparison of the virulence of field strains of the myxoma virus in Great Britain, Australia and France expressed as relative frequencies. The strains I and II are high virulence strains, IIIA and B are intermediate and IV and V are low virulence [4].

Virulence Strain	I	II	IIIA	IIIB	IV	V
Great Britain						
1953	100	-	-	-	-	-
1962-1967	3.0	15.1	48.4	22.7	10.3	0.7
1968-1970	0	0	78.0	22.0	0	0
1971-1973	0	3.3	36.7	56.7	3.3	0
1974-1976	1.3	23.3	55.0	11.8	8.6	0
1977-1980	0	30.4	56.5	8.7	4.3	0
Australia						
1950-1951	100	-	-	-	-	-
1958-1959	0	25.0	29.0	27.0	14.0	5.0
1963-1964	0	0.3	26.0	34.0	31.3	8.3
France						
1953	100	-	-	-	-	-
1962	11.0	19.3	34.6	20.8	13.5	0.8
1968	2.0	4.1	14.4	20.7	58.8	4.3

2.6 Rabbit haemorrhagic disease

2.6.1 Symptoms and disease progression

Rabbit haemorrhagic disease (RHD) is a viral disease caused by a calicivirus from the *lagovirus* genus called RHD virus (RHDV). It causes viral hepatitis resulting in a quick death within two to three days after infection. As opposed to myxomatosis, few symptoms can be observed apart from the occasional bloody mucous discharge from the nose [22]. The disease is transmitted through direct or indirect contact. Biting and non-biting arthropods are able to transmit the disease because only a few virions are required for infection via the conjunctiva [41]. Only 10% of adult rabbits survive infection while 40% of young rabbits recover [60, 107, 114]. The disease peaks during the winter [71].

2.6.2 History and impact of RHD

RHD was first observed in the People's Republic of China in 1984 among angora rabbits. Within a few months, the disease had spread widely across the country in commercial rabbit farms [114]. It is not certain where the virus originated from, but since related, harmless lagoviruses are present in Europe [60], it has been suggested it originated from there [71]. Despite measures to prevent the spread of the virus to other regions, it appeared in Italy in 1986. It spread to other European countries and subsequently appeared in wild populations in Spain in the summer of 1988, where the disease increased the pressure on its rabbit populations [22]. The first outbreak in the Iberian peninsula reduced populations already devastated by myxomatosis by an additional 50 to 70% [107].

The impact of RHD in Europe sparked interest in countries where rabbits had been introduced, as myxomatosis was becoming less effective at controlling populations [4, 71]. After a series of experiments to test its effectiveness at controlling rabbits and if it would cause disease in other animals [63], the virus spread beyond the quarantine fences of Wardang Island, a small 20 km island close to the coast of southern Australia, where the experiments took place, crossed several kilometres of sea to arrive in the dense inland rabbit populations, where it rapidly spread and became a useful control agent [22]. The first outbreak of RHD reduced populations up to 95%, spread initially 50 kilometres per week and was present in every part of Australia two years later [1].

2.6.3 RHDV2

In 2010, a new type of RHDV, called RHDV2, was discovered in northern France, infecting rabbits susceptible to RHDV as well as vaccinated animals. The estimated mortalities are unusually high at 80 to 90 %, similar to the mortalities during the first spread of RHDV [61]. The virus gives similar disease symptoms as RHDV but is classified as another genus of the *Lagovirus* indicating that it did not evolve from RHDV. There are two hypotheses explaining the origin of the virus. One is the evolution from a non-pathogenic *lagovirus* species, while the other is the species jump from another host animal to the European rabbit. Yet, none of these hypotheses has been proven [60]. Infections by RHDV2 last longer and are more variable, while the development of chronic disease instead of acute was more frequent. The disease spreads very fast, as the virus was already confirmed in Spain and Italy in 2011 [60]. RHDV2 has already replaced most of the RHDV isolates in France. The moderate virulence of RHDV2 can explain its selective advantage over more virulent RHDV strains (See Section 2.5.4) [60].

CHAPTER 3

Modelling Epidemical Diseases

In this chapter we will briefly outline the general principles of epidemical modelling after which some foundational epidemic models will be discussed. After that we will expand epidemic modelling into a spatial context after which a few examples of recent developments in epidemic modelling will be discussed. For the remaining chapters we will not differentiate between epizootics and epidemics since the processes governing them are similar.

3.1 General principles

There is a variety of mathematical approaches to epidemiology, but first some general principles need to be outlined. An epidemic can be characterized as the evolution of an infectious disease within a given population of individuals. The first group of assumptions concern the structure, dynamics and composition of the population are needed. This concerns the fact whether it consists of one homogenous group, multiple homogeneous strata that interact, or a completely heterogeneous group, which means that all individuals are different. For what concerns the population dynamics, a choice needs to be made between closed systems with a fixed number of individuals, or open systems, where individuals can migrate, die and/or give birth. The population composition is important to classify the individuals according to their disease status. More precisely at any time individuals are either susceptible to the disease, incubating it, infected, infected but without any symptoms i.e., a carrier, or removed, which means that they have been infected or a carrier but are so no longer, either through death, immunity or isolation. The second group of assumptions concern the disease itself. For instance, how does it spread and what is the mechanism for recovery or removal if this occurs. The third group of assumptions concern the mathematics necessary to specify the population and disease mechanics [25]. An important basis for epidemic modelling is the Law of Mass Action, postulated by Guldberg and Waage [42], which states that for a homogeneous system, the rate of chemical reaction is proportional to the active masses of the reacting substances [42]. This law can be applied in other contexts, including population processes. If the individuals in a population mix homogeneously, the rate of interaction between two different subsets of the population is proportional to the product of the numbers in each of the subsets concerned. This principle can be applied to deterministic and probabilistic epidemic models [25].

3.2 Foundational epidemic models

3.2.1 Contagious diseases

In deterministic models, the sizes of susceptible, infected and removed populations are assumed to be either functions of discrete time ($t = 0, 1, 2, \dots$) or differentiable functions of continuous time ($t \geq 0$). These approximations to the true, integer-valued numbers are a prerequisite for the derivation of systems of difference or differential equations governing the epidemic dynamics. The results of deterministic processes should be regarded as an approximation of the expected values of a random process [25]. One of the oldest and most frequently studied deterministic models is the model for the general epidemic by Kermack and McKendrick, describing a basic susceptible-infected-recovered model (SIR-model) [25, 55]. It is a simple system of differential equations describing an epidemic within a population of fixed size N , consisting of susceptibles $S(t)$, infected $I(t)$ and recovered individuals $R(t)$. By relying on the homogeneous mixing principle for continuous time the following system is obtained [55]:

$$\begin{cases} \frac{dS}{dt} = -\beta S I, \\ \frac{dI}{dt} = \beta S I - \gamma I, \\ \frac{dR}{dt} = \gamma I, \end{cases} \quad (3.1)$$

subject to the initial conditions $(S(0), I(0), R(0)) = (S_0, I_0, 0)$. In this system $\beta [T^{-1}]$ is the transmission rate that depends on the interaction between infected and susceptible individuals, while $\gamma [T^{-1}]$ is the removal rate, quantifying the rate at which infected subjects become immune. In cases where death or isolation occurs, $R(t)$ represents all removals from the population [25, 55]. The second equation of System (3.1) can be rewritten as:

$$\frac{dI}{dt} = \beta I \left(S - \frac{\gamma}{\beta} \right). \quad (3.2)$$

From this, it follows that the population of infected individuals I cannot increase if $S < \frac{\gamma}{\beta}$. This is called the threshold phenomenon [46, 48, 55]. Another important property relates to the basic reproductive number:

$$R_0 = \frac{\beta S}{\gamma}. \quad (3.3)$$

This is the average number of secondary disease cases caused by one primary disease case in a completely susceptible population [46, 48]. If $R_0 < 1$, the population of infected individuals cannot grow [48]. Furthermore, in a closed population, an infectious disease can only invade if $\frac{I_0}{N_0} > \frac{1}{R_0}$ [46].

System (3.1) assumes that there is no reproduction. In most populations, however, individuals can reproduce or die. Taking population dynamics into account the following system is obtained:

$$\begin{cases} \frac{dS}{dt} = r(S + I + R) - \beta SI - mS, \\ \frac{dI}{dt} = \beta SI - (\alpha + m + \nu)I, \\ \frac{dR}{dt} = \nu I - mR, \end{cases} \quad (3.4)$$

with $r[T^{-1}]$ the per capita birth rate, assumed here to be the same for susceptible, infected and recovered individuals, $m[T^{-1}]$ the mortality, which is assumed to be the same for susceptible and recovered individuals. The removal parameter γ from System (3.1) is replaced by $\alpha + m + \nu$ with $\alpha[T^{-1}]$ the death rate due to the disease and $\nu[T^{-1}]$ the rate at which infected individuals become resistant [32, 78]. The basic reproduction number R_0 for System (3.4) is

$$R_0 = \frac{\beta S}{\alpha + m + \nu}. \quad (3.5)$$

System (3.1) can also be expanded to a generic epidemic in a stratified population, where several homogeneous populations interact. Assume the population is divided in m strata, then we define pairwise transmission rates $\beta_{ij}[T^{-1}]$ for an infective in the i -th sub-population or stratum to infect a susceptible in the j -th stratum for $i, j = 1, \dots, m$. In addition, it is assumed that each stratum j has per capita removal rates $\gamma_j[T^{-1}]$ and $R_j(t)$ denotes the cumulative number of such removals at time t . In analogy with System (3.1) the following system is obtained

$$\begin{cases} \frac{dS_j}{dt} = -S_j \sum_{i=1}^m \beta_{ij} I_i, \\ \frac{dI_j}{dt} = S_j \sum_{i=1}^m \beta_{ij} I_i - \gamma_j I_j, \\ \frac{dR_j}{dt} = \gamma_j I_j, \end{cases} \quad (3.6)$$

for $j = 1, \dots, m$ with initial conditions $(S_j(0), I_j(0), R_j(0)) = (S_{j0}, I_{j0}, 0)$. A stratified SIR-model has been used to determine the effect of the combination of myxomatosis and RHD on population dynamics of wild rabbits [39]. The study concluded from the simulations that concurrent infections of RHD and myxomatosis lowered the maximum number of rabbits infected with RHD. Simulation results are shown in Figure 3.1.

Systems (3.4) and (3.6) are, however, only two ways to expand System (3.1). Other ways include the generation-wise spread of an epidemic or the consideration of a carrier-borne disease, where individuals can spread the disease, but do not develop symptoms [25]. Models of the SIR type and extensions thereof have been used in many epidemiological studies including the spread of cholera in Haiti [6, 113], the effect of vaccinations on epidemiological patterns [5], the spread of rabies through fox populations [98] and the dynamics of measles [12]. A SIR-model with stratified populations has also been used to determine the effect of different types of RHDV on the genetic diversity in rabbits [37].

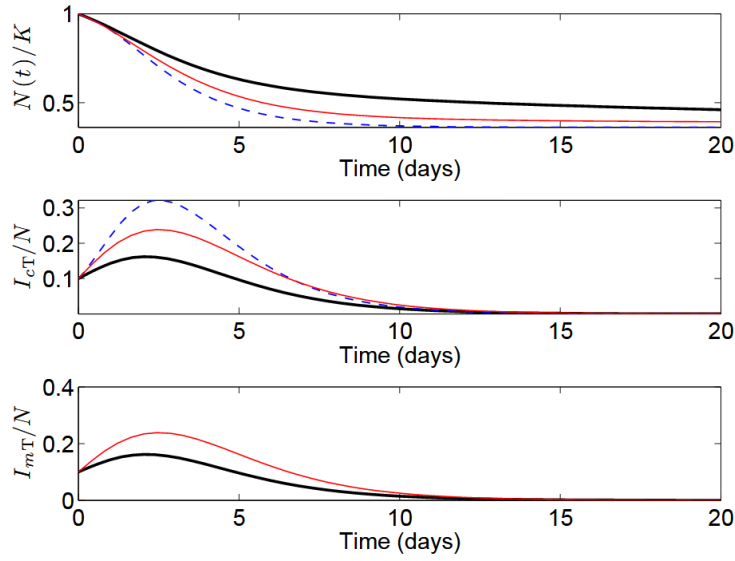


Figure 3.1: Simulation of the model without natural birth and death rates. $N(t)$ refers to the number of rabbits remaining. I_{cT} is the total prevalence of RHD while I_{mT} refers to the total prevalence of myxomatosis. The blue dashed line is the simulation with RHD without initial myxomatosis. The solid lines are simulations with both infections present. Only in the simulation resulting in the red curve the concurrent infection of RHD and myxomatosis is allowed [39].

3.2.2 Vector-borne diseases

The models introduced in Section 3.2.1 have one restriction in common in that they model the spread of a disease that is transmitted via direct contact, such as HIV, measles and smallpox. A vector-borne disease, like malaria, where the parasite responsible for the infection spends a part of its life cycle in *Anopheles* mosquitoes, needs a different approach since contact between infected and susceptible individuals does not transmit the disease [25, 74]. For that purpose two populations are considered, namely the population of hosts and the population of vectors, which are assumed to be of constant size N_1 and N_2 . Removals from both populations are neglected. So, the populations N_k are divided in a susceptible $S_k(t)$ and infected $I_k(t)$ population in such a way that $S_k(t) + I_k(t) = N_k$ for $k = 1, 2$. A human infected with malaria loses infectivity at rate $\mu_1 [T^{-1}]$ and infected mosquitoes die at rate $\mu_2 [T^{-1}]$. Because the populations are assumed to be of constant size, the dying mosquitoes are replaced with new uninfected individuals. A mosquito depends on biting a host, in this case a human, for a blood meal during which can ingest infected blood if the host is malarial. Subsequently, it can infect a susceptible host [9, 25]. Applying the Law of Mass Action, the following equation is obtained for the hosts:

$$\frac{dI_1}{dt} = \zeta \beta_{21} I_2 \frac{S_1}{N_1} - \gamma_1 I_1, \quad (3.7)$$

and for the vectors:

$$\frac{dI_2}{dt} = \zeta \beta_{12} S_2 \frac{I_1}{N_1} - \gamma_2 I_2, \quad (3.8)$$

with $\zeta [T^{-1}]$ the feeding rate per mosquito and $\beta_{ij} [T^{-1}]$ the disease transmission rate of an infected individual of type i with a susceptible of type j .

These equations can be reformulated in terms of proportions $x_k = S_k/N_k = 1 - y_k$ for $k = 1, 2$,

$$\begin{cases} \frac{dy_1}{dt} = \zeta \beta_{21} y_2 x_1 \frac{N_1}{N_2} - \gamma_1 y_1 \\ \frac{dy_2}{dt} = \zeta \beta_{12} y_1 x_2 - \gamma_2 y_2. \end{cases} \quad (3.9)$$

This is only a basic description of a vector-borne epidemic and can be improved in similar ways as non-vector borne epidemics (See [9]). Similar models have been used to study the transmission of the Chagas disease [106].

3.2.3 Discrete-time models

In Sections 3.2.1 and 3.2.2, the functions describing the epidemics were considered to be continuous. However, since epidemic data is gathered at discrete time instances, it makes sense to resort to discrete models [25]. An example of a discrete model is the model of Saunders [97]. It describes the evolution of myxomatosis (see Section 2.4) in a fixed population of European rabbits (see Section 2.2.1). It assumes that a rabbit gets infected on day t , enters a latent period of length l when the virus is incubating, and subsequently becomes infectious on day $t + l$ and remains so until day $t + l + k - 1$, after which it dies. Suppose I_1^t is the number of infectious rabbits on day t . These were infected on day $t - l$ and remain infectious until day $t + k - l$. Consequently, the total number of infectives on day t is

$$I^t = \sum_{j=0}^{k-1} I_1^{(t-j)}, \quad (3.10)$$

since any rabbits becoming infectious before day $t - k + 1$ have died by day t . Starting with S_0 susceptibles at time $t = 0$, the remaining number of susceptibles at time t is

$$S^t = S_0 - \sum_{j=1}^{t+l} I_1^j, \quad (3.11)$$

while the number of rabbits in the latent state is

$$W^t = \sum_{j=1}^l I_1^{t+j}, \quad (3.12)$$

such that the total number of living rabbits on day t is given by $N^t = S^t + I^t + W^t$. Saunders relies on homogeneous mixing to arrive at

$$I_1^{t+l} = \frac{a}{N^t} I^t S^t, \quad (3.13)$$

with $a [T^{-1}]$ the number of rabbits a diseased rabbit makes contact with each day.

Continuous models can also be discretized. For example, the model given by System (3.1) can be discretized for $t = 0, 1, \dots$ leading to

$$\begin{cases} S_{t+1} = S_t - \beta S_t I_t, \\ I_{t+1} = I_t + \beta S_t I_t - \gamma I_t, \\ R_{t+1} = R_t + \gamma I_t, \end{cases} \quad (3.14)$$

with $S_t + I_t + R_t = N$, and $\beta [T^{-1}]$, $\gamma [T^{-1}]$ are the infection and removal parameters, which may differ from those of the corresponding continuous models [25].

A discrete SIR-model based on (3.14) has been used to analyse a measles outbreak on a university campus and to determine the rate at which a population needs to be vaccinated to prevent an outbreak [3]. They concluded that more than 98 percent of a population needed to be immune to prevent an outbreak. A simulation of the model is given in Figure 3.2.

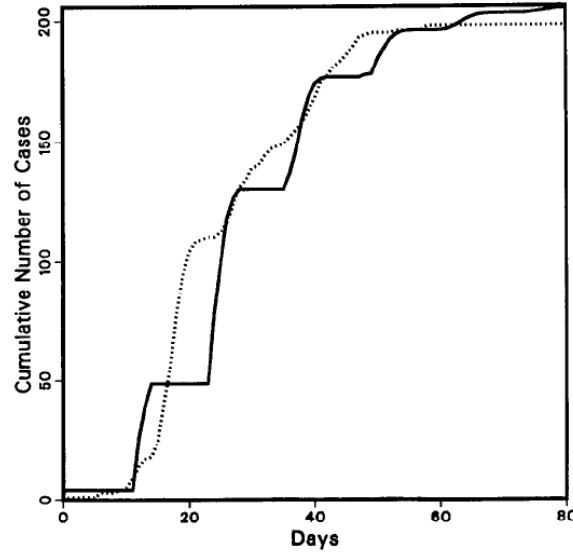


Figure 3.2: Simulation results of a discrete epidemic model for measles (thick line) compared to collected data (dashed line) [3].

Discrete models have also been used to study the outbreak of SARS and its transmission in China [115] among others.

3.2.4 Stochastic models

Deterministic models are adequate to characterize disease spread in large, uniform populations. In small populations, a stochastic approach is needed, especially if the population consists of only a few individuals. An example of a frequently used stochastic approach to epidemic modelling [25] is Markov chain analysis. Since the methods for analysis of Markov chains are quite elaborate, we will not discuss them further but refer the reader for detailed information and analytical solutions to [25]. The following approach is, however, suitable to analyse epidemics in small populations. If Y denotes the number of secondary infections that follow from a single infected individual, then the probability density function $f(y)$ describing the distribution of Y is referred to as the offspring distribution [43]. The number of secondary infections depends on the infectiousness of the first case over the time τ since it got infected, represented by a function $\beta(\tau)$. Now, the probability that an infective will infect a susceptible individual between time τ and $t + d\tau$ is

$$\beta(\tau)s d\tau, \quad (3.15)$$

with $d\tau$ the length of a short time period and $s[-]$ the probability that the other subject is susceptible to the disease [43].

Integrating Eq. (3.15) over the time since infection onset yields the expected number of offspring:

$$E(Y) = s \int_0^{\infty} \beta(\tau) d\tau. \quad (3.16)$$

In a population where contact between infectious and susceptible individuals is random, $E(Y)$ is the same as the reproduction number of an infection R [43, 48]. In an entirely susceptible population ($s = 1$), this is called the basic reproduction number R_0 (see Section 3.2.1). If a group of individuals has the same infectiousness, then the number of secondary infections caused by each individual is Poisson distributed with mean R [43]. Another important quantity is the time τ that has elapsed between one individual getting infected and that individual infecting another. The distribution of this time, also called the generation-time distribution $w(\tau)$, is related to the infectiousness $\beta(\tau)$ after rescaling by the reproduction number R :

$$w(\tau) = \beta(\tau)/R. \quad (3.17)$$

Equations (3.15) and (3.17) can be used for analysing and modelling the evolution of an epidemic in a population [43, 55]. Let $I(u)$ denote the number of newly infected individuals at time u , while at some later time point $t = u + \tau$ the infectiousness of these individuals is $\beta(\tau)$, then the number of susceptibles that they will infect during the next time step of duration $\delta\tau$ follows a Poisson distribution with mean $I(t - \tau)\beta(\tau)\delta\tau$. The total expected number of infected people at time t , is obtained by summing this quantity over all possible values of τ [43]:

$$I(t) = \int_0^{\infty} I(t - \tau) \beta(\tau) d\tau. \quad (3.18)$$

This formula is called the renewal equation. Using Eq. (3.17) to substitute $\beta(t)$ in Eq. (3.18), and recasting the resulting equation provides an estimator for the reproduction number R [38]:

$$R(t) = \frac{I(t)}{\int_0^{\infty} I(t - \tau) w(\tau) d\tau}. \quad (3.19)$$

This type of model is also used to analyse data and to analyse transmission trees (see Figure 3.3). Stochastic methods have been used for the analysis of the SARS outbreak in Singapore [21, 67], the spread of HIV-1 among risk groups and the spread of measles [43] among others.

3.3 Spatial models

Hidden in the proportionality aspect of the Law of Mass Action (See Section 3.1) is the assumption that all individuals interact equally likely with each other. Clearly, in reality this is not always the case. Another concern with the models in Section 3.2 is that they do not improve the understanding of how the wave-front of a an epidemic progresses [82]. In the remainder of this chapter different approaches to spatio-temporal modelling of epidemics will be discussed.

3.3.1 Reaction-diffusion models

Individuals moving through space and time can be envisaged as a diffusion process of particles through time and space. This process is governed by the diffusion equation [35, 52]:

$$\frac{\partial\psi}{\partial t} = D \nabla^2 \psi, \quad (3.20)$$

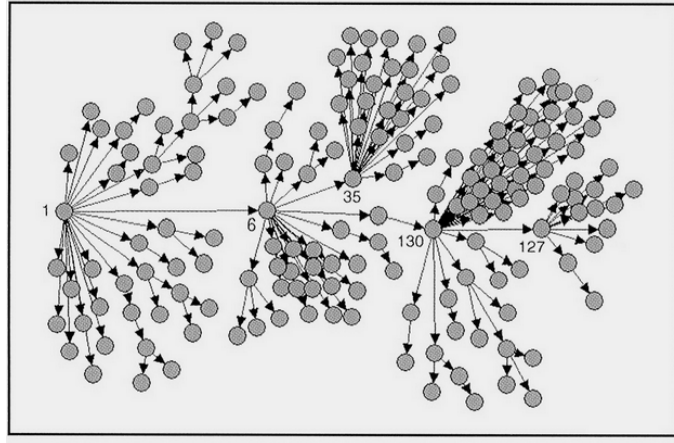


Figure 3.3: Transmission tree of an SARS outbreak in Singapore in 2003. The dots represent infected individuals connected by arrows showing which individual have infected each other [21].

with $\psi(x, y, z, t)$ the concentration of a compound at (x, y, z) at time t , $D [L^2, T^{-1}]$ the diffusion coefficient, here assumed to be constant and

$$\nabla^2 \psi = \frac{\partial^2 \psi}{\partial x^2} + \frac{\partial^2 \psi}{\partial y^2} + \frac{\partial^2 \psi}{\partial z^2} \quad (3.21)$$

the Laplacian operator denoting the divergence of the gradient of a function in Euclidean space [52]. Equation (3.20) has a variety of applications, and is also used in population modelling [84] and epidemic modelling [82] to incorporate spatiality. A diffusion-based SIR-model has been used to successfully model the general wave-like spread of rabies among foxes [82]. The system used in [82] in reads:

$$\begin{cases} \frac{\partial S}{\partial t} = -\beta I S + (r - m) \left(1 - \frac{N}{K}\right) S \\ \frac{\partial E}{\partial t} = \beta I S - \sigma E + \left[m + (r - m) \frac{N}{K}\right] E \\ \frac{\partial I}{\partial t} = \sigma E - \alpha I - \left[m + (r - m) \frac{N}{K}\right] I + D \nabla^2 I, \end{cases} \quad (3.22)$$

with $N = S + E + I$ the total number of foxes, $S[-]$ the number of susceptible foxes, $E[-]$ the number of infected foxes that do not show symptoms yet and $I[-]$ the number of infectious foxes. It is assumed that the spatial dispersal of rabies originates from the random wandering of rabid foxes [82]. It is also assumed that the population follows a logistic population dynamic instead of an exponential one, contrary to System (3.4) from Section 3.2 for example. Therefore the carrying capacity $K[-]$ is added, denoting the maximum number of foxes in the environment. The parameters are similar to those of System (3.4), with the addition of $\sigma [T^{-1}]$ denoting the rate at which infected foxes become rabid and $D [L^2, T^{-1}]$ the diffusion parameter. The parameter ν is not incorporated since it is assumed that foxes do not develop resistance and never recover from rabies [82]. The model was used to simulate the wavefront following an introduction of rabies in fox populations in the southern half of England with known fox densities (see Figure 3.4).

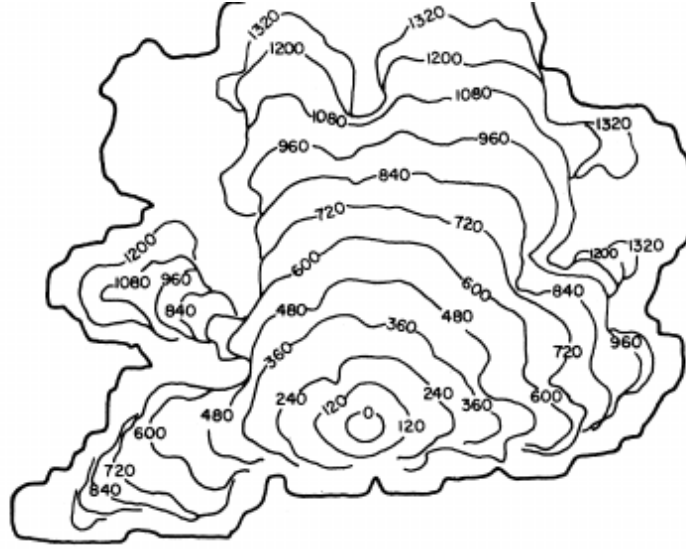


Figure 3.4: The position of the wavefront every 120 days following the introduction of rabies in southern England [82].

Another example is the epidemic model of the spread of a pathogen in insect populations by [31], where the system of PDEs reads:

$$\begin{cases} \frac{\partial S}{\partial t} = -\beta P S + D\nabla^2 S, \\ \frac{\partial I}{\partial t} = \beta P S - \gamma I + D\nabla^2 I, \\ \frac{\partial P}{\partial t} = \lambda I - \mu P, \end{cases} \quad (3.23)$$

with $P [L^{-2}]$ the density of pathogen particles, $\beta [T^{-1}]$ the rate at which contact between susceptible individuals and pathogens causes infection through ingestion of pathogen particles by the insects (note the similarity with System (3.2.2)), $S [L^{-2}]$ and $I [L^{-2}]$ the density of susceptible and infected individuals, respectively, $\gamma [T^{-1}]$ the death rate of infected individuals, and $\lambda [T^{-1}]$ and $\mu [T^{-1}]$ the dispersal rate of pathogen survival stages from diseased individuals and the death rate of the pathogens, respectively [31]. Diffusion-based epidemic models have also been used in the analysis of an Avian-human influenza system [57] and the spread of human influenza [95], among others. This approach to spatial modelling, however, has a few limitations. First, the equations need to be solved numerically since they do not have a closed-form solution. Second, they are not suitable to model complex patterns that sometimes arise in spatial processes, due to the fact that the variability of the environment that causes these patterns is neglected [86]. Third, they still represent an approximation of a stochastic process, limiting diffusion-based epidemic models to epidemics in large, uniform populations [51] and fourth, they assume that infected individuals move from regions of higher densities of infected individuals to regions with lower densities, which is sometimes not the case. For example, rabbits infected with myxomatosis become highly immobile (see Section 2.4).

3.3.2 Agent-based complex systems

An epidemic is typically governed by a large number of individuals that make autonomous decisions, have their own distinct behaviour and interact with the environment. It is one example of a process governed by autonomous, adaptive agents, like cells of the immune system, stock market investors, and so on [45]. Systems governed by such agents are called agent-based complex systems (ACSSs) [45]. Their interaction gives rise to complex patterns that are not easily modelled by standard mathematical methods like differential equations. An ACS has three elements: the first being a set of agents, their attributes and behaviours; the second being a set of agent relationships and methods of interaction describing how and with whom agents interact among themselves, and the third being the environment with which the agents interact [72]. Models with this bottom-up approach have been developed for several types of ACSs, especially in ecology. The bottom-up approach has two big challenges: the complexity of the models and the uncertainty of the output [44, 45]. These models are often computationally expensive, limiting their use in the past due to limited computing power [112].

Individual-based models

An individual-based model (IBM) tries to model phenomena caused by the interaction of multiple individuals by modelling them as single agents and letting them mutually interact and with their environment. An example of a well-known basic IBM is the boids model [91]. This model reproduces schooling behaviour through simple rules in that individual boids try to avoid collision, match the velocity of neighbouring individuals and stay close to their neighbours [45, 91]. In epidemiology an IBM has been used to model the spatio-temporal spread of malaria in a Peruvian village in the rainforest. It is based on the interaction between mosquitoes and humans in a spatially explicit way. The modelled environment includes: climate, peoples houses and their positions, and elevation. The changes in the mosquito breeding areas because of flooding is also included [88]. The individuals follow a decision tree each time step to determine their next action (see Figure 3.5 and 3.6). By letting the mosquito agents interact with the human hosts and the environment during subsequent time steps this model simulates the process of malaria incidence in a rainforest village in great detail. It is clear that this model has complicated interactions with a variety of possible actions that each individual human or mosquito can take [88]. This however, also introduces some random factors, which inadvertently makes the model outcome harder to predict, but is also closer to a real epidemic, which is the result of a random process [25]. The results of a simulation of this model are given in Figure 3.7.

IBMs have been used to model bioattacks [20], the spread of HIV [103] and the epidemiological and evolutionary dynamics of influenza viruses [92] among others. IBMs are very suitable to model spatial patterns, but modelling the entire life history of each individual in time and space generates an enormous complexity of information, making the results sometimes difficult to interpret and limiting their applications [51]. They are typically very good at generating data, but finding parameter values that approximate experimental data sufficiently is typically very hard for this type of models [66].

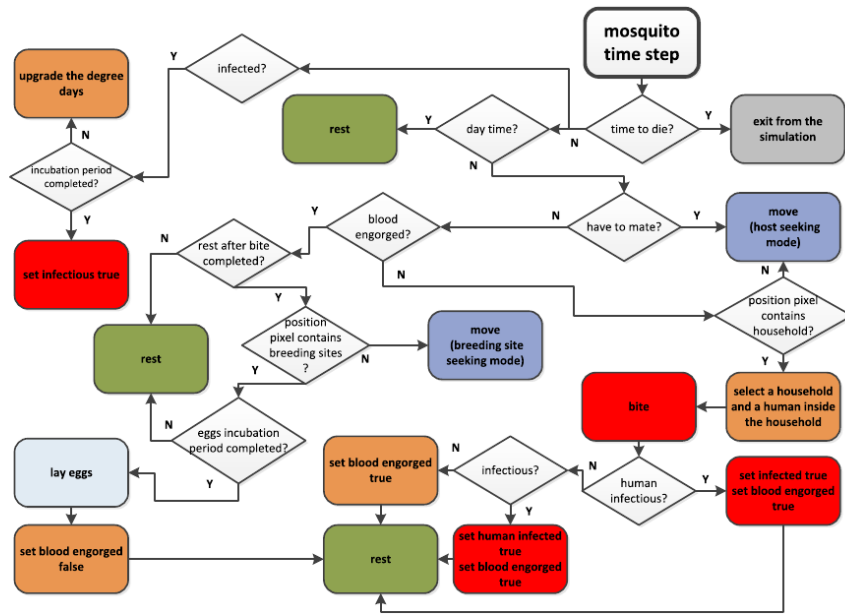


Figure 3.5: Decision tree of the mosquitoes [88].

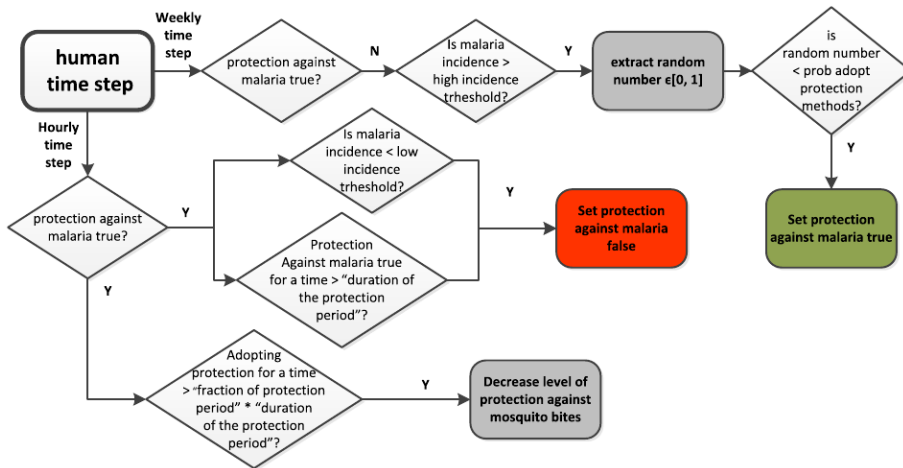


Figure 3.6: Decision tree of the humans [88].

Cellular automata

For the study of systems that lead to complex patterns cellular automata (CAs) have become quite popular. They are based on a discretized 2D or 3D grid. Each of those cells bears one of a finite number of states [2, 112], and has a number of cells in its neighborhood \mathcal{N}_i with which they can interact. After assigning an initial state to each cell, every cell gets a new state according to a fixed rule that depends on the state of the cell c_i considered and the cells $c_j \in \mathcal{N}_i$ in its neighbourhood in subsequent discrete time steps $t = 1, 2, 3, \dots$ [112]. CAs are agent-based systems in the sense that each individual cell can be considered an autonomous agent interacting with its neighbourhood [72]. The best known example of a CA is Conway's Game of Life [40], but CAs have found their way in a multitude of applications, including chemistry, microbiology, geology,

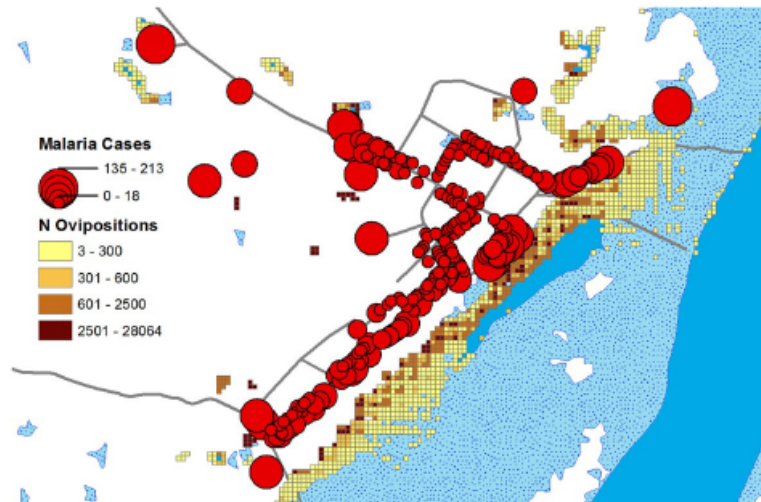


Figure 3.7: Oviposition sites and malaria cases during the simulation period [88].

geography and epidemiology [2, 112]. In epidemic modelling, an example is the CA-like model that has been used to model the pattern formation in red fox (*Vulpes vulpes*) populations following an outbreak of rabies [51]. It is based on a spatial grid of fox home ranges that feature a healthy population, an infectious population or no population at all. It is not a pure cellular automaton since it also features an IBM to model the dispersal of young foxes and wandering rabid foxes [51]. A schematic representation of the model is given in Figure 3.8. The cells in the grid shown in this figure are home ranges of foxes. The local dynamics in a fox home range are aggregated into three discrete states: the cells with a healthy population denoted by H , the cells with an infected population denoted by I , and the empty cells denoted by E . Transitions between those states occur throughout the year with certain probabilities (transition from I to either E or H and from H to I through infection by neighbouring infected home ranges), or only during dispersal of young foxes governed by the IBM (transition from H to I through infection by rabid, young foxes and transition from E to H by arrival of healthy, young foxes).

Using this model, the effect of the dispersal function on the disease front was observed (see Figure 3.9). They concluded that the dispersal of young foxes in a random direction along a straight line was necessary to develop a disease front [51].

CAs have been used to simulate the spatial dynamics of foot and mouth disease outbreaks in feral pigs in Australia among others [28]. They are restricted in the sense that the cells can only be assigned one out of a finite set of discrete states. The latter can be overcome by resorting to so-called coupled-map lattices (CMLs), often called continuous CAs. They are similar to CAs in the sense that they are also based on the subdivision of space and time, but they feature a set of continuous state variables [53]. ABSs in general are very good at simulating patterns, but can get computationally expensive. They are also not suitable to infer general epidemic theories [45].

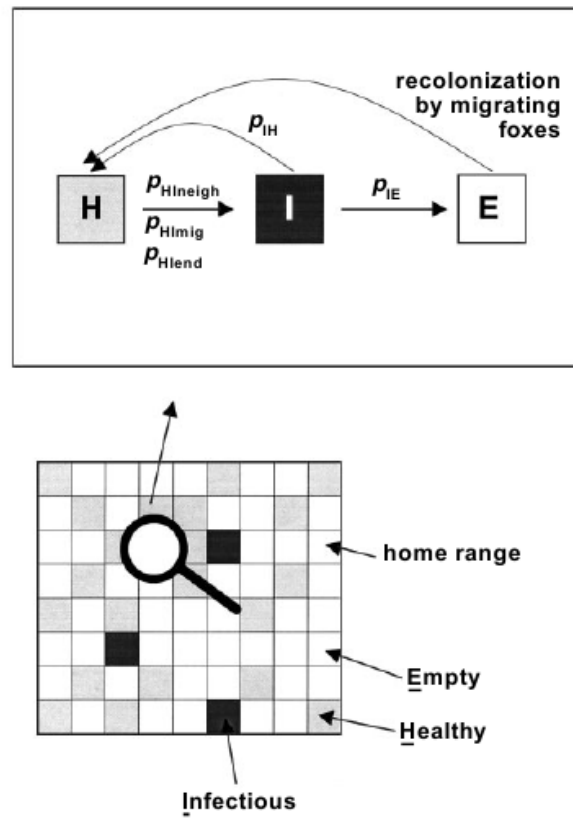


Figure 3.8: Schematic representation of the rabies model with transition probabilities [51].

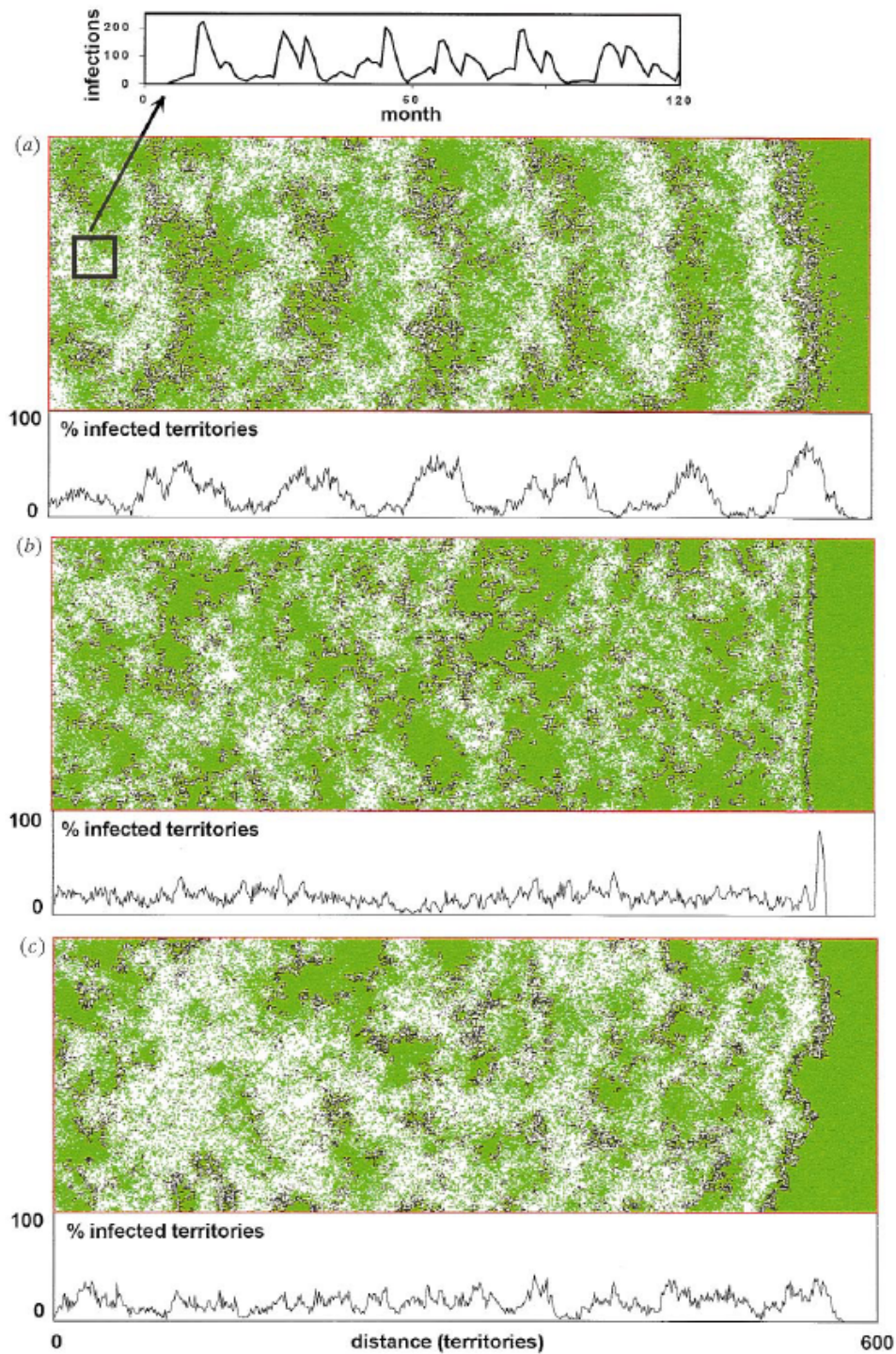


Figure 3.9: Large-scale pattern formation using different dispersal functions and their one-dimensional projections. a) Dispersal of young foxes along a straight line starting from a random direction. b) No dispersal of young foxes. c) Dispersal using a random-walk model. Healthy home ranges are green, infected home ranges black, and empty home ranges white [51].

CHAPTER 4

The 1953-1954 Myxomatosis Epidemic in Belgium

4.1 The dataset

4.1.1 The Bulletin Sanitaire

As mentioned in Section 2.5.2, myxomatosis was introduced in the European mainland in 1952. According to the Bulletin Sanitaire [80], the disease spread into Belgium from the French border in September 1953. The Bulletin Sanitaire is a report that was published every two weeks from 1929 to 1983 by the Ministry of Agriculture of the Belgian government about animal diseases that are harmful for agriculture. Since September 1953 these also included myxomatosis [80]. For this disease, every two weeks, the number of nidi were reported together with the towns where they were found. A nidus is a pathogen reservoir from which one or more cases of a disease originate. It was also mentioned if these were nidi in wild or domesticated rabbits. This data was collected from the Bulletin Sanitaire for the period of 15 September 1953, till 31 December 1956. Separate datasets were generated for domesticated and wild rabbits, containing the number of nidi at subsequent points in time. From these datasets it was also possible to derive the number of nidi that have been reported per town up to a point in time.

The model that will be used to reconstruct the introduction of myxomatosis (see Chapter 5) only takes short range disease transfer into account. Nidi, that could not have been caused by such short-range interactions, were eliminated as follows. If a nidus appeared in a town for the first time and if none were reported in the same town or its neighbours for the next four weeks, then the data point was eliminated. It should also be noted that, since the data were collected more than sixty years ago, the conclusions drawn from the analyses should be interpreted with care.

4.1.2 Data exploration

In Figure 4.1 the number of reported nidi in Belgium over time and the cumulative number of nidi are plotted for both wild and domesticated rabbits. There is a clear difference in the number of nidi and the timing of the peaks between Figures 4.1(a) and 4.1(c), and 4.1(b) and 4.1(d). That is, for wild rabbits, the number of nidi peaks at about 50 weeks after the introduction and decreases

quickly after that resulting in a smooth sigmoid curve for the corresponding cumulative disease cases (see Figure 4.1(c)). For domestic rabbits, the number of nidi peaks directly after the start of the epizootic, decreasing quickly afterwards with sudden and short-lasting rises every fifty weeks. This results in a stepwise sigmoid curve for the cumulative number of nidi.

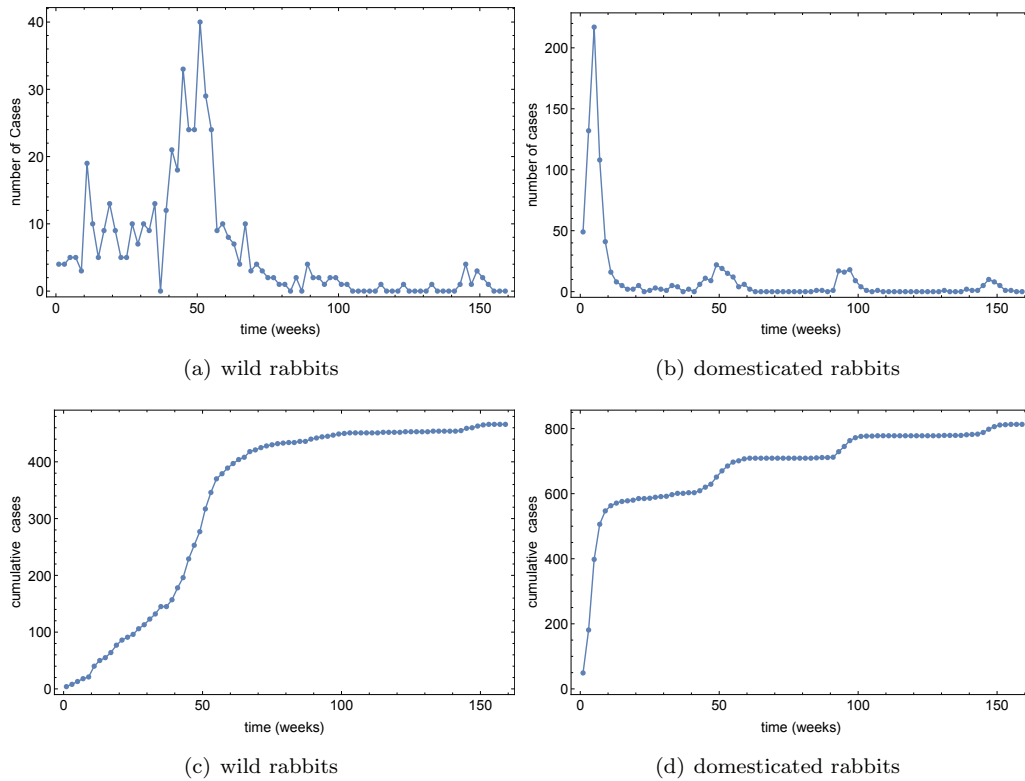


Figure 4.1: nidi of myxomatosis in the 1953-1954 epidemic

Figure 4.2 displays the percentage of the towns in Belgium where at least one nidus in wild or domesticated rabbits was reported. Normally, one would expect that after some time, all towns of Belgium would have been infected, but this is not the case. It seems that after about 50 weeks, only a few additional towns got infected. This could be attributed to underreporting once the disease had become commonplace. It is clear, however, that the number of towns with a nidus in wild rabbits is at least the double of those with a nidus in domesticated rabbits, though, for those, more nidi were reported in total. This suggests that the reports of wild rabbits contain more information on the spatial spread of myxomatosis.

Figures 4.3 and 4.4 show the observed spatial distribution of nidi for the first four seasons after the introduction of myxomatosis for wild and domesticated rabbits respectively. In the former, we can see that in autumn, the epidemic wave enters Belgium at different points along the French border, after which it spreads to the center of Belgium during the subsequent winter and spring. In the summer it seems the disease is present in large parts of Belgium, although not uniformly across all towns. In the latter, we see many nidi at the coast, but not much changes afterwards. It follows from comparing Figures 4.3 and 4.4 that nidi in domesticated rabbits are clustered in the North of West Flanders with only sporadic occurrences in other parts of the country, while

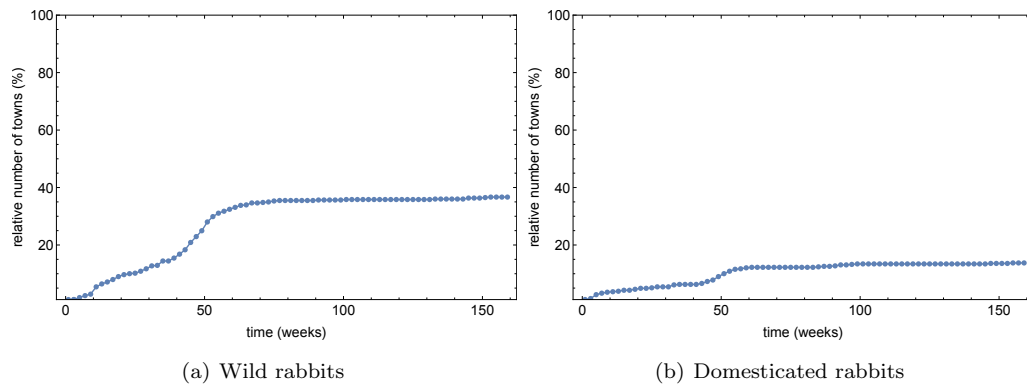


Figure 4.2: Relative number of towns with at least one nidus.

the nidi of wild rabbits are distributed more evenly across the country. These maps show that the dataset of the wild rabbits contains the most information concerning the spatial spread of myxomatosis.

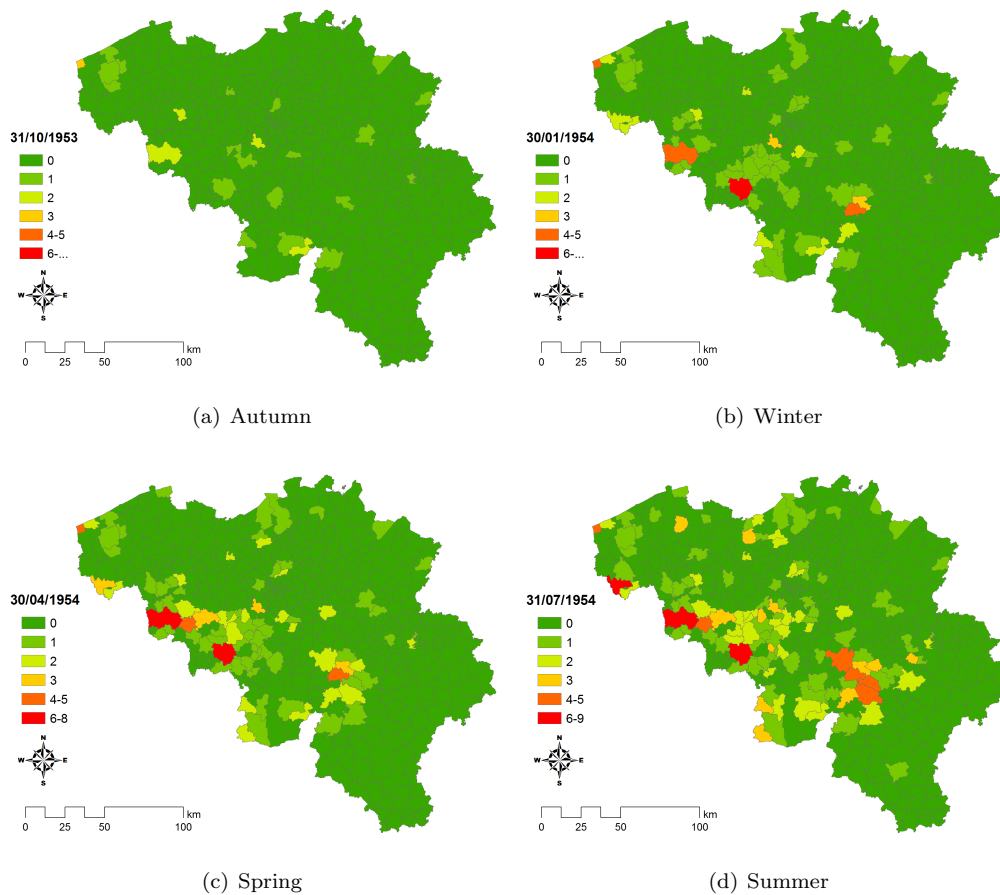


Figure 4.3: Cumulative number of nidi during the first four seasons of the 1953-1954 epidemic: wild rabbits.

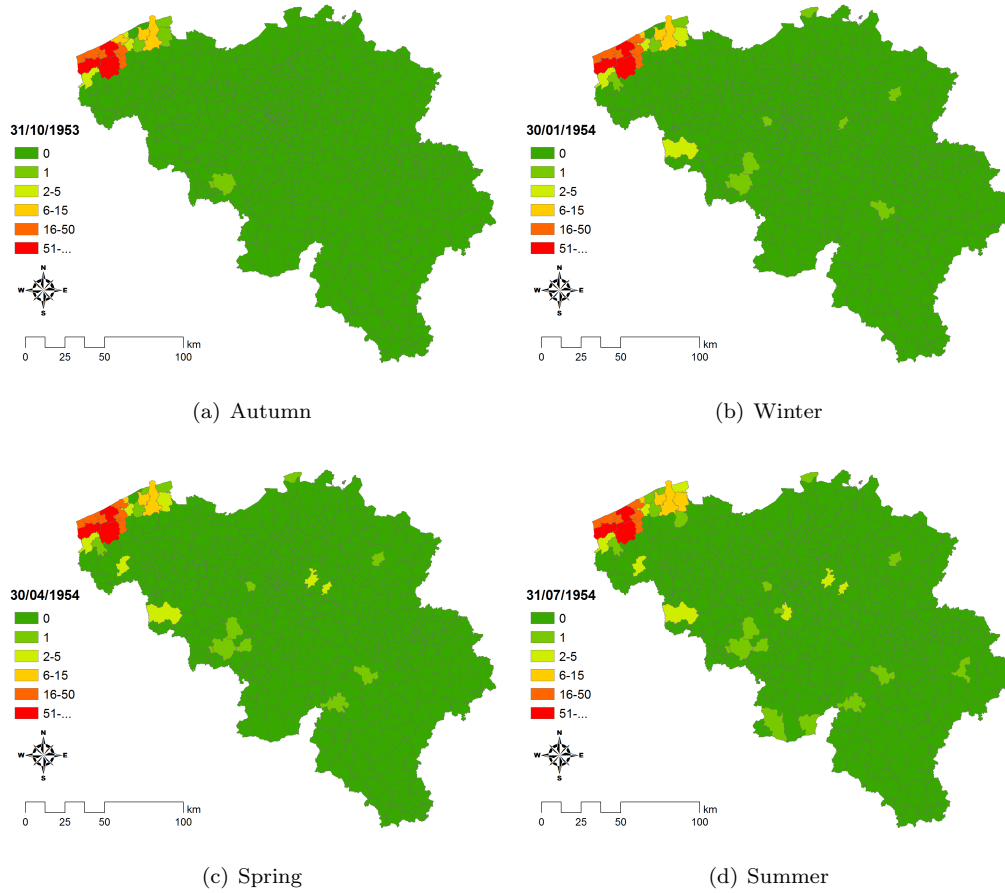


Figure 4.4: Cumulative number of nidi during the first four seasons of the 1953-1954 epidemic: domesticated rabbits.

4.1.3 Epidemic progress

Based on the observations in Section 4.1.2, we can investigate how the disease spread through Belgium. Since the nidi in wild rabbits are the most informative for what concerns the spatial disease dynamics, these will be used for this analysis. Roughly speaking, the disease spread from the French border to the other side of the country. However, the disease did not spread gradually into Belgium along the French border. To distinguish between the infected areas a hull enclosing the infected towns was constructed each time point during the first year after the introduction. Similar procedures have been performed to construct epidemic wave fronts from historic data of a rabies epidemic in France [73, 82] and the progression of the Black Death across Europe [59, 82]. On the basis of observations during the first few weeks, four primary outbreaks were identified; the first in the province of West Flanders, near the coast, the second in the southern part of Hainaut, and the third at the indent of the French border in the province of Namur. Shortly thereafter a fourth outbreak occurred at the northern part of Hainaut, near the city of Tournai. Starting from the second, third and fourth primary outbreaks the disease quickly spread towards the center of Belgium. The outbreak in West-Flanders remained isolated for a few weeks before fusing with the

other three epidemic waves. At the end of November, the disease suddenly appears in wild rabbits in Antwerp (Figure 4.6(c)). A possible cause for this could be the outbreak of myxomatosis in domesticated rabbits in the north of Antwerp (Figure 4.6(a)). Since the travelling wave seems to have skipped a bunch of towns before appearing in Antwerp, we assumed that, in the preceding weeks, the nidi in Antwerp were caused by a fifth outbreak, which supposedly originated from the border with the Netherlands. If the infected towns from the different primary outbreaks are still discernible, a separate disease hull was constructed for each outbreak, otherwise they were merged. The edges of the hulls were constructed such that if a town got infected, at least part of the towns' area is included in the disease hull. Moreover, the edges also have to move at least some distance every two weeks since the epidemic wave should keep moving if there is no external interference. Sometimes large areas got infected at once without any prior infections in the vicinity. We presume that the disease was already present beforehand, such that areas were enclosed in the hull without any reported nidi. After the last outbreak, the epidemic wave slowed down in winter, during which the wave from Antwerp fused with the other outbreaks. New nidi appeared in the summer and following autumn, after which no uninfected areas remained, apart from the southernmost part of Belgium, which remains seemingly uninfected, except for the city of Arlon. From middle of the autumn of 1954 on, not much changes. Therefore, we assumed that the disease had infected most of Belgium by that time. The disease hulls and infected towns are given in Figure 4.7. In Figure 4.7(a) the first two outbreaks and their respective disease hulls are given. In Figure 4.7(b) the third outbreak is presented and in Figure 4.7(c) the fourth and fifth outbreaks appear, while, at the same time, the hulls from the second and third outbreak merge. In Figure 4.7(d) the fourth outbreak merges with the second and third outbreak. The result of merging the first outbreak and the combined hull of the second till the fourth outbreak is shown in Figure 4.7(e). The appearance of the nidi in Antwerp and the resulting hull are shown in Figure 4.7(f). Furthermore, for each disease hull every two weeks, the surface area was calculated (see

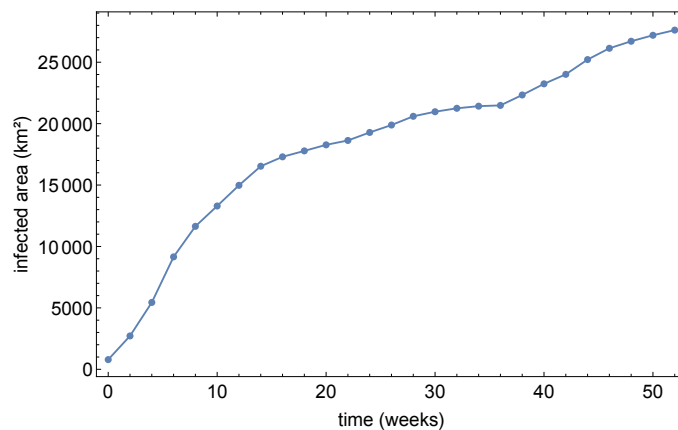


Figure 4.5: Total area enclosed in the epidemic wave.

Figure 4.5). The surface area follows a sigmoid curve that rises steadily, with a slight increase at 40 weeks.

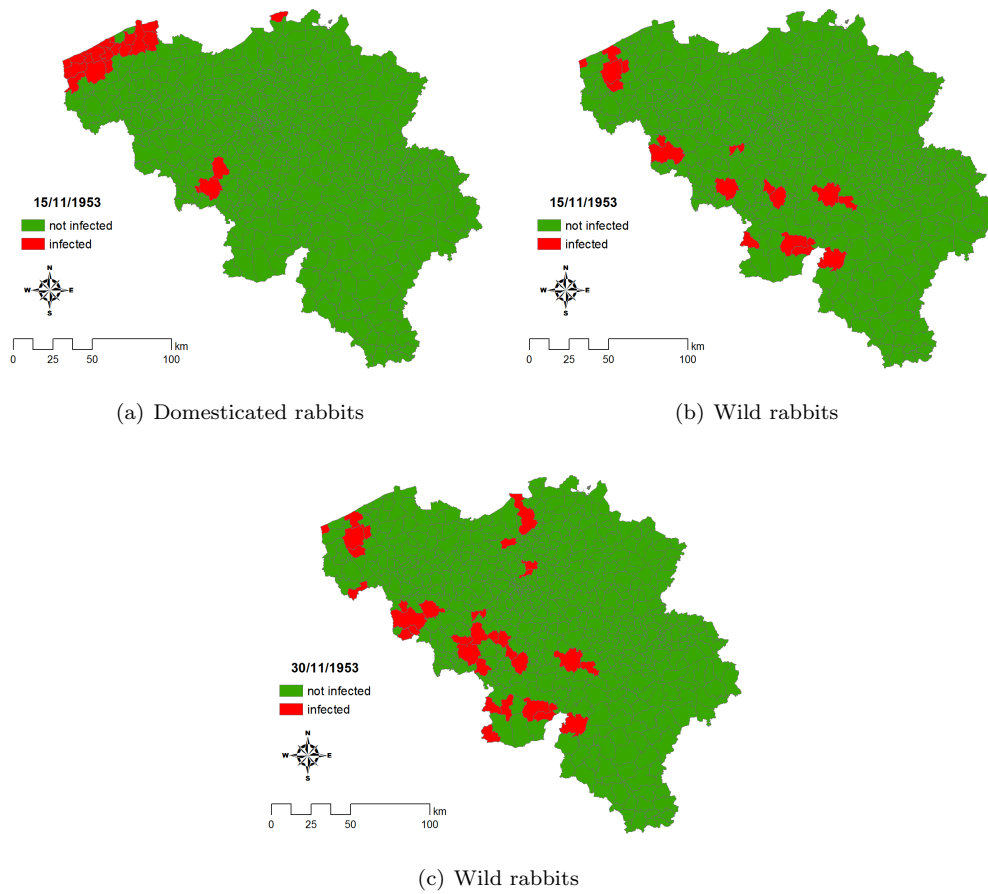


Figure 4.6: A nidus in a town in the North of the province of Antwerp in domesticated rabbits (a) is followed by nidi in wild rabbits in other towns in Antwerp in the following weeks (c) without a nidus in wild rabbits beforehand (b). The maps display the towns where at least one nidus case took place up to that point.

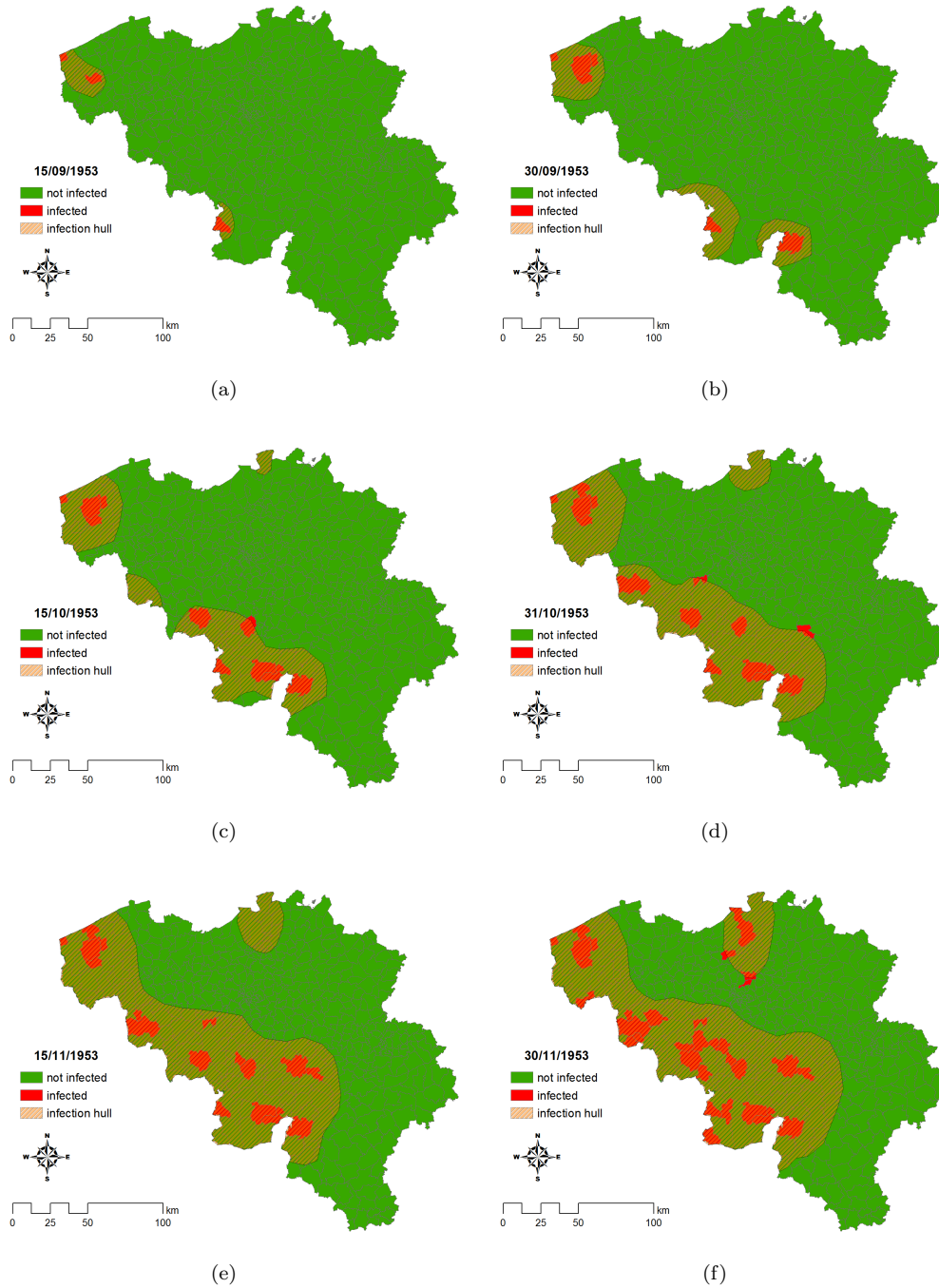


Figure 4.7: Epidemic wavefronts during the first three months.

4.2 Myxomatosis and land cover

4.2.1 Overall analysis

As mentioned in Section 2.2.2, rabbits behave and cohabit differently in different habitats [69, 70, 71, 87]. This also influences the dynamics of myxomatosis [70], as well as RHD [18, 70]. Therefore it makes sense to investigate the land cover of the towns where myxomatosis was reported. For that purpose, a map of the land cover from 2006 was used. It would make more sense to use an older land cover map, but a digital version of such a map was not available, and constructing it from scratch would have required a disproportionate amount of resources and time.

The CORINE map divides Europe in polygons covered by one out of 44 possible different classes. The 44 classes were reduced to six main classes (Figure 4.8) for the sake of this work: urban area, which contains residential areas, industry and cities, arable land, where the main agricultural activities consists of growing crops, pasture for grazing cattle, forested areas, water-rich areas, like fens, marches and rivers, and the undefined class which contains miscellaneous areas, like sea areas, where rabbits do not live. This last class is not considered for further analysis. The histogram of the land cover for Belgium is given in Figure 4.9. It is clear that arable land has the

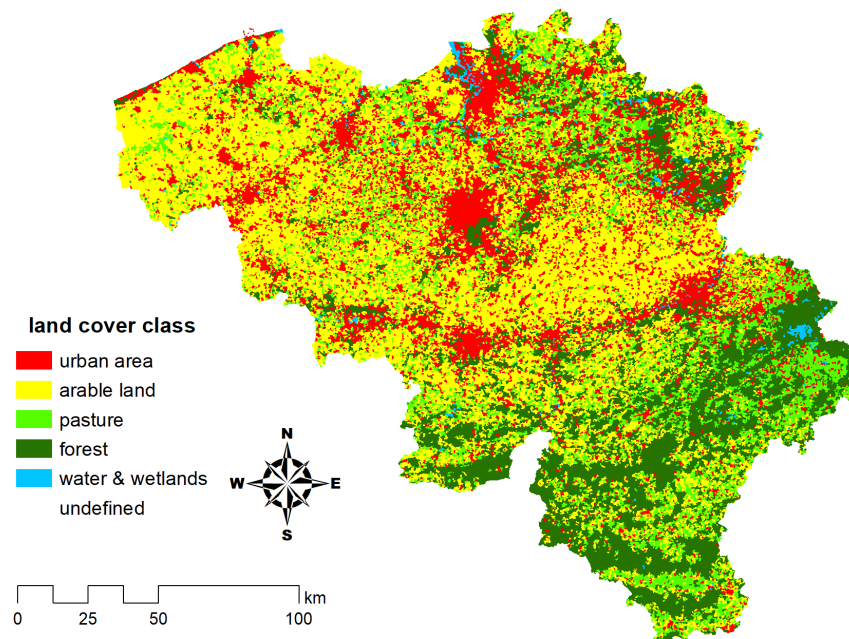


Figure 4.8: The CORINE map with the 6 land cover classes.

largest surface area, and water the lowest. The other three classes do not differ much in surface area. The relative land cover of the towns where myxomatosis was reported among wild rabbits, and the infection hulls are presented in Figure 4.10.

For the infected towns, the relative surface areas does not change by much over time after about 50 weeks, which is caused by the reduced number of new cases and newly infected towns (See section 4.1.2). It can be observed that the relative area occupied by forest in the infected towns

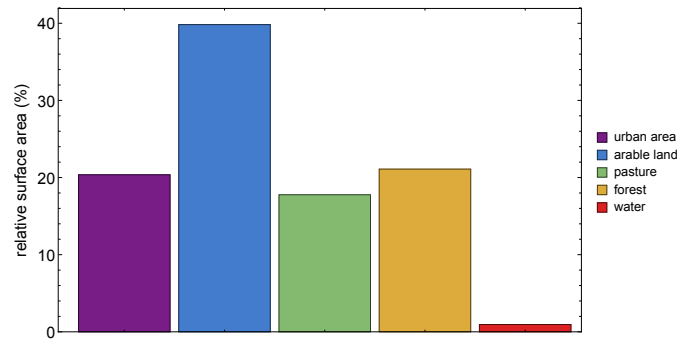
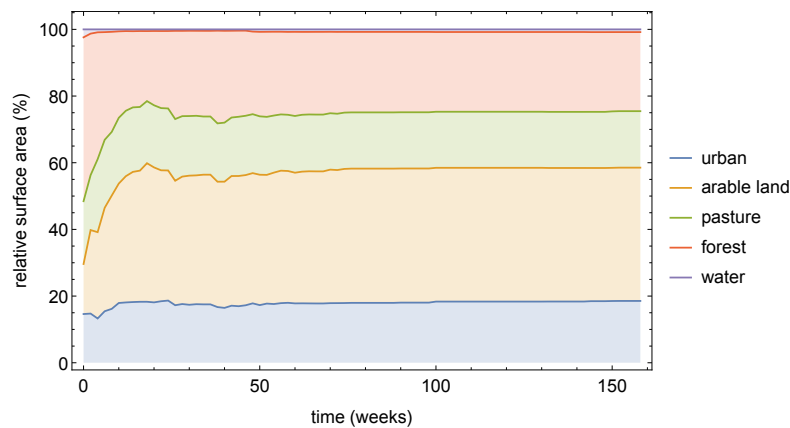
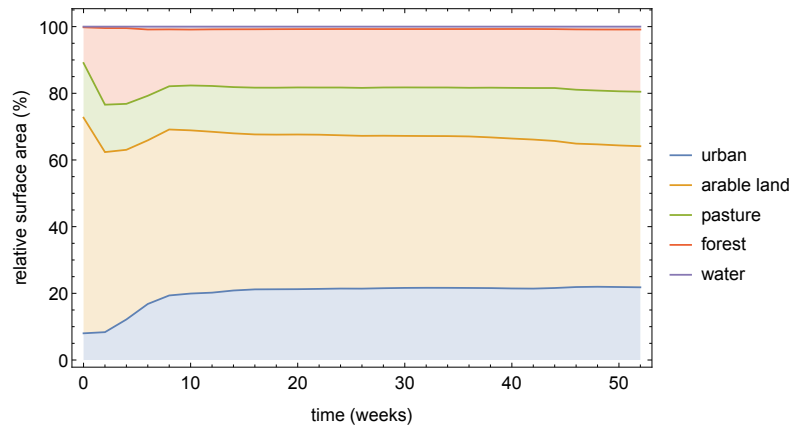


Figure 4.9: Histogram of the land cover of Belgium according to the CORINE-map.



(a) Infected towns



(b) Infection hulls

Figure 4.10: Relative surface areas for the infected towns and the infection hulls.

is very high at the epidemic onset and steadily decreases afterwards, while the opposite is true for the arable land. The relative areas of other land cover types do not change much over time. Interestingly, a different pattern can be discerned for the infected hulls. Here, the relative area of the arable land is very important at the beginning and decreases steadily afterwards in favour of forest and urban area. This means that nidi were reported first in towns with relatively large

forest and urban areas, while the disease probably remained unnoticed or were not reported in the towns with more arable areas.

4.2.2 Investigating the link between land cover and myxomatosis spread

Since the model from Section 5.1 can incorporate spatial information, it is interesting to compare the differences in relative land cover across the infected areas and Belgium as a whole, as well as their evolution over time. An important aspect of the infection hulls is that they are composed of different outbreaks. In this section we will analyse those hulls as a whole and for different outbreaks separately. Figure 4.11 shows the differences in land cover between Belgium, the infected towns, and the infection hulls as a whole respectively, for the first four seasons of the epidemic.

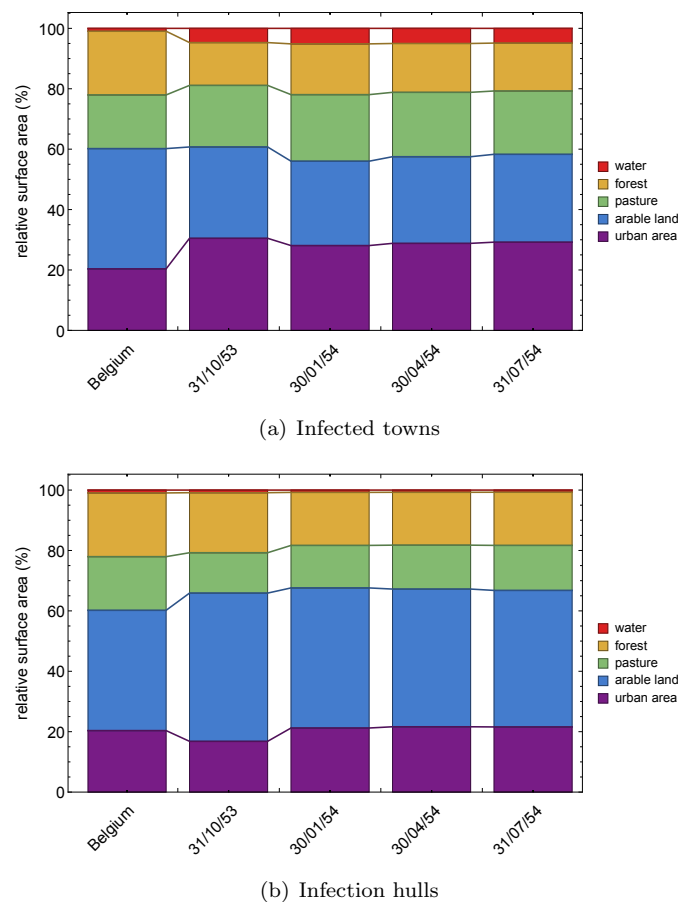


Figure 4.11: Evolution of the relative land cover areas of the infected towns and the infection hulls for the first four seasons

For what concerns the infected towns, it is clear that the relative areas differs slightly from those found for Belgium as a whole. In autumn, it seems that the infected towns are relatively rich in forests, while relatively poor in agricultural areas. The opposite can be observed during the winter. In the subsequent seasons, the relative land cover aligns with the relative land cover of Belgium, which is to be expected as increasingly more towns get infected. For what concerns the infection hulls, the trends are less pronounced. Pasture, forest and urban area are relatively unimportant in

comparison to arable land at the beginning. The importance of urban area and pasture increases a bit afterwards in comparison to the arable land, which becomes slightly less important. Forest area keeps decreasing slightly in importance, but stabilizes afterwards. In the summer, it seems that the urban area and arable land are the two most important land covers. Regardless of these trends it should be noted that the differences in relative land cover areas compared to those for Belgium as a whole remain quite small.

The relative land cover of the separate hulls is given in Figure 4.12, where outbreak 2, 3 and 4 were grouped together since their corresponding epidemic waves fused relatively quickly.

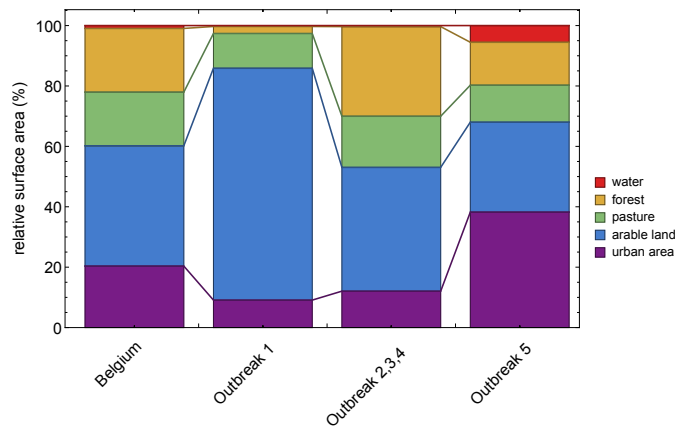


Figure 4.12: Relative land cover area in the outbreaks and Belgium

It is clear that the relative land cover area differs between the outbreaks. The majority of the land in outbreak 1 is arable land with almost no forests and few urban areas. Outbreaks 2,3 and 4 have a lot of forested areas in comparison to the other outbreaks, while outbreak 5 occurs in a region that is a lot more urbanised, with fewer arable land and also relatively water-rich.

4.2.3 Hypothesis tests

Since there are visible changes and shifts in land cover as discussed in Section 4.2.2, it could be interesting to test whether there is a significant difference in the relative land cover areas of the infected regions in comparison to those of Belgium. The relative land cover areas of Belgium are computed on the basis of the relative land cover areas of all Belgian towns. The histograms of the different relative land covers of all the Belgian towns are given in Figure 4.13.

As concluded on the basis of a Cramér-Von Mises test for normality [29, 30] (see Table 4.1), that the histograms in Figure 4.13 are not normally distributed,

Table 4.1: Results from the Cramér-Von Mises test for normality.

Land use	urban area	arable land	pasture	forest	water
test statistic & p-value	3.289 0.	0.331 0.	0.734 0.	7.819 0.	23.736 0.

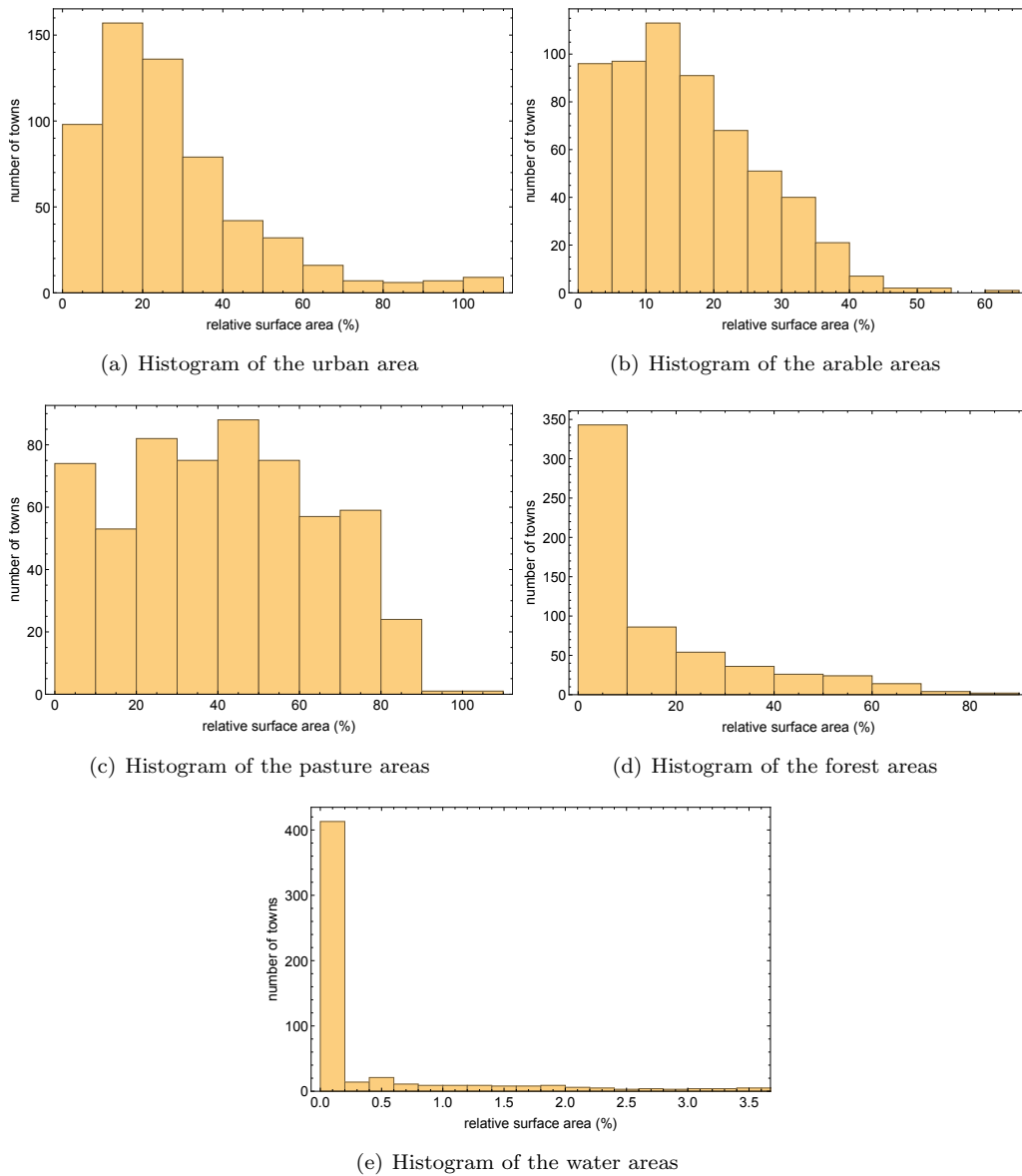


Figure 4.13: Marginal histograms of the different relative land covers.

we compared the medians of the land cover distributions of the infected towns and Belgium using the non-parametric Mann-Whitney-Wilcoxon test [75]. Since the relative land cover distribution for the infected towns changes through time, this test was performed separately for every two weeks (see Figure 4.14).

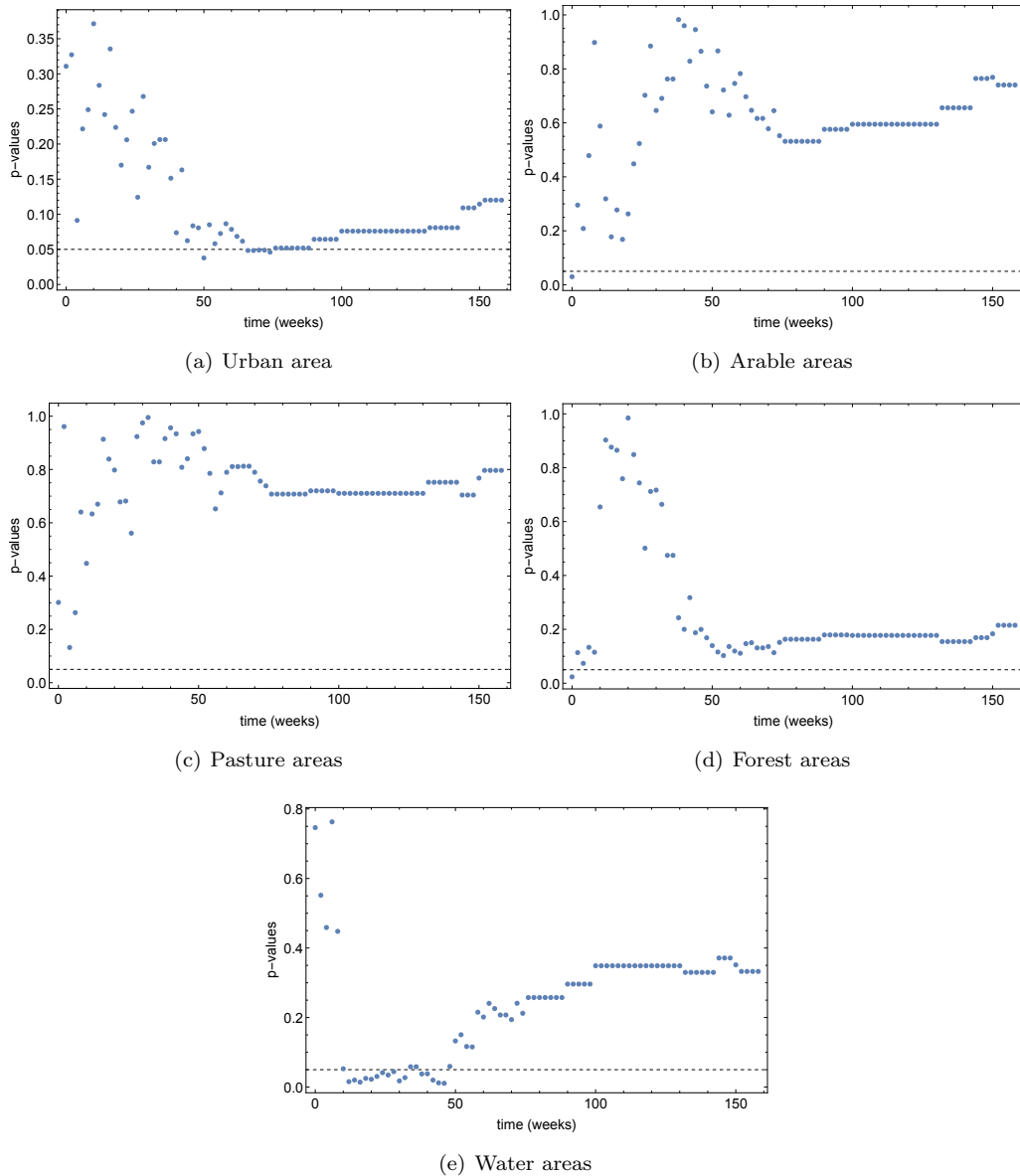


Figure 4.14: p-values resulting from the Mann-Whitney-Wilcoxon test for the different relative land covers and their evolution over time.

It is clear that only for a few time points for the urban areas and the water-rich areas, the null hypothesis can be rejected at a significance level of 0.05. So, this is not enough proof that there is a significant effect of the land cover on the spread of myxomatosis. However, since those p -values still are quite low, it seems that further research may be useful. Moreover, we know from literature (see Section 2.2.2) that rabbits cohabit and behave differently under different land cover types,

which influences the disease dynamics of myxomatosis [69, 70]. In addition to that, the land cover map is not from the same time period as the introduction of the disease, which could have had some influence on the results.

CHAPTER 5

A Spatially Explicit Model for the 1953-1954 Outbreak of Myxomatosis in Belgium

5.1 The spatially explicit myxomatosis model

In Chapter 4, the first outbreak of myxomatosis in Belgium was discussed and analysed. The goal of this master thesis is to reconstruct the progression of this outbreak with an epidemic model, to understand the importance of different factors for the epidemic process and their variation in a temporal as well as a spatial way. This can also help us to analyse and possibly assist in forecasting the progression of new epidemics. In the subsequent sections, the used spatio-temporal epidemic model will be discussed.

5.1.1 The non-spatial model

The spatially explicit model of myxomatosis is based on the non-spatial model for contagious disease transmission of Anderson and May (see System (3.4)) [78], introduced in Section 3.2.1. This system of differential equations assumes that myxomatosis is transmitted by contact, since the infection only depends on contact between susceptibles and individuals, which means that no vector population is considered. Yet, as discussed in Section 2.4, the disease can also be transmitted by vectors. In Europe, its most important vector is the rabbit flea (*Spilopsyllus cuniculi*) (see Section 2.5). Since rabbit fleas are transmitted by contact between rabbits and are closely tied to rabbit populations, we may assume that myxomatosis spreads via contact for the sake of simplicity.

System (5.1) extends System (3.1)), taking the reproductive and natural death rate of rabbits into account:

$$\begin{cases} \frac{dS}{dt} = r(S + I + R) - \beta SI - mS, \\ \frac{dI}{dt} = \beta SI - (\alpha + m + \nu)I, \\ \frac{dR}{dt} = \nu I - mR, \\ \frac{dD}{dt} = \alpha I + m(S + I + R), \end{cases} \quad (5.1)$$

with S , I , R and D the number of susceptible, infected, recovered and deceased individuals, respectively, $r [T^{-1}]$ the natural per capita birthrate, $m [T^{-1}]$ the natural per capita death rate, $\alpha [T^{-1}]$ the additional per capita death rate of infected individuals caused by the disease, $\beta [T^{-1}]$ the disease transmission rate and $\nu [T^{-1}]$ the per capita recovery rate [4, 8, 32, 78]. Comparing Systems (3.1) and (5.1), it follows that $\gamma = \nu + \alpha$, since $\gamma [T^{-1}]$ in System (3.1) denotes the removal rate of infected individuals from the population either through death (α), or becoming resistant (ν). It is assumed that all newly born individuals are susceptible to myxomatosis, which is indeed the case in reality (see Section 2.4). Based on a study by Dwyer et al. [32], some parameters of System (5.1) were modified for the sake of comprehension:

$$\nu = (1 - C_M)\epsilon, \quad (5.2)$$

$$\alpha = C_M\epsilon, \quad (5.3)$$

with $\epsilon [T^{-1}]$ the reciprocal of the mean disease duration and $C_M [-]$ the case mortality, which denotes the proportion of individuals that die due to the disease. It follows from Equations (5.2) and (5.3) that $\nu + \alpha = \epsilon$, so $\epsilon = \gamma$. Using Equations (5.2) and (5.3) in System (5.1) gives

$$\begin{cases} \frac{dS}{dt} = r(S + I + R) - \beta SI - mS, \\ \frac{dI}{dt} = \beta SI - (\epsilon C_M + m + \epsilon(1 - C_M))I, \\ \frac{dR}{dt} = \epsilon(1 - C_M)I - mR, \\ \frac{dD}{dt} = \epsilon C_M I + m(S + I + R). \end{cases} \quad (5.4)$$

5.1.2 A spatially explicit model for myxomatosis

There are different spatially explicit modelling paradigms, like individual-based modelling, cellular automata and partial differential equations (see Section 3.3). Here, we chose the coupled-map lattice (CML) which are also referred to as continuous cellular automata [53]. They feature continuous variables, which are modelled on a discrete, tessellated space, at discrete time steps. We preferred not to use an individual-based model, since the number of rabbits is large, which would imply substantial computing time. We also did not use a partial differential equations since those assume that diseased animals move from areas with higher concentrations of diseased animals, to areas with a lower concentration [31]. Since infected rabbits tend to become highly immobile [25], we cannot assume they behave that way.

The first step in transforming System (5.4) into a CML proceeds by discretizing it into a system of discrete difference equations. In the same way System (3.1) can be transformed into System (3.14), System (5.4) can be transformed into

$$\begin{cases} S(t+1) = S(t) + r \Delta t (S(t) + R(t)) - \beta \Delta t S(t) I(t) - m \Delta t S(t), \\ I(t+1) = I(t) + \beta \Delta t S(t) I(t) - (\epsilon C_M + m + \epsilon(1 - C_M)) \Delta t I(t), \\ R(t+1) = R(t) + \epsilon(1 - C_M) \Delta t I(t) - m \Delta t R(t), \\ D(t+1) = D(t) + m \Delta t (S(t) + I(t) + R(t)) + \epsilon C_M \Delta t I(t). \end{cases} \quad (5.5)$$

The meaning of the parameters is the same as in System (5.4), and $\Delta t[-]$ is the length of one time step. This system, however, still does not have a spatial component. Therefore, the study area was discretized, by subdividing it in 250 000 irregular Voronoi polygons c_i , $i = 1, \dots, 250000$ [7]. So, we have one system, like System (5.5) for every polygon, which are mutually coupled. Therefore, the parameter β is split in an internal component $\underline{\beta}$, which governs the disease transmission in a polygon, representing disease spread at short ranges and the external component $\bar{\beta}$, which governs the disease transmission between the susceptible population in a polygon and the infected populations in the polygons of its neighbourhood, representing the disease spread at longer ranges. Essentially, we get

$$\begin{cases} S(c_i, t+1) = S(c_i, t) + r \Delta t (S(c_i, t) + R(c_i, t)) - \underline{\beta} \Delta t S(c_i, t) I(c_i, t) - \\ \Delta t S(c_i, t) \sum_{c_j \in \mathcal{N}_i} \bar{\beta} O_{ij} I(c_j, t) - m \Delta t S(c_i, t) \\ I(c_i, t+1) = I(c_i, t) + \underline{\beta} \Delta t S(c_i, t) I(c_i, t) + \Delta t S(c_i, t) \sum_{c_j \in \mathcal{N}_i} \bar{\beta} O_{ij} I(c_j, t) \\ - (\epsilon C_M + m + \epsilon(1 - C_M)) \Delta t I(c_i, t) \\ R(c_i, t+1) = R(c_i, t) + \epsilon(1 - C_M) \Delta t I(c_i, t) - m \Delta t R(c_i, t) \\ D(c_i, t+1) = D(c_i, t) + m \Delta t (S(c_i, t) + I(c_i, t) + R(c_i, t)) + \epsilon C_M \Delta t I(c_i, t), \end{cases} \quad (5.6)$$

where c_j are the polygons in c_i 's neighbourhood. The most notable change from System (5.5), however, is the addition of the term

$$\sum_{c_j \in \mathcal{N}_i} \bar{\beta} O_{ij} I(c_j, t). \quad (5.7)$$

To explain what this term does, a polygon c_0 and its neighbourhood \mathcal{N}_0 containing cells c_0, c_1, \dots, c_5 is given in Figure 5.1. For this polygon, the aforementioned term becomes:

$$\sum_{j=1}^5 \bar{\beta} O_{0j} I(c_j, t). \quad (5.8)$$

The factor $O_{0j}[-]$ is the length of the edge connecting c_0 and c_j divided by the circumference of c_0 . This means that neighbouring polygons sharing relatively long sides contribute more to the disease dynamics of c_i . Due to a CML being an assembly of individual systems, instead of keeping the parameters the same for each polygon, we can change the parameter values for each polygon separately.

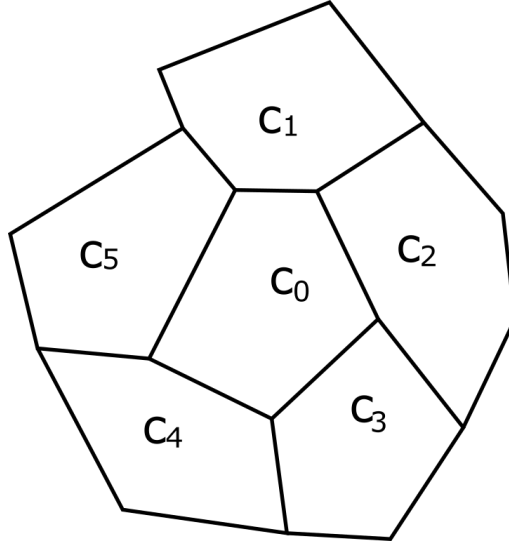


Figure 5.1: A cell of the grid and its five neighbouring cells.

This enables us to incorporate spatial information in this model structure, in this case the land cover classes of the CORINE map. In this thesis we will do this for the transmission rates and as such the system incorporated with the land cover information is

$$\left\{ \begin{array}{l}
 S(c_i, t+1) = S(c_i, t) + r \Delta t (S(c_i, t) + R(c_i, t)) - \underline{\beta}_i \Delta t S(c_i, t) I(c_i, t) - \\
 \quad \Delta t S(c_i, t) \sum_{c_j \in \mathcal{N}_i} \bar{\beta}_i O_{ij} I(c_j, t) - m \Delta t S(c_i, t) \\
 I(c_i, t+1) = I(c_i, t) + \underline{\beta}_i \Delta t S(c_i, t) I(c_i, t) + \Delta t S(c_i, t) \sum_{c_j \in \mathcal{N}_i} \bar{\beta}_i O_{ij} I(c_j, t) - \\
 \quad (\epsilon C_M + m + \epsilon(1 - C_M)) \Delta t I(c_i, t) \\
 R(c_i, t+1) = R(c_i, t) + \epsilon(1 - C_M) \Delta t I(c_i, t) - m \Delta t R(c_i, t) \\
 D(c_i, t+1) = D(c_i, t) + m \Delta t (S(c_i, t) + I(c_i, t) + R(c_i, t)) + \epsilon C_M \Delta t I(c_i, t).
 \end{array} \right. \quad (5.9)$$

We will use the five land cover classes of the CORINE as discussed in Section 4.2.1, which results in five possible $\underline{\beta}_i$ s and $\bar{\beta}_i$ s for this system.

5.2 Preliminary sensitivity analysis

In this section we will investigate the overall role of the parameters in System (5.6). For this purpose, we will visually compare the difference between three simulations; the first being a benchmark simulation with parameter values derived from literature (see Chapter 2 and Table 5.1), the second with one of the parameters lowered and the third with the same parameter raised relatively to the benchmark. We presume that the β s are spatially homogeneous for the sake of simplicity. All simulations were run in Mathematica (version 10.0.0, Wolfram Research Inc., Champaign, United States) using the high-performance infrastructure of Ghent University for 7560 time steps, corresponding to 378 days as $\Delta t = 0.05$ d. The initial population of rabbits was assumed to be the same for all cells with a density of five rabbits per hectare [8, 71].

We assumed that, at the start of the simulation, the cells bordering the French province of French Flanders are infected with myxomatosis, since the disease entered Belgium at that location [8, 80].

Table 5.1: Benchmark parameter values

parameter	value
$\underline{\beta}$	0.01
$\overline{\beta}$	0.01
C_M	0.9
ϵ	1/12
r	$1/(1.5 \times 365)$
m	$1/(1.5 \times 365)$

For the sake of comprehensiveness, the output variables are aggregated in space, by focusing on the sum of all susceptible, diseased, resistant and dead rabbits in Belgium over time. Figure 5.2 shows the simulated rabbits susceptible to, infected with, resistant to, dead regardless of, and dead due to myxomatosis. These numbers appear to reach an equilibrium after about 150 days. It is clear that the numbers of susceptible rabbits declines rapidly, giving rise to large numbers of dead individuals, of which the largest fraction is caused by the disease. The number of infected rabbits never reach that magnitude, but still peak during the decline of the susceptibles. The number of resistant rabbits remain relatively low. Given the high mortality rates and low survival times, this result is reasonable. Furthermore, Figure 5.3 shows that the model is capable of generating

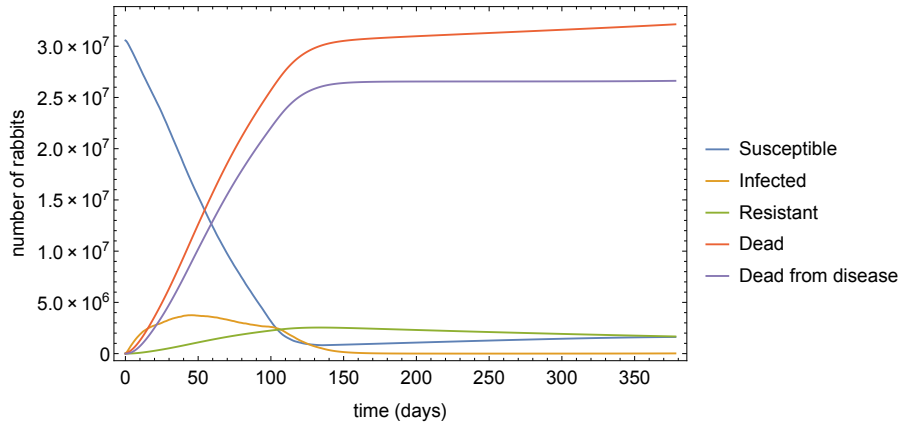


Figure 5.2: Simulated number of susceptible, infected, resistant, and dead rabbits with parameter values from Table 5.1.

an epidemic wavefront, which is an important feature in spatial epidemic models (see Section 3).

5.2.1 Disease mortality

The disease mortality (C_M) is the proportion of individuals that do not survive infection. Its effect on the simulated dynamics is shown in Figure 5.4. The largest effect of lowering C_M (Figure 5.4(b)) is the appearance of high numbers of resistant individuals. Furthermore, the number of casualties from the disease is significantly lowered in comparison to the total number of deaths.

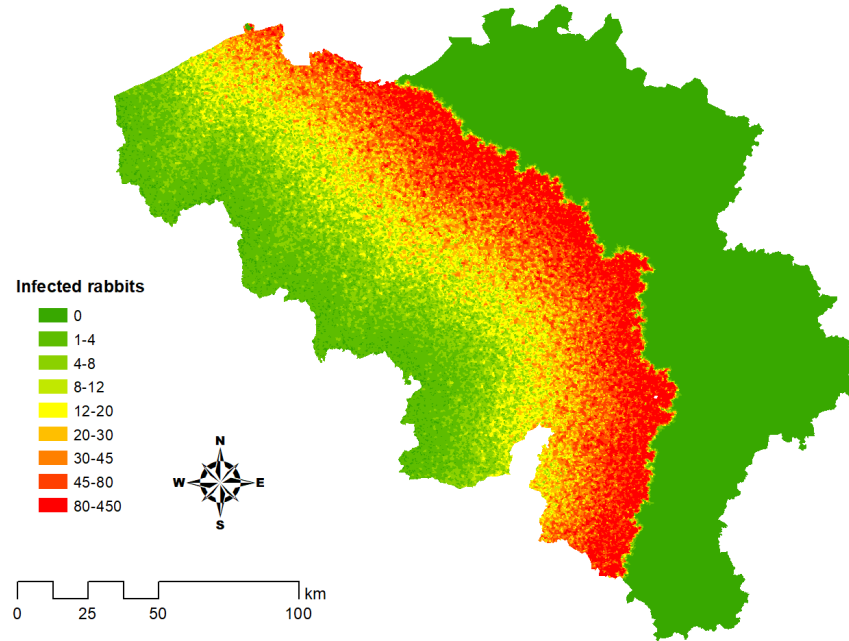


Figure 5.3: Simulation of the infected individuals on $t = 56$ d.

The number of susceptible rabbits in the long term is also a bit higher in comparison to the benchmark. Raising C_M gives the opposite effect. Changing this parameter appears to have no effect on the number of infected individuals.

5.2.2 Disease duration

The parameter ϵ is the reciprocal of the amount of time an individual is infected before either dying or becoming resistant. Therefore, raising ϵ equals a shorter disease duration. The effects of these changes on the model output are shown in Figure 5.5. The main effect of changing ϵ appears to be an increase of infected population if the parameter is lower than in the benchmark, whereas the reverse happens if ϵ rises.

5.2.3 Reproductive rate

The reproductive rate r is the reciprocal of the amount of time it takes to add an extra individual to the population. If this takes longer, the parameter is lowered. The effects of these changes are shown in Figure 5.6 and appear to be quite limited. In Figure 5.6(a), the higher reproductive rate results in higher numbers of casualties in the long term. Also, the number of susceptibles raises slightly at the end of the simulation. Lowering the reproductive rate (Figure 5.6(b)) results in no clear visible changes.

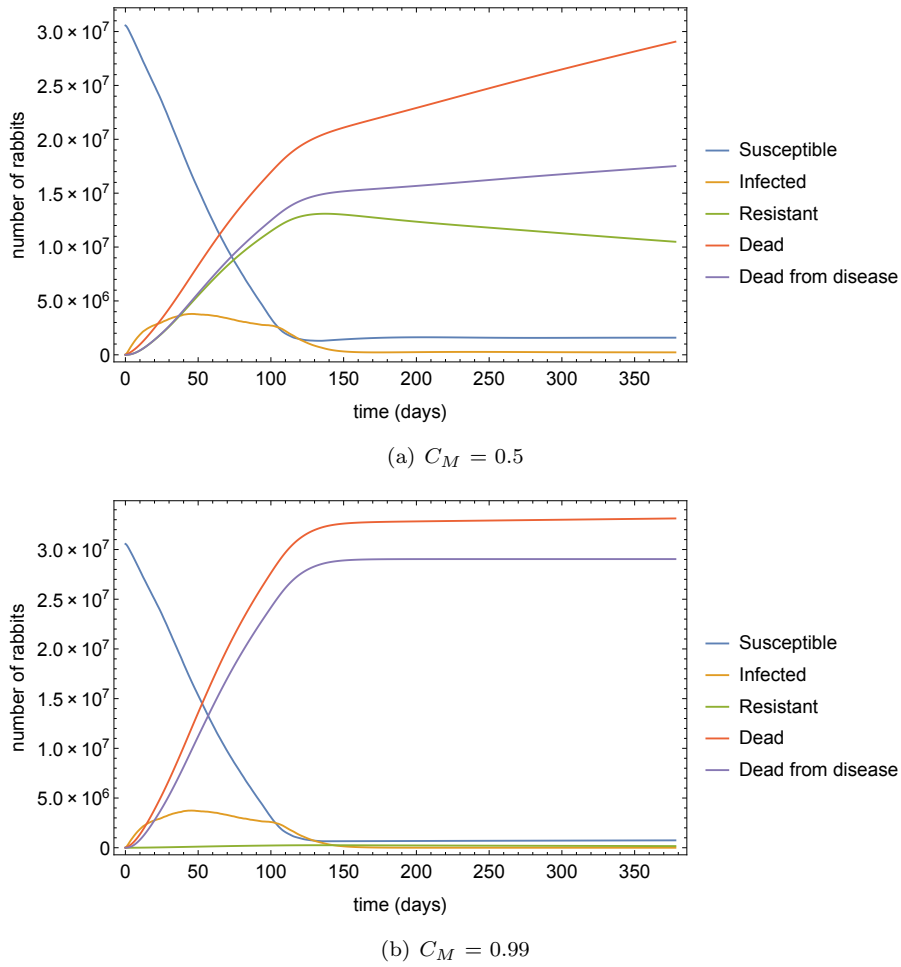


Figure 5.4: Effect of changing C_M on the numbers of susceptible, infected, resistant, and dead rabbits.

5.2.4 Natural mortality

The natural mortality m is the reciprocal of the natural life span of an individual without contracting the disease. If this parameter raises, the individuals have shorter life spans on average. The effects of changing it are shown in Figure 5.7.

The effects of m are quite small. The clearest effect is that raising m lowers the fraction of dead individuals caused by the infection and vice versa.

5.2.5 Short range transmission rate

The parameter β_i is the rate at which susceptible individuals in c_i become infected by the infected population of c_i . The effects of changing this parameter are shown in Figure 5.8.

Raising this parameter (Figure 5.8(b)) causes all the output variables to change faster. Since this parameter seems important, maps of the epidemic wave at $t = 56$ d are shown in Figure 5.9 for the infected rabbits. Raising β_i (Figure 5.9(b)) makes the epidemic wave propagate faster and increases its width. The opposite is true if the parameter is lowered (Figure 5.8(a), 5.9(a)).

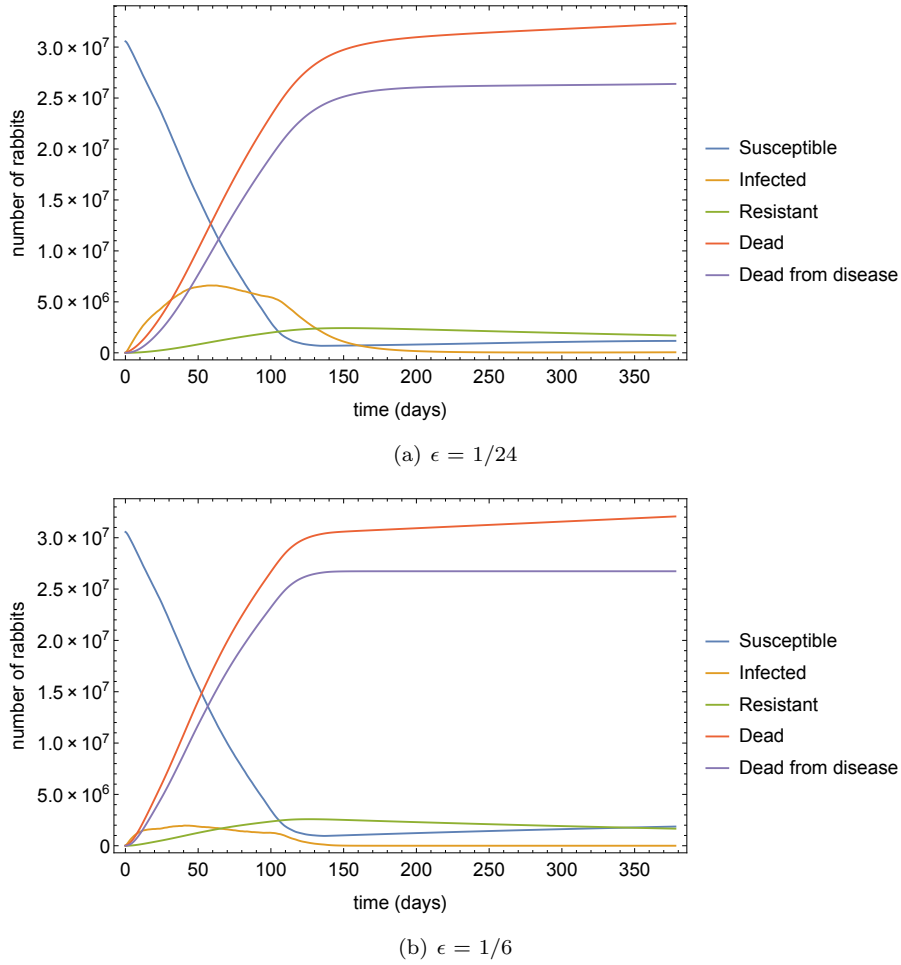


Figure 5.5: Effect of changing ϵ on the numbers of susceptible, infected, resistant, and dead rabbits.

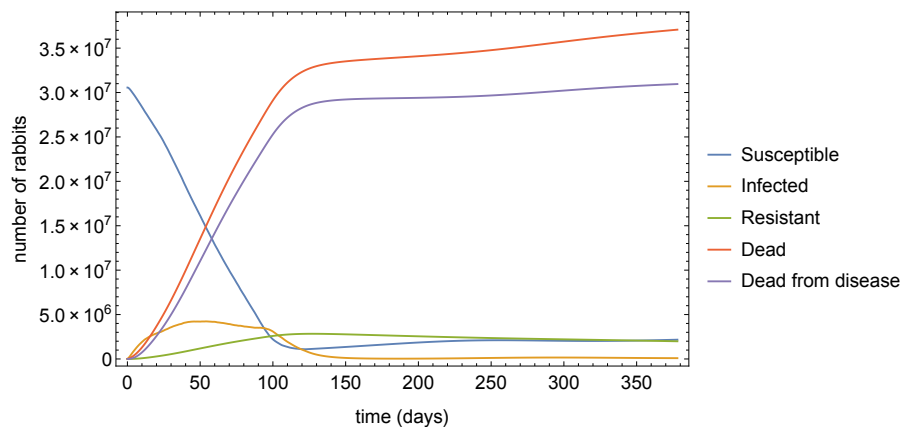
This means that raising or lowering the parameter speeds up or slows down the epidemic process, respectively.

5.2.6 Long range transmission rate

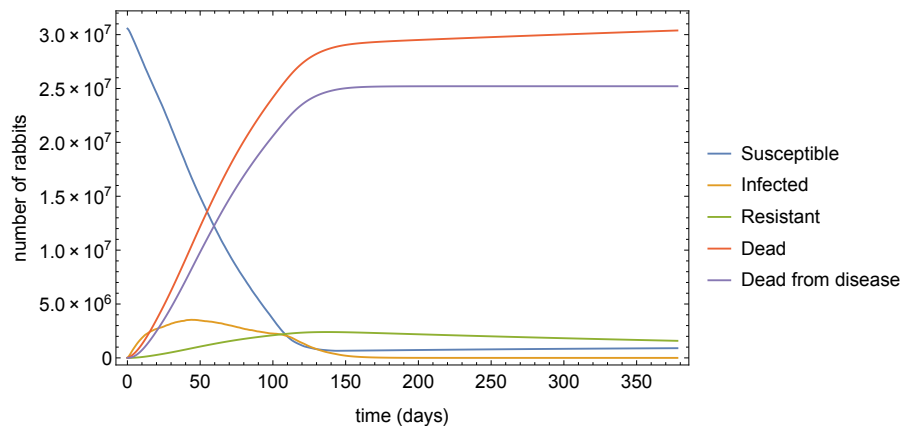
The parameter $\bar{\beta}_i$ is the rate at which susceptible individuals in a polygon c_i become infected by the infected populations of the polygons c_j in its neighbourhood. The effects of changing it are shown in Figure 5.10.

The effects of this parameter are similar to the ones of $\underline{\beta}_i$ (see Section 5.2.5). However, by comparing Figures 5.8(a) and 5.10(a), and 5.8(b) and 5.10(b), it seems that changing $\bar{\beta}_i$ has a bigger impact than changing $\underline{\beta}_i$. The same conclusion can be drawn by comparing Figures 5.9 and 5.11.

It follows that it would be interesting to be able to compare the effect and importance of the different parameters of System 5.6 in a more quantitative manner. For this purpose, it is necessary to perform a sensitivity analysis, which we will get to in Chapter 6.



(a) $r = 1/(0.75 \times 365)$



(b) $r = 1/(3 \times 365)$

Figure 5.6: Effect of changing r on the numbers of susceptible, infected, resistant, and dead rabbits.

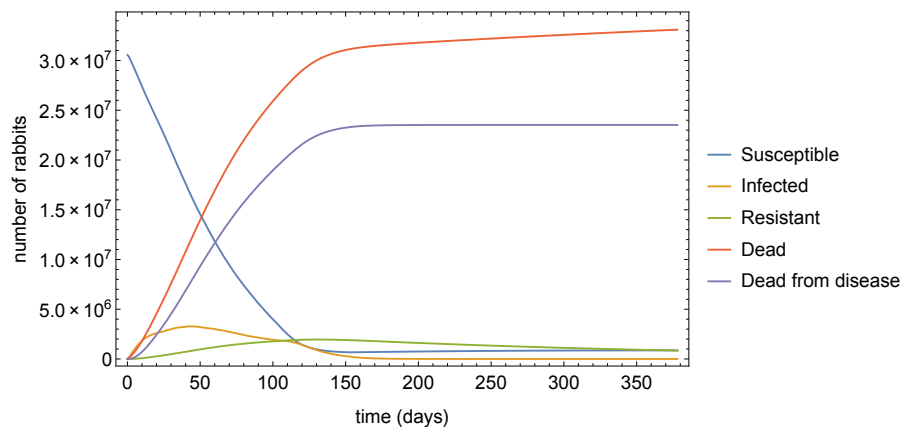
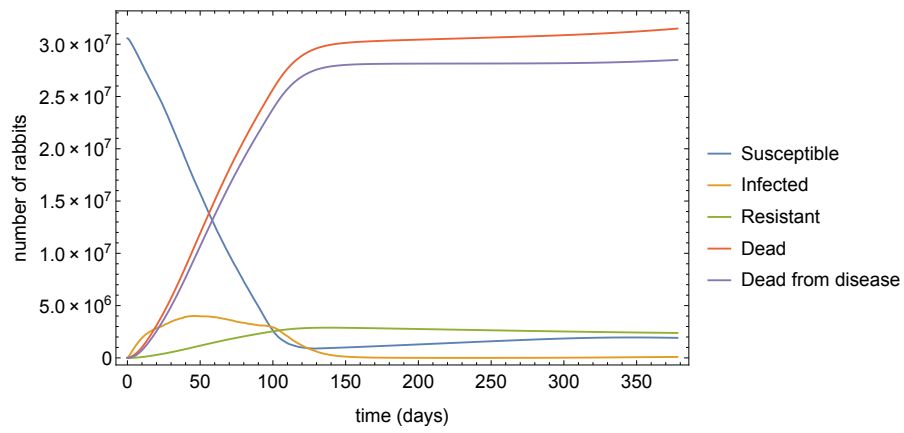
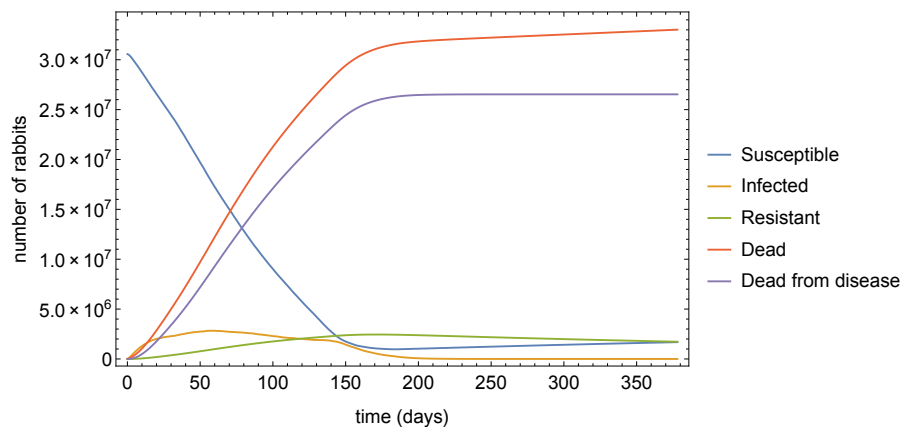
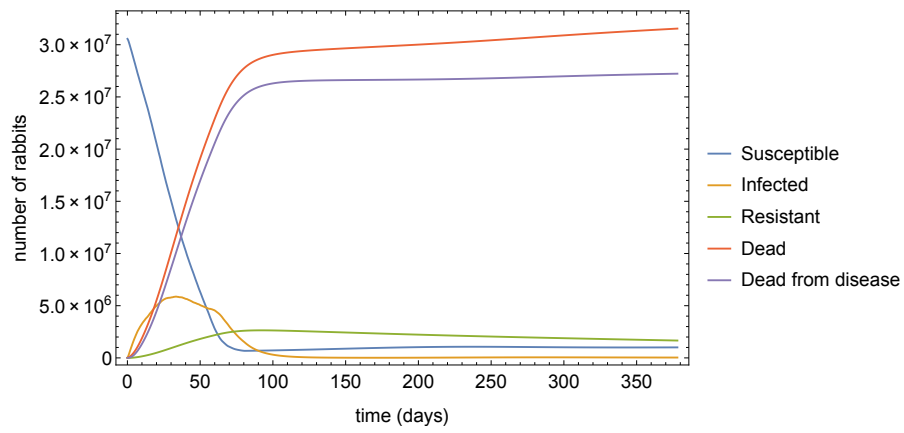
(a) $m = 1/(0.75 \times 365)$ (b) $m = 1/(3 \times 365)$

Figure 5.7: Effect of changing m on the numbers of susceptible, infected, resistant, and dead rabbits.

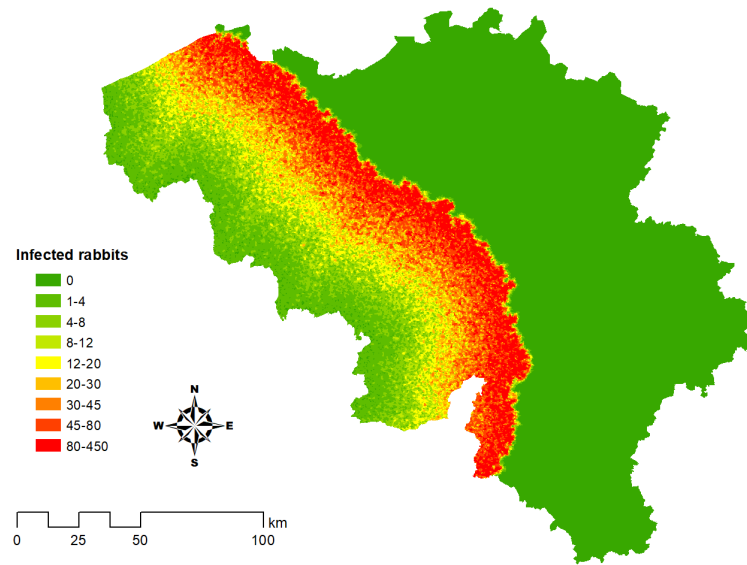
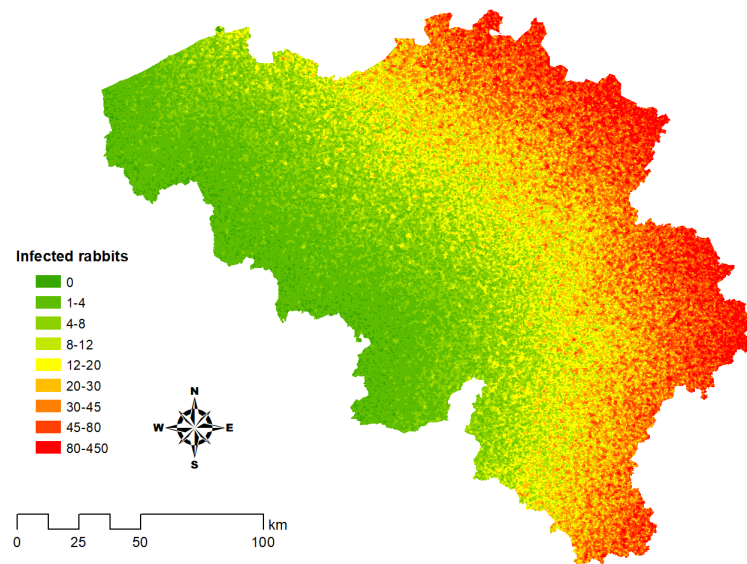


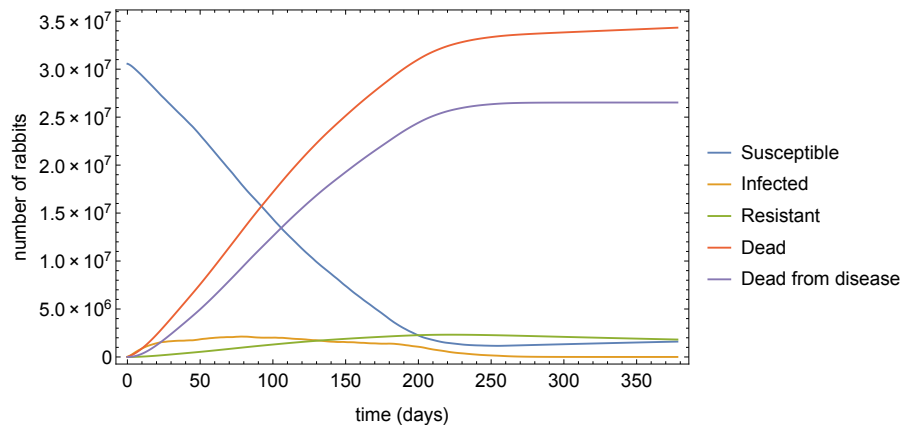
(a) $\beta = 0.0025$



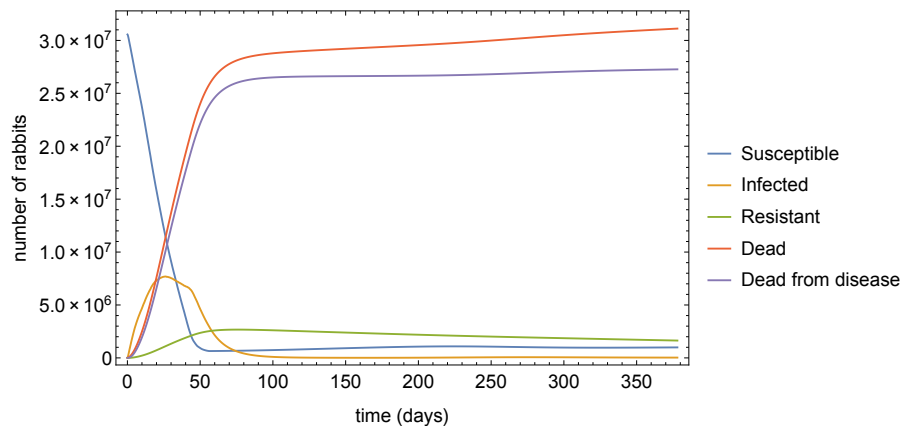
(b) $\beta = 0.05$

Figure 5.8: Effect of changing β on the numbers of susceptible, infected, resistant, and dead rabbits.

(a) $\underline{\beta} = 0.0025$ (b) $\underline{\beta} = 0.05$ **Figure 5.9:** The effect of changing $\underline{\beta}$ on the number of infected rabbits at $t = 56$ d.

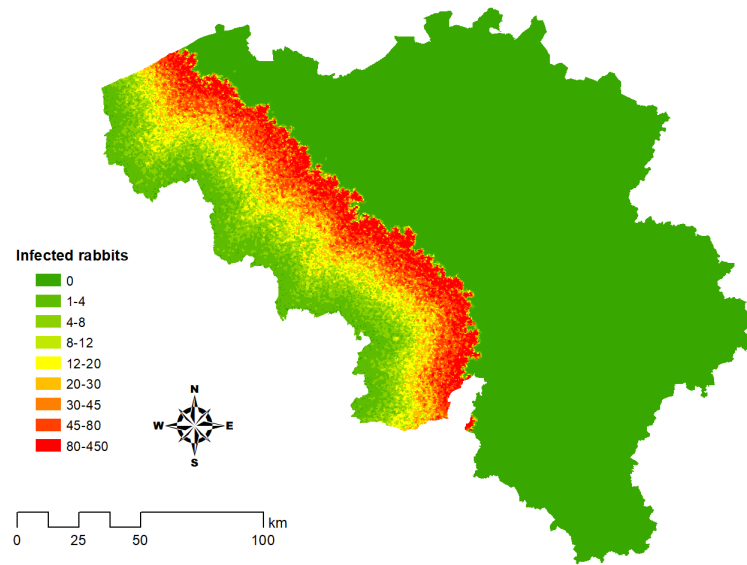
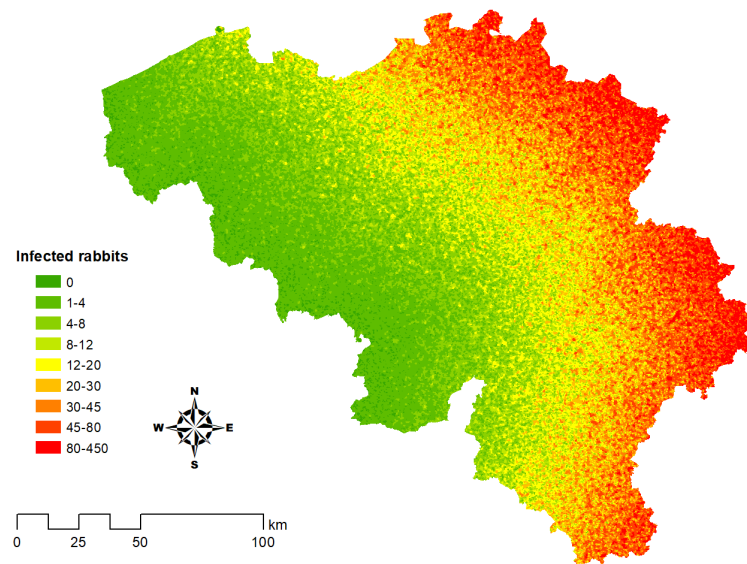


(a) $\bar{\beta} = 0.0025$



(b) $\bar{\beta} = 0.05$

Figure 5.10: Effect of changing $\bar{\beta}$ on the numbers of susceptible, infected, resistant, and dead rabbits.

(a) $\bar{\beta} = 0.0025$ (b) $\bar{\beta} = 0.05$ **Figure 5.11:** Effect of changing $\bar{\beta}$ The number of infected individuals at $t = 56$ d.

CHAPTER 6

Sensitivity Analysis of the Spatially Explicit Myxomatosis Model

A step often overlooked in spatio-temporal modelling, but crucial to the modelling process is a sensitivity analysis [8]. This is the study of how uncertainty in the output of a model can be appointed to different sources of uncertainty in the model input/parameters [93, 94]. Sensitivity analyses are important as they allow researchers to identify critical regions in the input/parameter space, establish priorities for research, simplify the model structure and defend against falsifications of the analysis [93]. In this chapter we will discuss the most important methods for sensitivity analysis, and we will subsequently perform a global sensitivity analysis of the myxomatosis model presented in Section 5.1.

6.1 Local sensitivity analysis

The best known and easiest method to perform sensitivity analyses is the local sensitivity analysis, also referred to as the one-at-a-time (OAT) approach. This involves quantifying the effect of perturbing one model input/parameter at a time, while keeping the others constant. This essentially involves the calculation of a partial derivative from the model output with respect to the input/parameter concerned. If we have a model F with input/parameter p its absolute sensitivity with respect to that to that input/parameter can be written as:

$$\frac{\partial F}{\partial p} \approx \frac{F - \tilde{F}}{\Delta p}, \quad (6.1)$$

with F the simulated model output and \tilde{F} the simulated model output with a input/parameter perturbed by a factor δ , such that $\Delta p = \delta p$. If we want to compare the sensitivity across different model inputs/parameters, it is better to calculate the relative sensitivity:

$$p \frac{\partial F}{\partial p} \approx p \frac{F - \tilde{F}}{\Delta p}. \quad (6.2)$$

This derivative-based approach has been applied to System (5.6)[8]. It has the advantage that it is very easy to perform for most models and has very low computational demands [65, 113]. However, it is not informative if the model inputs/parameters are uncertain, since the perturbation needs

to happen in a small range around a nominal value, or if the system is of unknown linearity [93]. Since our model parameters are uncertain, we will not use this approach.

6.2 Global sensitivity analysis

The second, more recent approach to model sensitivity is the global one. In contrary to a local sensitivity analysis all the parameters are varied the same time over a large feasible range, resulting in broader understanding of model sensitivity [50, 113]. There are many approaches and aims for this type of analysis [50, 93]. In the context of this thesis, a small selection will be discussed.

6.2.1 Morris screening

When the number of inputs/parameters is too large to apply variance-based methods, the elementary effect (EE) method developed by Morris [81] can be used to screen which inputs/parameters are the most important [93]. This technique is relatively simple and shares some similarities with the OAT method (Section 6.1) in that it also uses local variations around a fixed point in the input/parameter space. The difference lies in the fact that it uses multiple of those perturbations over a larger range and averages them, to remove the dependence on a single point [93].

Consider a model with k independent parameters $X_i \in \mathbf{X}, i = (1, \dots, k)$, which vary in the k -dimensional unit cube across p fixed levels, which means that the parameter space is discretized into a p -level grid Ω . The elementary effect of the i th parameter is

$$EE_i = \frac{[Y(X_1, \dots, X_i + \Delta, \dots, X_k) - Y(X_1, \dots, X_i, \dots, X_k)]}{\Delta}, \quad (6.3)$$

with Δ a value in $\{1/(p-1), \dots, 1-1/(p-1)\}$, \mathbf{X} is chosen such that each point $\mathbf{X} + \mathbf{e}_i \Delta$, with \mathbf{e}_i a zero vector with its i th component equal to one, is still in Ω for every i . By randomly sampling different \mathbf{X} from Ω , the distribution of elementary effects associated with the i th parameter, F_i is obtained, with $EE_i \sim F_i$ [50, 81, 93]. To illustrate this more clearly, the arrows in Figure 6.1 depict the eight EE s for the situation with $k = 2, p = 4$ and $\Delta = 2/3$.

The two sensitivity measures, μ and σ , proposed by Morris [81] are the estimates of the mean and standard deviation of the distribution F_i . The mean μ is a measure for the overall influence of the factor on the output. The standard deviation σ yields an estimate of the ensemble of the factor's effect, be it nonlinear, or interaction effects with other parameters [93]. The measure μ is quite sensitive to type II errors (failing to find an influential factor) if the distribution F_i contains both negative and positive numbers. For that reason, it has been proposed that the mean μ should be replaced by the mean of the distribution of the absolute values of the EE s [19]. For more details about Morris screening, we refer the reader to [50] and [93].

This technique is the most suitable for a sensitivity analysis of models with many parameter and long execution times, since the number of evaluations is limited. We will not use this technique since the ones in Section 6.2.2 provide a more detailed criterion for sensitivity [93, 113].

6.2.2 The Sobol' method

A more recently developed method for sensitivity analysis is the approach of Sobol' [99, 100]. Here, instead of studying the effect of changing one input/parameter at a time, multiple the input/pa-

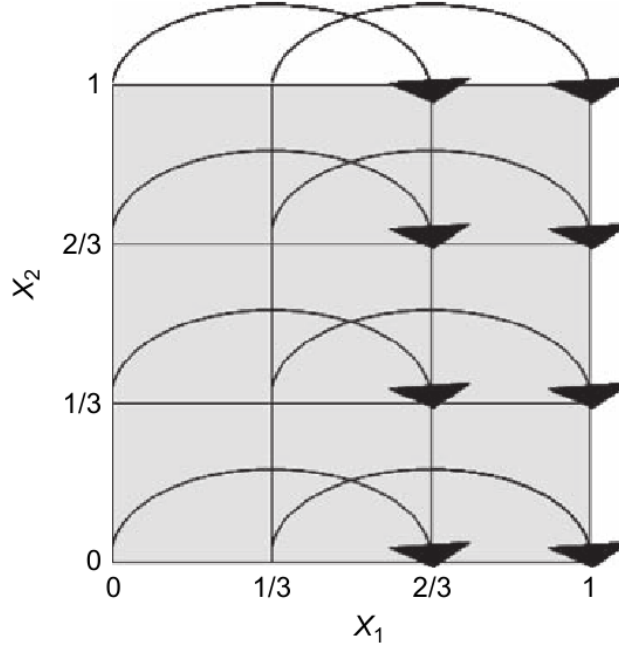


Figure 6.1: Illustration of the Morris method [93].

rameters are varied simultaneously. In essence, methods based on Sobol's theorem generate several different model outputs from randomly sampled input/parameter combinations and analyse the generated variance [93]. Such methods are capable of estimating the influence of individual and groups of inputs/parameters on a non-linear model [93, 99, 113]. Given a model

$$\mathbf{Y} = f(X_1, X_2, \dots, X_k), \quad (6.4)$$

describing the relationship between k inputs/parameters $\mathbf{X} = (X_1, X_2, \dots, X_k)$ and the output variables \mathbf{Y} , Sobol' showed that f can be decomposed for each output variable $Y \in \mathbf{Y}$ into a finite sum of terms with increasing dimensionality, known as a high-dimensional model representation (HDMR) [93, 99]:

$$f(\mathbf{X}) = f_0 + \sum_{i=1}^k f_i(X_i) + \sum_{j>i}^k f_{ij}(X_i, X_j) + \dots + f_{1,2,\dots,k}(X_1, X_2, \dots, X_k), \quad (6.5)$$

with f_0 the zeroth-order component function, which is the mean response, $f_i(X_i)$ the first-order component function, which denotes the independent contribution to $f(\mathbf{X})$ by the input/parameter X_i alone. Then, $f_{ij}(X_i, X_j)$, the second-order component function gives the correlated contribution of the pair X_i, X_j to the model $f(\mathbf{X})$, and so on, until the the last term $f_{1,2,\dots,k}(X_1, X_2, \dots, X_k)$, which denotes any residual contribution to $f(\mathbf{X})$ by all inputs/parameters together [64].

Sobol showed that if each term in this expansion has a zero mean, the variance of an output variable can be decomposed into

$$V(Y) = \int f(\mathbf{X})^2 d\mathbf{X} - f_0 = \sum_{i=1}^k V_i + \sum_{i=1}^k \sum_{j>i}^k V_{ij} + \dots + V_{1,2,\dots,k}, \quad (6.6)$$

with

$$V_{i_1, i_2, \dots, i_s} = \int f_{i_1, i_2, \dots, i_s}^2 dX_{i_1} dX_{i_2}, \dots, dX_{i_s}, \quad (6.7)$$

for a given set of indices i_1, \dots, i_s . The Sobol' sensitivity indices that we want to calculate are the ratios of the partial variances in Equation (6.6) versus the total variance [93, 99, 113]. So, if we divide Equation (6.6) by $V(Y)$ we arrive at these indices [93]:

$$\sum_{i=1}^k S_i + \sum_{i=1}^k \sum_{j>i}^k S_{ij} + \dots + S_{1,2,\dots,k} = 1. \quad (6.8)$$

From these indices, only two are calculated on a regular basis [93, 113]: the first order sensitivity indices, S_i , and the total order sensitivity indices, S_{T_i} . The former show the main effect contribution of each input/parameter to the variance of the output, and are given by:

$$S_i = \frac{V[f_i(X_i)]}{V(Y)} = \frac{V[E(Y|X_i)]}{V(Y)}. \quad (6.9)$$

It is easy to see that Equation (6.9) contains the first terms of Equation (6.8). The other terms in Equation (6.8) are the higher-order Sobol' indices that show how much of the variance can be attributed to interaction effects between inputs/parameters. The number of those higher order terms increases exponentially with increasing numbers of inputs and parameters, and as such require many calculations for more complex models [93]. The total-order Sobol' indices provide a way to estimate the total contribution to the output variation by a given input/parameter, taking first and higher order effects into account. For instance, given a model with three parameters ($k = 3$), the total effect of X_1 is the sum of all the terms in Equation (6.8) for this parameter:

$$S_{T_1} = S_1 + S_{12} + S_{13} + S_{123}. \quad (6.10)$$

It seems that all the higher-order terms of Equation (6.8) still need to be calculated. There is, however, a way around. The first order Sobol' index from Equation (6.9) follows from decomposing the variance $V(Y)$ in its main effect in regard to that input/parameter, which is the Sobol' index and the residual. We can also do this for all but one input/parameter, i.e. $\mathbf{X}_{\sim i}$:

$$V(Y) = V[E(Y|\mathbf{X}_{\sim i})] + E[V(Y|\mathbf{X}_{\sim i})]. \quad (6.11)$$

The difference $V(Y) - V[E(Y|\mathbf{X}_{\sim i})] = E[V(Y|\mathbf{X}_{\sim i})]$ is the remaining variance of Y that would be left on average, if we would determine the true values of $\mathbf{X}_{\sim i}$. Dividing Equation (6.11) by $V(Y)$ gives the total Sobol' index for a given input/parameter:

$$S_{T_i} = \frac{E[V(Y|\mathbf{X}_{\sim i})]}{V(Y)} = 1 - \frac{V[E(Y|\mathbf{X}_{\sim i})]}{V(Y)}. \quad (6.12)$$

The first and total order indices have the property that $S_i \leq S_{T_i} \leq 1$. Moreover, if $S_i = S_{T_i} = 0$ it may be concluded that $f(\mathbf{X})$ does not depend on X_i , while $S_i = S_{T_i} = 1$ indicates that $f(\mathbf{X})$ solely depends on X_i .

This method for global sensitivity has several advantages in comparison to other alternatives in that it is independent from the model structure, captures effects of individual inputs/parameters as well as their interaction effects, and is able to rank the importance of different inputs/parameters with respect to their share in the output variance. Yet, it is computationally expensive [113].

Given a model with k parameters and N samples from each parameter, at least $N(k + 1)$ model runs are necessary to calculate partial variances for individual parameters [93]. N needs to be larger if there are more inputs/parameters due to the exponentially growing size of the parameter space from which there needs to be sampled, also known as the curse of dimensionality [54]. When sensitivities are very low, there can also arise some computational difficulties [101].

6.2.3 Calculating Sobol' indices in practice

For the sake of explaining the procedure we will represent the myxomatosis models from Section 5.1 as

$$\mathbf{Y} = f(\mathbf{X}), \quad (6.13)$$

with $y \in \mathbf{Y}$ a model output and k parameters such that $(x_1, x_2, \dots, x_i, \dots, x_k) = \mathbf{X}$. The first thing to decide is the number of model runs (N) for the analysis. The computational strategy to arrive at Sobol' indices is based on Monte Carlo simulations in that many model evaluations are necessary to give reliable estimates, especially for nonlinear models [65]. Then, we generated a matrix of $2N$ rows and k columns, representing N quasirandom samples from the k parameters which were then split into two matrices A and B , with N rows and k columns. After that, for each parameter $x_i \in \mathbf{X}$, a matrix D_i was defined by all columns of A except the i th column, which was taken from B , and a matrix C_i formed by all columns of B except the i th column, which was taken from A . This resulted in $2k + 2$ matrices, two for each parameter, and the A and B matrix (Figure 6.2).

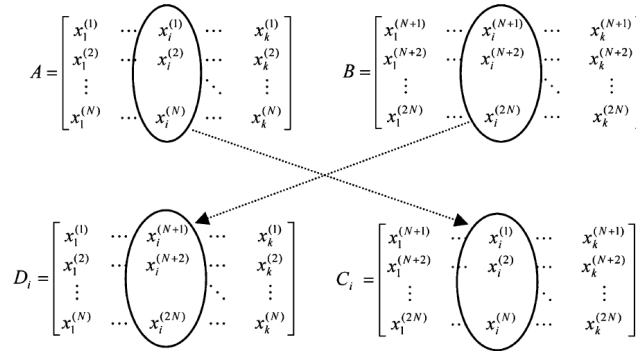


Figure 6.2: Generating one pair of C and D parameter matrices from A and B [65].

To obtain the estimates of the first and total order Sobol' indices for a given parameter, three output vectors are needed of length N :

$$\mathbf{y}_A = f(A), \mathbf{y}_{C_i} = f(C_i), \mathbf{y}_{D_i} = f(D_i). \quad (6.14)$$

Using those three output vectors, the first order Sobol' index can be estimated as

$$S_i = \frac{\frac{1}{N} \sum_{j=1}^N y_A^{(j)} y_{C_i}^{(j)} - \left(\frac{1}{N} \sum_{j=1}^N y_A^{(j)} \right)^2}{\frac{1}{N} \sum_{j=1}^N (y_A^{(j)})^2 - \left(\frac{1}{N} \sum_{j=1}^N y_A^{(j)} \right)^2}, \quad (6.15)$$

with $j = 1, \dots, N$. The total order Sobol' index is estimated by

$$S_{T_i} = 1 - \frac{\frac{1}{N} \sum_{j=1}^N y_A^{(j)} y_{D_i}^{(j)} - \left(\frac{1}{N} \sum_{j=1}^N y_A^{(j)} \right)^2}{\frac{1}{N} \sum_{j=1}^N (y_A^{(j)})^2 - \left(\frac{1}{N} \sum_{j=1}^N y_A^{(j)} \right)^2}. \quad (6.16)$$

The matrices C_i and D_i are different for each parameter concerned and are generated for each parameter/input separately, such that the total number of model evaluations needed for calculating the first and total order Sobol' indices for k model parameters is $N(2k + 1)$, which explains the computational demand of this method [65]. For Equations (6.15) and (6.16) the output vectors need to consist of scalars [65, 93], which is often not the cases. Sometimes, the model output is a time series, which implies that the sensitivity indices need to be calculated at each time step separately, or by aggregating the output in a statistic. If the output of the model is spatial, like in our myxomatosis model (see Section 5.1), then there are two options to calculate the Sobol' indices. The first is to aggregate the spatial variables into an aggregated statistic, like the area of a surface or its circumference, and continue with those statistics, or the Sobol' indices can be calculated for each grid cell separately [65]. The last approach results in a map of sensitivity.

6.3 Global sensitivity analysis of the myxomatosis model

In this section we will put the method of Sobol' into practice according to [65]. First the selected output will be outlined, after which the results for the spatially explicit myxomatosis model from Chapter 5 will be discussed.

6.3.1 Selecting the model output

The first step in a global sensitivity analysis always involves determining the model output for which we want to calculate sensitivity indices. For System (5.6) the generated outputs are maps composed of cells with numbers of susceptible, infected, resistant and deceased rabbits, that vary through time. As explained in Section 6.2.3, we need to have a scalar value to calculate the Sobol' indices, which means that we need to aggregate our output by considering:

1. total number of susceptible rabbits;
2. total number of infected rabbits;
3. total number of rabbits killed by the disease.
4. total area of the cells with at least one infected rabbit present;

5. total area of the cells with at least one rabbit that died from the disease;
6. total area of the cells with at least 10 percent of the population infected;
7. total area of the cells with at least 30 percent of the population infected;
8. area of the convex hull around the cells with at least one infected rabbit;
9. area of the convex hull around the cells with at least 10 percent of the population infected;

The convex hull is the smallest convex set that contains S if and only if for any pair of points $p, q \in S$ the line segment \overline{pq} is completely contained in S (Figure 6.3) [85].

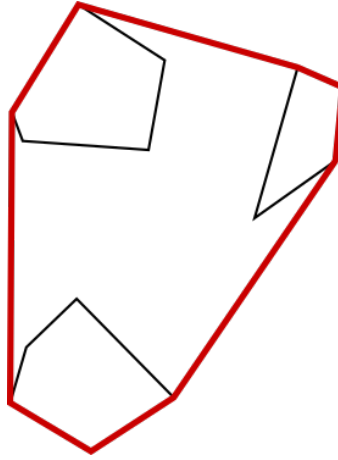


Figure 6.3: Convex hull around three polygons.

6.3.2 Input selection and sampling procedure

The next step in the sensitivity analysis considers the selection of inputs/parameters. In case of System (5.6) we want to know the sensitivity with respect to six parameters $(C_M, \epsilon, r, m, \underline{\beta}, \overline{\beta})$. We chose to keep the initial rabbit densities, and the location of the initial infected cells fixed. Subsequently, it is necessary to define intervals for parameters from which to sample. For $\overline{\beta}$ and $\underline{\beta}$, we took the values from [32]. Since [32] involved a non-spatial myxomatosis model, it is not clear whether these values will be the same for the spatially explicit model. For the other parameters, we found substantial information on myxomatosis and rabbit population dynamics (see Chapter 2). Feasible and realistic parameter ranges were defined using this information (Table 6.1). The ranges of the case mortality C_M and the reciprocal of the survival time ϵ were largely based on the studies of Anderson [4] and Dwyer [32]. For the mortality rate m , we constructed an interval enclosing the reciprocal of the mean survival time of adult rabbits as reported by [71], and for the reproductive rate r we calculated the ranges with values found in literature with

$$r = \frac{\text{females}}{\text{rabbits per warren}} \times \frac{\text{nests per year}}{\text{female}} \times \frac{\text{young rabbits}}{\text{nest}} \times \frac{\text{adults}}{\text{young rabbits}}, \quad (6.17)$$

by inserting the highest and lowest values of those proportions found in [71].

Now we needed to assign a statistical distribution from which to sample our parameters [65]. We assumed that all parameters are uniformly distributed in their respective ranges since we

Table 6.1: Sampled parameter ranges for System (5.6)

parameter	range
$\underline{\beta}$	[0.00025,0.02]
$\overline{\beta}$	[0.00025,0.02]
C_M	[0.50, 0.99]
ϵ	[1/50, 1/10]
m	[1/(2.5×365),1/(0.8×365)]
r	[(1/2×3×4×0.20)/365,(5/7×8×5×0.20)/365]

had no further information to underpin another choice. To arrive at the matrices A and B from Section 6.2.3, we needed to sample combinations of parameter values from their respective marginal distributions. Since our parameter space is relatively high-dimensional, we used latin hypercube sampling (LHS) [93]. Often, multiple thousands of runs are needed for the calculation of Sobol' indices, but this stratified sampling design allowed to sample the parameter space more uniformly with fewer samples needed than using standard Monte-Carlo sampling [79], which was useful, given the computational demand of System 5.6. Subsequently, for each parameter individually the matrices C and D were assembled.

With $N = 1000$ and $k = 6$ this resulted in $N(k + 1) = 13\,000$ model runs. With $\Delta t = 0.05$ d and 7560 time steps, this corresponds to a time frame of 378 days or 54 weeks, which was the time frame during which the myxomatosis epidemic developed in Belgium (see Section 4.1.3). Each simulation took about 14 hours. All simulations were run in Mathematica (version 10.0.0, Wolfram Research Inc., Champaign, United States) on the high-performance infrastructure of Ghent University.

6.3.3 Homogeneous land cover

The first GSA is performed under homogeneous land cover, so the transmission rates $\underline{\beta}_i$ and $\overline{\beta}_i$ are equal for each polygon c_i . For the most relevant aggregated statistic from Section 6.3.1 the time series of the first and total order Sobol' indices will be given, as well as the corresponding variances. The convex hulls were calculated every 280 time steps, instead of every time step due to high memory demands of their calculation.

Total of the susceptible rabbits

For the total number of susceptible rabbits (Figure 6.4), initially the most important parameter is $\overline{\beta}$, followed by r . The importance of the latter quickly declines in favour of $\underline{\beta}$. Subsequently, the first order indices (Figure 6.4(a)) of $\underline{\beta}$ and $\overline{\beta}$ steadily dwindle in favour of r , which becomes the most important parameter after about 200 days. Before this shift, the total order indices (Figure 6.4(c)) of both $\underline{\beta}$ and $\overline{\beta}$ stay relatively high. This indicates that there are substantial interaction effects. The other three parameters (C_m, m, ϵ) remain insignificant for this aggregated statistic.

Infected rabbits

For the total number of infected rabbits (Figure 6.5), the two transmission rates ($\underline{\beta}$ and $\overline{\beta}$) start off as the most prominent. However at about thirty days, the former is overtaken in favour of the disease duration (ϵ) and the reproductive rate (r), and the latter shrinks again shortly thereafter.

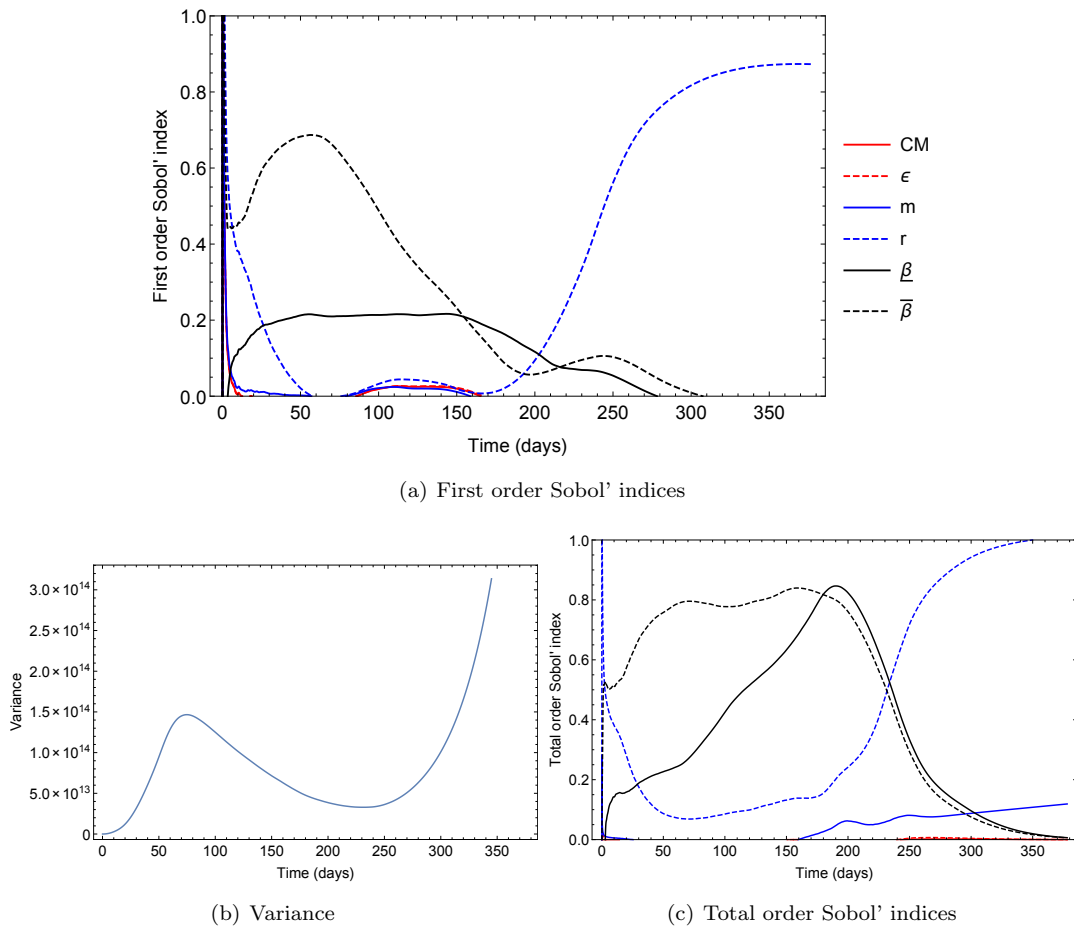


Figure 6.4: Variance and Sobol' indices of the total number of susceptible rabbits.

The sensitivity with respect to the long-range transmission rate ($\overline{\beta}$) has a small resurgence in its first order sensitivity afterwards. After 150 days, the first order indices (Figure 6.5(a)) dwindle for all parameters. By comparing them to the total order indices (Figure 6.5(c)), it is clear that after that point in time the interaction effects become manifold and difficult to disentangle.

Rabbits that die due to the disease

For the total number of rabbits that die due to the disease (Figure 6.6), the long range transmission rate $\overline{\beta}$ and the survival time ϵ are the two most important parameter at the onset, but are overtaken at about 100 days by r . This seems contradictory, given that r governs the population increase. Yet, as newly born rabbits are susceptible to the disease, an increase in r indirectly causes more rabbits to die from myxomatosis.

Area with at least one infected rabbit

The first spatial statistic is total area of cells where at least one infected rabbit is present (Figure 6.7). The two disease transmission rates ($\underline{\beta}$ and $\overline{\beta}$) explain almost all variance at the start of the simulation. To elucidate this, we compare the first order (Figure 6.7(a)) and total order (Figure

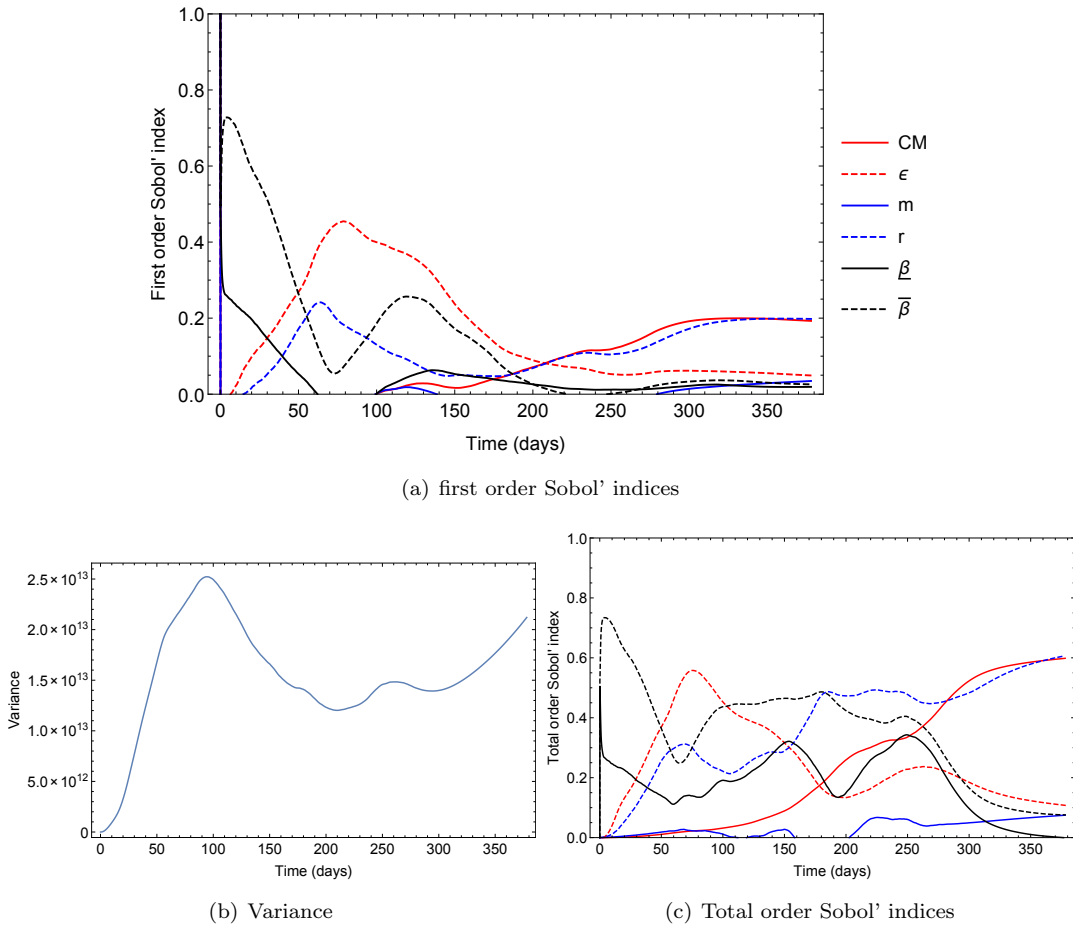


Figure 6.5: Variance and Sobol' indices of the total number of infected rabbits.

6.7(c)) indices. It is clear that at the start, the first and total order indices are almost equal for both $\underline{\beta}$ and $\bar{\beta}$ up to about 80 days. This means that this statistic solely depends on those two parameters up to the point where C_M , ϵ and r gain importance, with C_M becoming the most prominent.

For the area of the convex hull enclosing the cells with at least one diseased rabbit, the sensitivities are similar to those of the the total area of those cells (Figure 6.7), except that it is unclear which parameters become important after the decline of the sensitivity to the transmission rates ($\underline{\beta}$ and $\bar{\beta}$).

Area where at least one rabbit died due to the disease

For the total area of the cells that contain at least one rabbit that died to the disease, the transmission rates $\underline{\beta}$ and $\bar{\beta}$, again, contribute the most to the variance at the earlier time frame of the simulations (Figure 6.8). After 100 days, the sensitivity with regard to $\underline{\beta}$ and $\bar{\beta}$ shifts first to r , C_M , ϵ and m . After about 200 days, the indices suddenly shoot upwards to theoretically impossible values, and this for the first order (Figure 6.8(a)) and the total order indices as well (Figure 6.8(c)). This is a prime example why it is good practice to always examine the variance (Figure 6.8(b)) when performing a sensitivity analysis. Since the calculation of both Sobol' indices

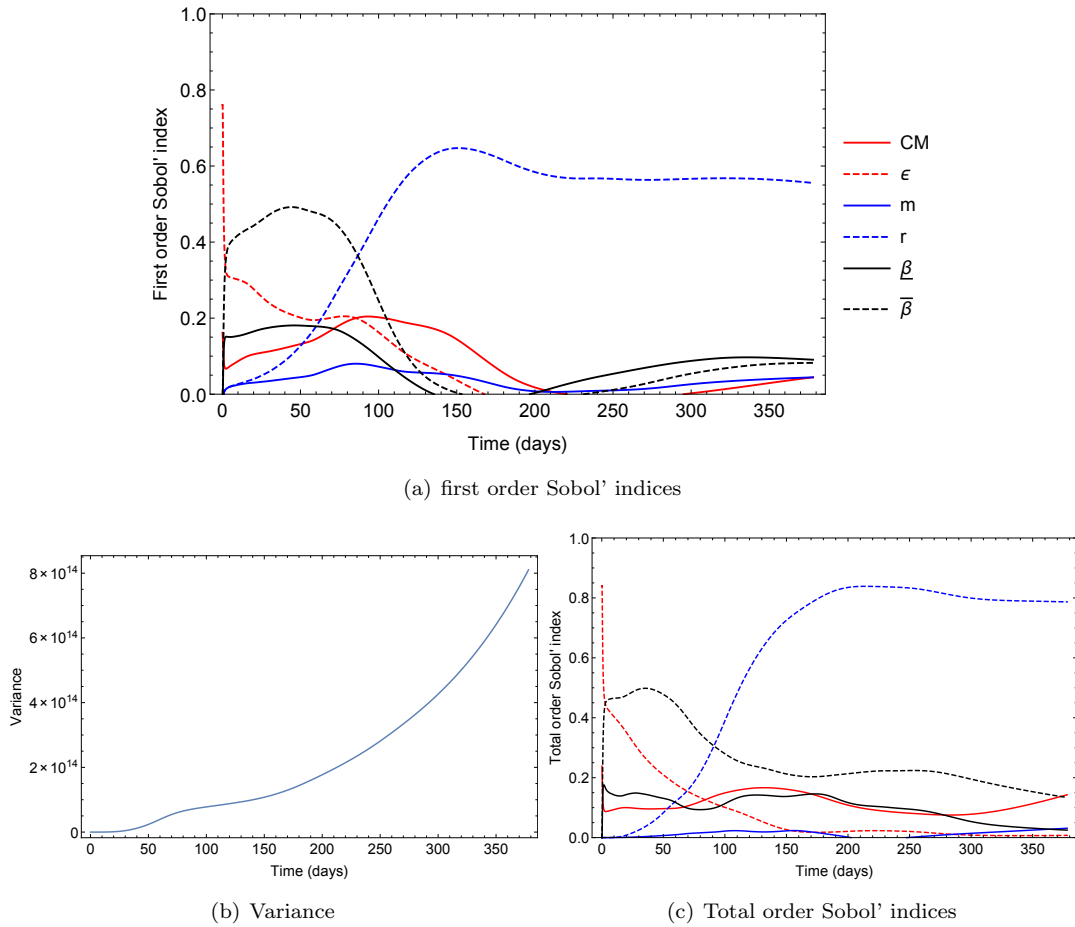


Figure 6.6: Variance and Sobol' indices of the total number of rabbits that died from the disease.

requires the division by the total variance (Equations 6.9, 6.12), this means we get indeterminate values for those indices if said variance reaches zero. The low variance can be explained as follows. After about 200 days, for all the simulations, all the cells have been infected at least once, therefore, the calculated area remains constant. Since myxomatosis took longer than the simulation time to spread across Belgium (see Section 4.1.3), we may state that the combination of parameter values that can lead to a realistic simulation result to mimic the myxomatosis epidemic is not contained in the sampled parameter space.

Area with at least 10 percent infected

The trends for the sensitivity indices for the total area of cells, and the convex hull around those cells, where at least 10 percent of the population is infected (Figure 6.9) are similar to those where at least one infected rabbit is present (Figure 6.7). However, there are some key differences. The sensitivities to the transmission rates ($\underline{\beta}$ and $\bar{\beta}$) dwindle a bit earlier, and the two parameters replacing those as the most important ones, are ϵ and r , instead of C_M and r . This shift becomes even more apparent for the sensitivities of the total area of the cells with at least 30 percent of the population infected. Besides, the parameters ϵ and r also show strong interaction effects (Figure

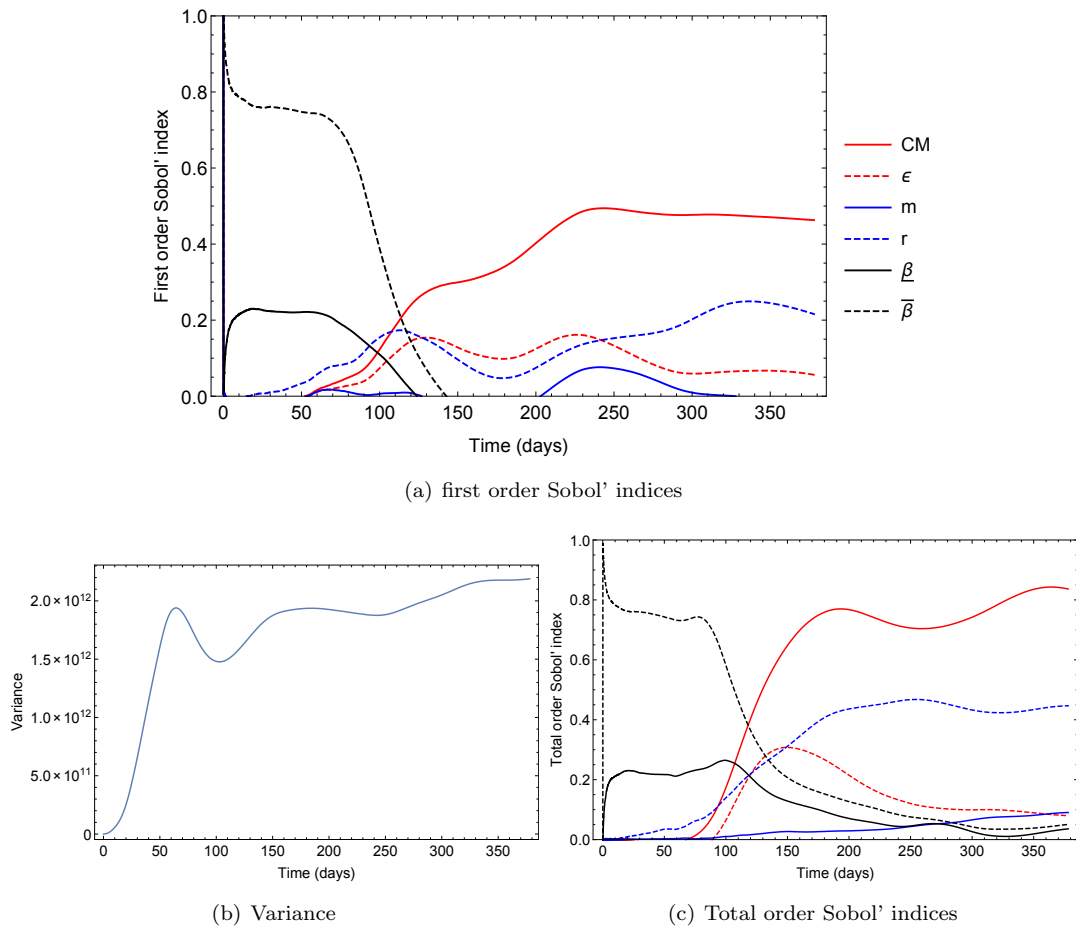
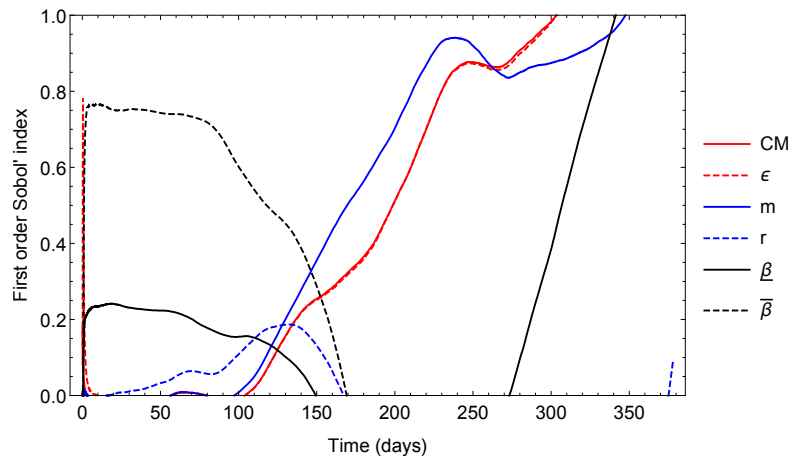


Figure 6.7: Variance and Sobol' indices of the area of the polygons with at least one diseased rabbit present

6.9(c)). The fact that ϵ gets increasingly important if the statistic is based on larger numbers of infected rabbits is not unexpected, since a longer survival of infected individuals contributes to larger populations of infected rabbits.



(a) first order Sobol' indices

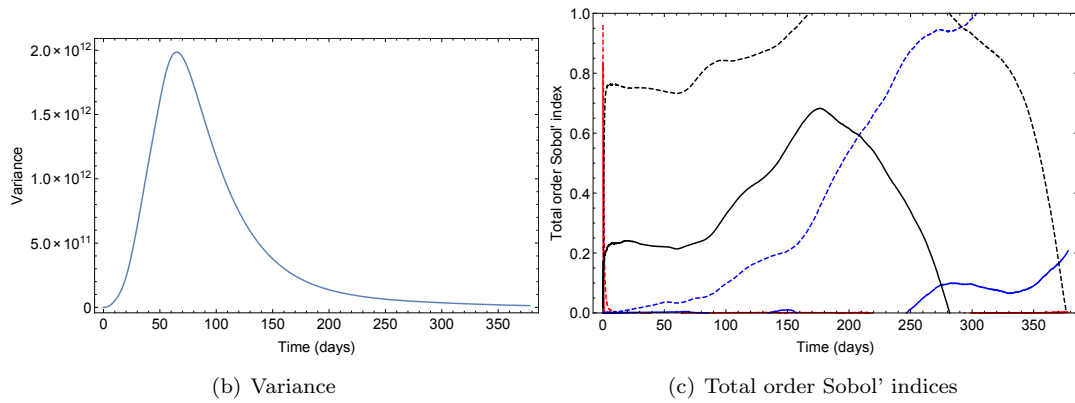
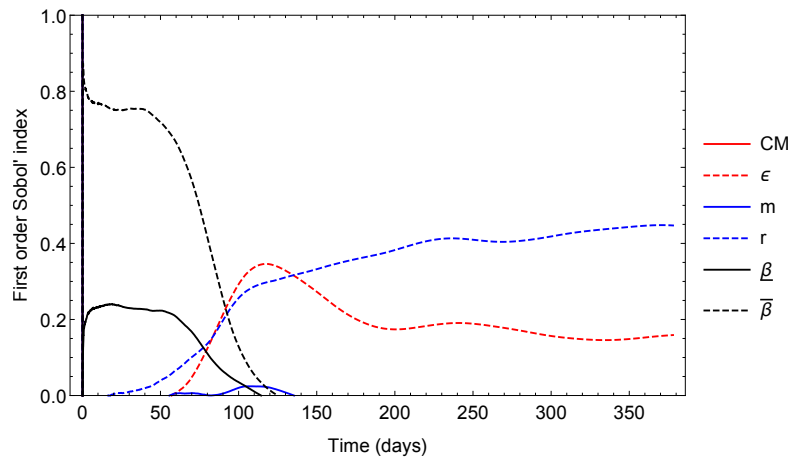
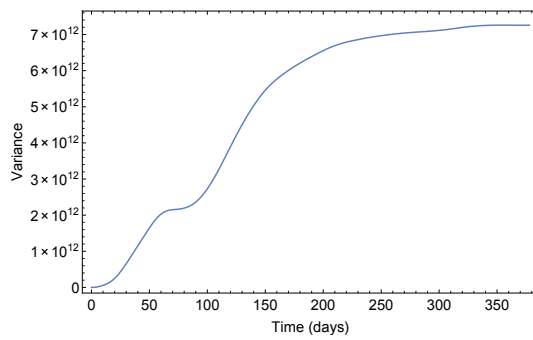


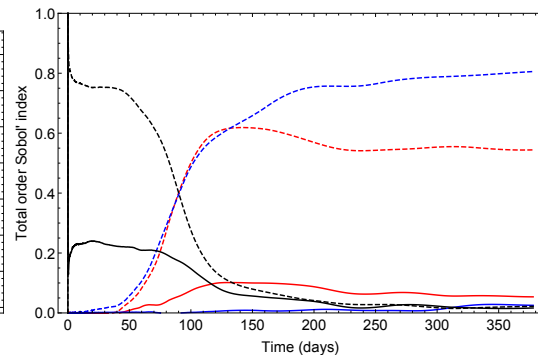
Figure 6.8: Variance and Sobol' indices of the total area where at least one rabbit died to the disease.



(a) first order Sobol' indices



(b) Variance plot



(c) Total order Sobol' indices

Figure 6.9: Variance and Sobol' indices of the area where at least 10 percent of the population is infected.

6.3.4 Heterogeneous land cover

Since System 5.9 can incorporate land cover information, we decided to perform a global sensitivity analysis on the transmission rates of different land cover classes, so we can identify which are the most important. We only varied the transmission rates $\underline{\beta}_i$ and $\overline{\beta}_i$ in such a way that $\underline{\beta}_i = \overline{\beta}_i$ for each land cover class, resulting in five different transmission rates; one for each land cover class of the CORINE map (Figure 4.8). The parameters were sampled in the same way as in Section 6.3.2, with a LHS design for the five transmission rates. The same aggregated statistics were calculated as in Section 6.3.1. The other parameters (C_M , ϵ , r , m) were kept constant at the values from Table 5.1, while the heterogeneous transmission rates were sampled from their distributions given in Table 6.1. With $N = 1000$ and $k = 5$ this results in 11 000 simulations for this analysis. For the sake of conciseness, we will restrict our discussion to a small selection of the aggregated statistics of Section 6.3.3 since some were not informative or yielded very similar results.

Total number of susceptible rabbits

For the total of the susceptible rabbits (Figure 6.10), it is clear that the transmission rate of the arable land class is the most important, with the other land cover classes trailing far behind. There are, however, some interaction effects with the other transmission rates (Figure 6.10(c)).

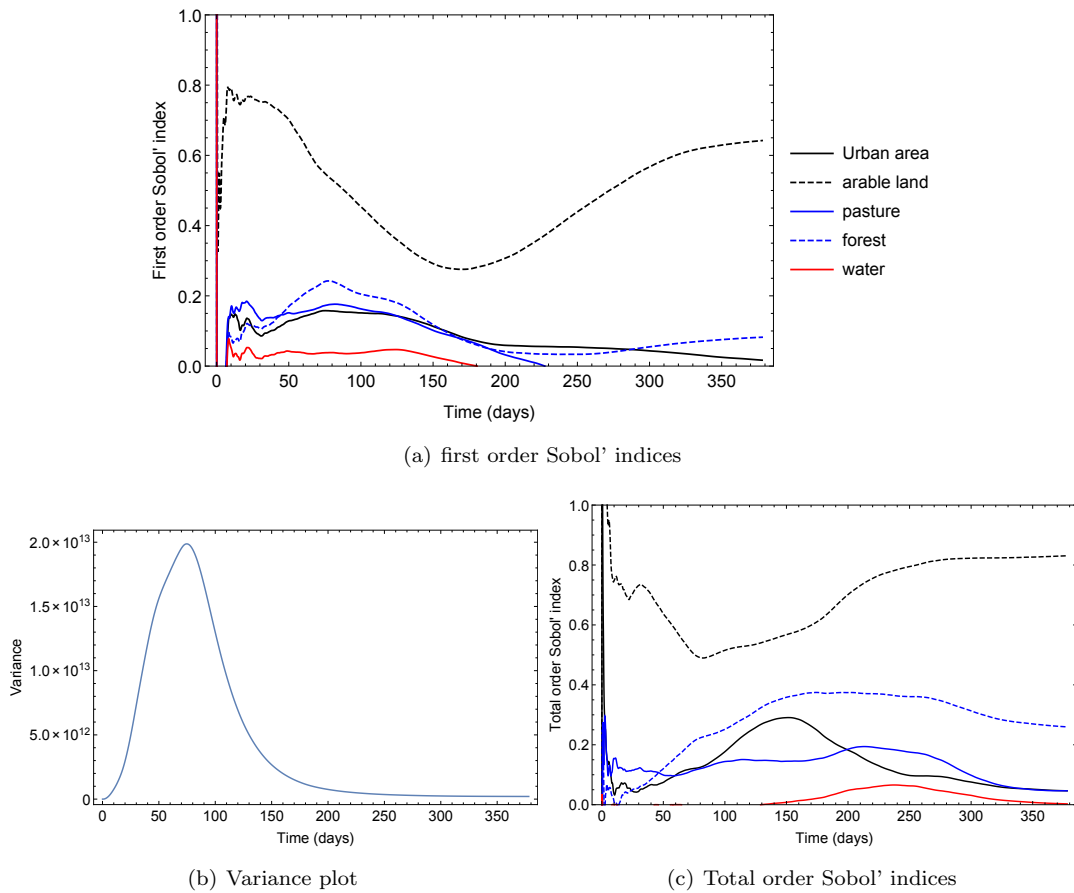


Figure 6.10: Variance, and Sobol' indices of the total number of susceptible rabbits

Total number of infected rabbits and the total area where at least one rabbit is infected

For the total number of infected rabbits (Figure 6.11), the transmission rate of the arable land also is the most important. By comparing Figures 6.11(a) and 6.11(c), it is clear that at about 75 days there are almost no linear effects, inflating the total order indices. At that same point in time the variance plot (Figure 6.11(b)) shows a dip, after which the variance raises again. After 250 days the graphs of the sensitivity indices become difficult to interpret, because the variance approaches zero from that point on (Figure 6.11(b)). The other statistics provided similar results, so they are not included. The most striking features of the two aggregated statistics are their variance graphs (Figures 6.10(b), 6.11(b)). Except for the dent in the variance at about 75 days for last two, they all approach zero after 250 days. The same thing happened with the variance of the total area where at least one rabbit died due to the disease (Figure 6.8(b)). From this, we already stated that the parameter space did not include the values for which the model can mimic the myxomatosis epidemic. Here, only the transmission rates (β_i and $\bar{\beta}_i$) were varied over different land cover classes. This indicates that the ranges of those parameters were not wide enough.

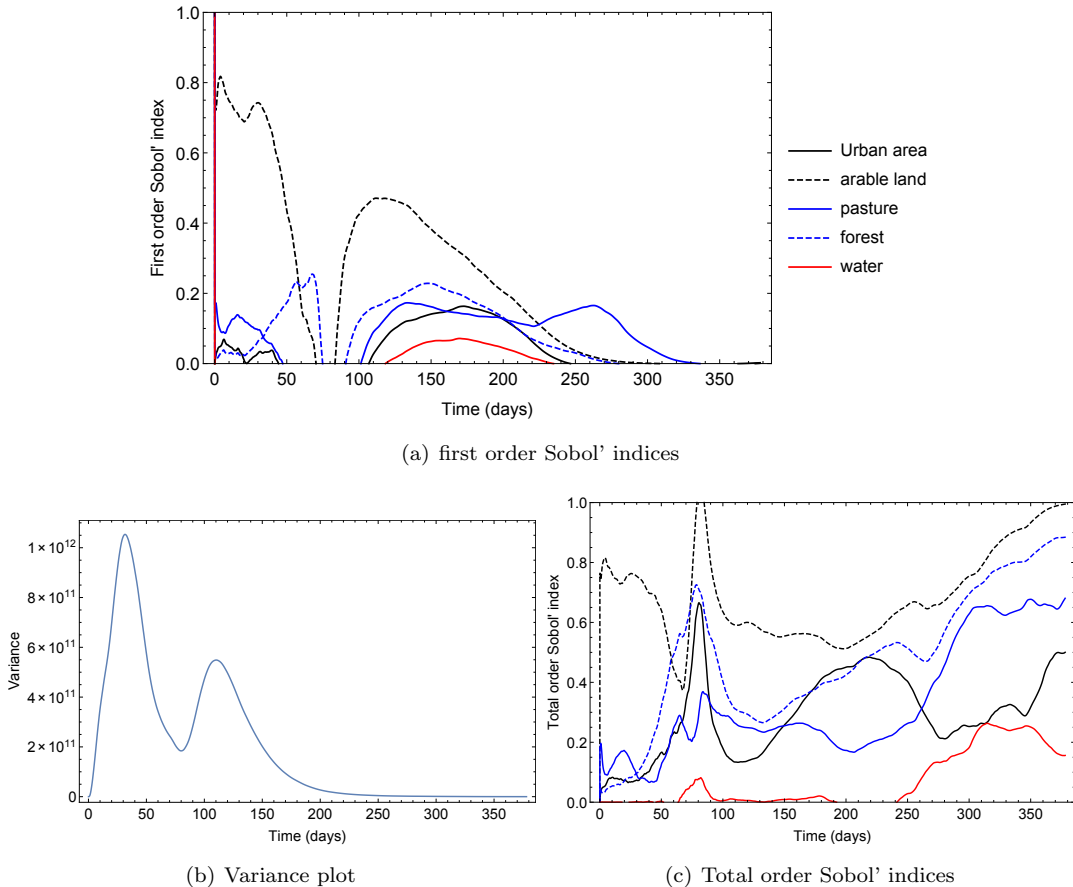


Figure 6.11: Variance and Sobol' indices of the total number of infected rabbits.

6.3.5 Conclusion

The main conclusions from these GSA's are the following. In general, the two transmission rates ($\underline{\beta}$ and $\overline{\beta}$) are the most important parameters at the start of the simulation, with the long range transmission rate ($\overline{\beta}$) being more important than the short range transmission rate ($\underline{\beta}$). By examining the variances, we may conclude that the sampled parameter space does not include the parameter values able to simulate the myxomatosis epidemic, since all simulations have already spread across the study area, on a moment that the epidemic from the data did not. Moreover, the GSA concerning the $\underline{\beta}_i$ s and $\overline{\beta}_i$ s under heterogeneous land cover also resulted in low variances further in the simulations, from which we may conclude that the transmission rates were not sampled in wide enough ranges.

6.4 Spatial sensitivity analysis

From the GSA concerning the heterogeneous transmission rates (Section 6.3.4) one might conclude that, given the land cover distribution of Belgium (Figure 4.9), the transmission rates of the arable land are relatively more important for the disease spread. It should be pointed out, that the land cover distribution of Belgium does not contain the complete simulation area, as parts outside the Belgian border are included to avoid influence of it on the simulations. Therefore it could be interesting to further investigate the transmission rates under heterogeneous land cover.

6.4.1 Method and input selection

Here, we want to extend Sobol's method to a spatial context, i.e., we want to calculate a map of sensitivity indices. This also means that we will not calculate a time series of Sobol' indices, but we will select a point in time and assess the sensitivity at that time instance instead. This means that we will calculate Equation (6.15) for each polygon for a given model output, in this case the number of infected rabbits in that polygon. From Section 6.3 we learned that the two transmission rates ($\underline{\beta}$ and $\overline{\beta}$) are the two most influential parameters in general, and that under heterogeneous land cover the transmission rates of the arable land cover class are the most important. It is still not clear, however, if its transmission rates are the most important across Belgium, or if in certain areas, the transmission rates of another land cover class may be more important. For this we chose to compare the transmission rates of the arable land with the transmission rates of the forest area. We chose this class' transmission rates as a comparison, since the forest area is quite concentrated in the southern part of Belgium, while the pasture area and the urban area are more spread evenly across Belgium (see Figure 4.8). From Section 4.1.2 we also know that in the southern part of Belgium, not many nidi of myxomatosis were reported, and although there is no statistical proof of an effect of the forest area on the number of reported nidi in a town (see Section 4.2.3) it is still a good reason investigate the effect of its transmission rates.

We did not assume that $\underline{\beta}_i = \overline{\beta}_i$, so we varied them separately for each land cover class. This results in four different sampled transmission rates. Since we concluded that the sampled ranges for the β s were too narrow we changed their sample ranges to $[0.25e^{-4}, 0.02]$. The transmission rates of the other land cover classes remained fixed at $\underline{\beta}_i = \overline{\beta}_i = 0.005$, while the other parameters are given in Table 5.1. The parameters were sampled using a LHS design, but there is a major

difference in the number of used samples. This time, $N = 500$, because our parameter space is not as high-dimensional as the GSAs of Section 6.3. We also only needed the A and C matrices this time, since we will not be calculating total order Sobol' indices. With $k = 4$, this results in a total of $N(k + 1) = 2500$ simulations. We limited the simulations to 2000 time steps, which is equivalent to 100 days, and at the end of the simulations, we calculated the sensitivity maps. We also calculated sensitivity maps for $t = 1000$ which is equivalent to 50 days, to check if those indices change over time.

6.4.2 Results and conclusions

The sensitivity maps at 50 days are given in Figure 6.12. It is clear that, for the largest part of Belgium, the long range transmission rate of the arable land (Figure 6.12(b)) is the most important parameter. However, in the south, the long range transmission rate of the forest area is the most important (Figure 6.12(d)). The two short range transmission rates are minor in comparison. From the variance map of this time instance (Figure 6.14(a)), we can see that at this time instance, none of the simulations have reached the north-eastern part of Belgium, meaning no sensitivity indices can be calculated.

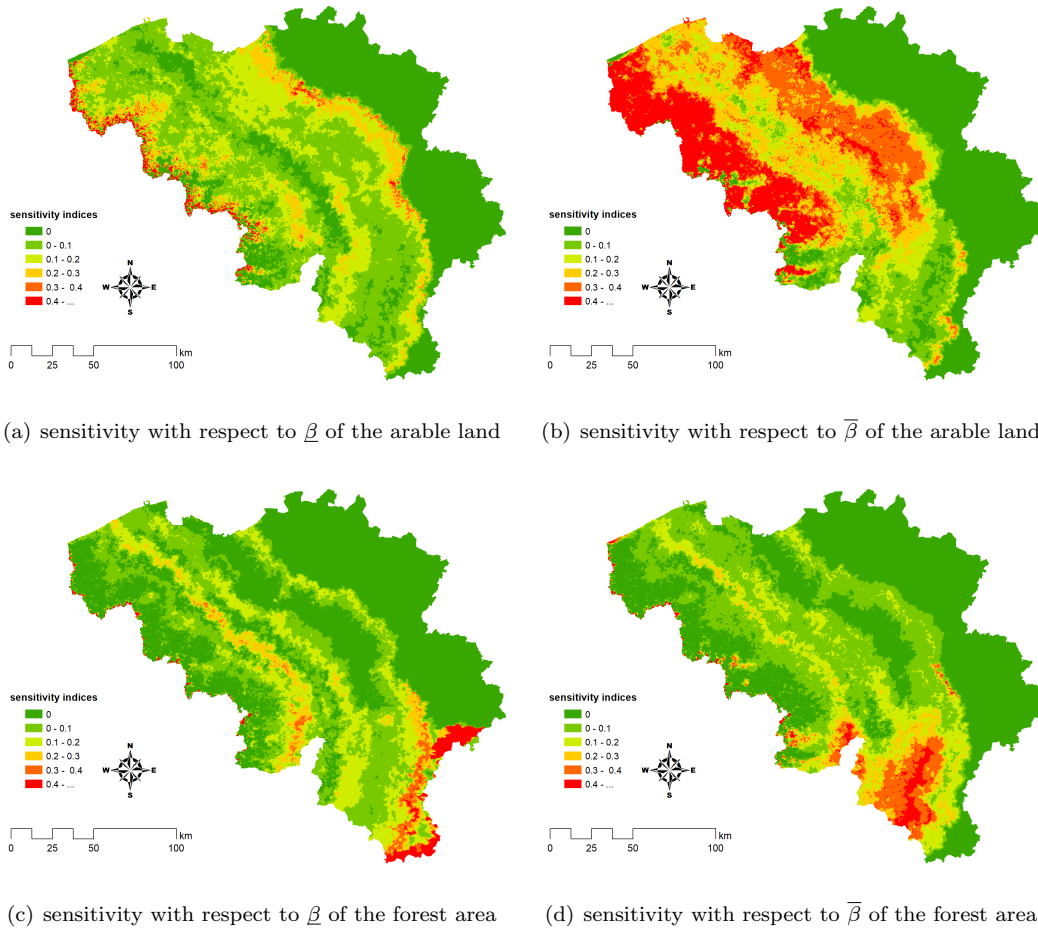


Figure 6.12: Sensitivity maps for the infected rabbits $t = 50$ d.

At $t = 100$ days, the sensitivity maps are more informative (Figure 6.13). Though, the same conclusions can be drawn as from the maps at $t = 50$ d.(Figure 6.12). Now, the waves have reached the north-eastern part of the country, where it seems that the first order sensitivity indices are low, irrespective of the parameter. This probably means that there are some interaction effects in between them, as the variance in those regions is high at that moment (Figure 6.14(b)). This shows that a spatial parameter that explains only a minor part of the variance in a non-spatial statistic, can still be the most important one in certain regions of the simulated space.

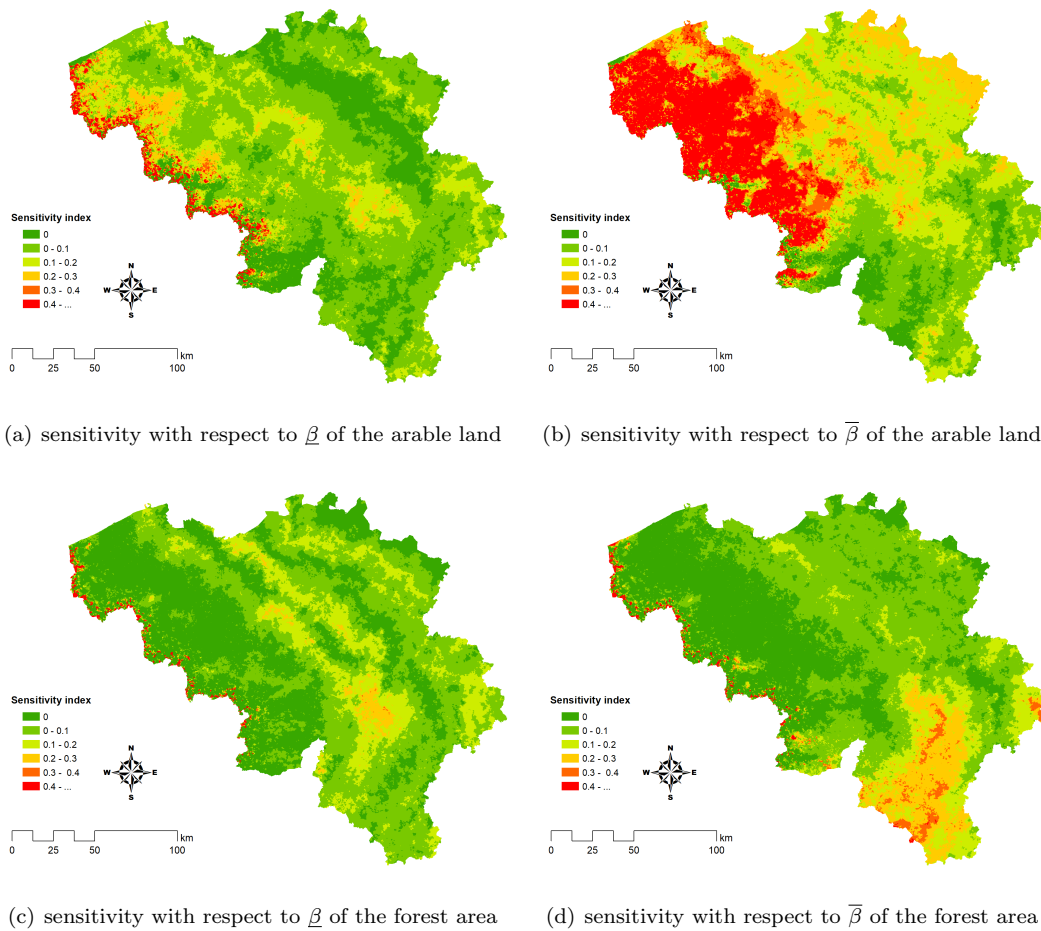


Figure 6.13: Sensitivity maps for the infected rabbits $t = 100$ d.

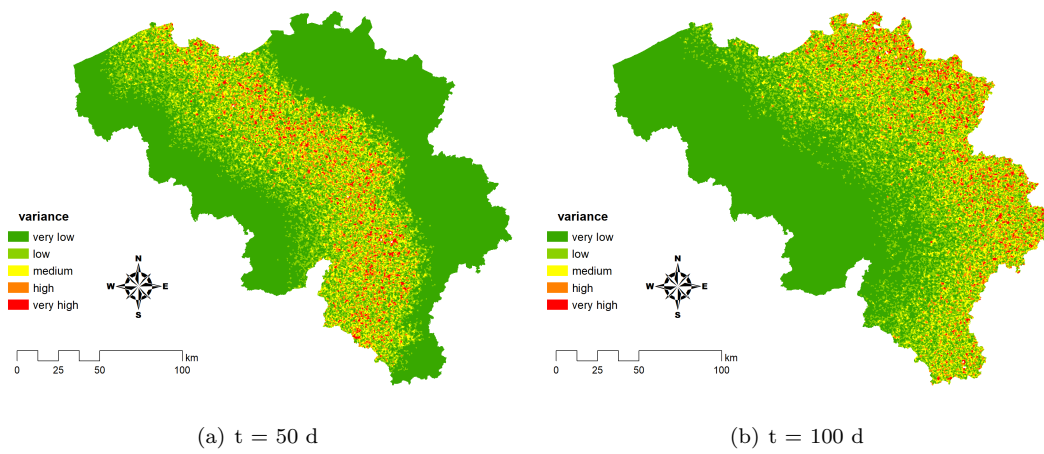


Figure 6.14: The variance maps

CHAPTER 7

Calibration of the Spatially Explicit Myxomatosis Model

In this chapter we will discuss the theoretical principles of approximate Bayesian computation. Subsequently, we will use this technique to infer parameters of the myxomatosis model (System (5.6)) based on the observed disease spread (Section 4.2.3). Then, we will check if the calibrated model is able to simulate the 1953-1954 myxomatosis epidemic. Subsequently, the model will be used to simulate some different scenarios.

7.1 Model calibration

Many recent models in computational biology are able to describe nature to a high degree of accuracy. They cannot be treated in an analytical way, but can be simulated on a computer, replicating many complex phenomena [66]. While it is easy to generate data from those models for different parameter values, the inverse problem, that is, identifying parameters that lead to simulated data that are sufficiently similar to the observed data is very difficult to solve [66]. For more simple models, like systems of ordinary differential equations, a variety of different methods and algorithms are available, such as maximum-likelihood estimation, genetic algorithms and simulated annealing [105]. Applying these methods to complex models with long simulation times, often stochastic, and very complex, or intractable likelihood surfaces can be challenging or practically impossible [66].

7.1.1 From Bayesian inference to approximate Bayesian computation

Approximate Bayesian computation has its roots in Bayesian inference [66]. It is a statistical method in which Bayes' theorem is used to update the probability of a hypothesis as it is given additional information [14]. Let $\mathbf{y} = (y_1, \dots, y_n)$ be a vector of observations whose probability distribution $P(\mathbf{y}|\mathbf{X})$ depends on the values of k parameters $\mathbf{X} = (X_1, \dots, X_k)$. Suppose that \mathbf{X} itself has a probability distribution $P(\mathbf{X})$, then we can use Bayes' theorem to arrive at [14]:

$$P(\mathbf{X}|\mathbf{y}) = \frac{P(\mathbf{y}|\mathbf{X})P(\mathbf{X})}{P(\mathbf{y})} \propto P(\mathbf{y}|\mathbf{X})P(\mathbf{X}). \quad (7.1)$$

Here, $P(\mathbf{X})$ tells us what is known of \mathbf{X} without knowledge of the data and is called the prior distribution. Correspondingly, $P(\mathbf{X}|\mathbf{y})$ tells us what we know about \mathbf{X} given our observations \mathbf{y} , and is called the posterior distribution [14]. The posterior is the distribution of interest as it shows what parameter values are likely to explain the data. To link it to the prior $P(\mathbf{X})$, $P(\mathbf{y}|\mathbf{X})$ needs to be calculated. This term can also be written in function of \mathbf{X} as the likelihood function of \mathbf{X} given \mathbf{y} , or $\mathcal{L}(\mathbf{X}|\mathbf{y})$ [14], so Equation (7.1) becomes

$$P(\mathbf{X}|\mathbf{y}) \propto \mathcal{L}(\mathbf{X}|\mathbf{y}) P(\mathbf{X}). \quad (7.2)$$

In classical Bayesian inference, $\mathcal{L}(\mathbf{X}|\mathbf{y})$ is needed to link the prior and posterior distributions. In the case of more complex models, the calculation of this likelihood function can be very difficult or completely impossible [66]. Approximate Bayesian computation (ABC) overcomes this problem by replacing $\mathcal{L}(\mathbf{X}|\mathbf{y})$ with a sampling procedure [24, 66]. Algorithms for ABC have the following generic form:

1. sample a candidate parameter vector \mathbf{X}^* from some prior distribution $P(\mathbf{X})$;
2. simulate a dataset \mathbf{y}^* using the model with a conditional probability distribution $P(\mathbf{y}|\mathbf{X}^*)$;
3. compare the simulated dataset, \mathbf{y}^* , with the experimental data, \mathbf{y}_0 , using a distance function d ;
4. specify a tolerance level ϵ , which is the desirable level of agreement between \mathbf{y}^* and \mathbf{y}_0 ;
5. if $d(\mathbf{y}_0, \mathbf{y}^*) \leq \epsilon$ accept \mathbf{y}^* .

This procedure results in a sample of parameters from a distribution $P(\mathbf{X}|d(\mathbf{y}_0, \mathbf{y}^*) \leq \epsilon)$ [105]. If ϵ is sufficiently small, $P(\mathbf{X}|d(\mathbf{y}_0, \mathbf{y}^*) \leq \epsilon)$ will be a good approximation of the posterior distribution $P(\mathbf{X}|\mathbf{y}_0)$. The biggest advantage of ABC-methods is that they only require the calculation of a distance function to be able to infer posterior distributions. The fact that this procedure results in a distribution and not a point estimate can also be more informative in certain situations. Some algorithms can also be easily parallelised [76]. The biggest disadvantage of ABC methods is that they require many model evaluations to infer the posterior distributions, which gets increasingly problematic if the number of parameters increase, or if the prior distribution differs much from the posterior one [66].

7.1.2 Applying ABC to the myxomatosis model

The ABC-algorithm that will be used to infer parameter distributions is a variation on the ABC rejection sampler [76, 89, 105]. Its pseudo code is given below.

This algorithm is one of the simplest ABC-algorithms, and is still quite inefficient [66]. It is, however, very easy to parallelize the for-loop since all the simulations are independent. This is a clear advantage in our case, due to the long computing times. Other, more sophisticated ABC-algorithms, like sequential Monte Carlo-ABC and Markov Chain-ABC are more efficient at finding good posteriors, but cannot be as easily parallelized [76].

There were, however, slight modifications to the model needed before proceeding. All presented simulations have been performed assuming that the disease entered at the French border. As discussed in Section 4.2.3, there were a few different entry points along the French border and

```

Initialization:
Choose the prior distribution  $P(\mathbf{X})$ 
Choose the number of samples  $N$ 
Choose a fraction  $\theta$ 
for  $i \in [1, 2, \dots, N]$  do
  | Generate  $\mathbf{X}_i^*$  from  $P(\mathbf{X})$ 
  | Generate  $\mathbf{y}_i^*$  from the model  $F(\mathbf{X}_i^*)$ 
end
Sort all samples  $(\mathbf{X}_i^*, \mathbf{y}_i^*)$  based on the distance of  $\mathbf{y}_i^*$  to the observations  $\mathbf{y}_0$  in increasing order.
Choose only the first  $\theta N$  samples to generate the posterior distribution of the parameters.

```

one in Antwerp, and these introductions happened at different times. Since System (5.6) can only simulate disease transmission at relatively short ranges, the areas where the different outbreaks started, were assumed to contain 10 % infected rabbits at their time of appearance in the dataset. As summary statistic to compare our data and simulation results, we decided to compare the surface areas of the observed epidemic wave fronts, at a given time with the area that has contained at least 10 % infected rabbits up to that point. More precisely, both time series of areas can be seen as vectors between which we can calculate the Euclidean distance, which is the distance measure we used.

We restricted the parameter inference to the two transmission rates $\underline{\beta}$ and $\bar{\beta}$ under homogeneous land cover since there is no sufficient proof for an effect of the land cover on the spread of myxomatosis (See Section 4.2.3). Also, the other parameters can easily be derived from literature (see Section 6.3.2 and Table 7.1). In addition to that, the model is not sensitive to them when the disease is still spreading (see Chapter 6), which means they are more difficult to infer [105]. We assumed a stable population with equal reproduction and natural mortality rates. The parameter values for the fixed parameters are given in Table 7.1. for the transmission rates, we chose the

Table 7.1: Parameter values for the calibration.

parameter	value
C_M	0.95
ϵ	1/12
m	$1/(1.5 \times 365)$
r	$1/(1.5 \times 365)$

same sampling distributions ($[0.25e^{-4}, 0.02]$) as in Section 6.4 for both. We did not use a LHS design this time, since it is not necessary for low-dimensional sampling procedures. We took $N = 1000$ samples from those distributions and chose $\theta = 0.1$. So, the posteriors were constructed from the 100 samples that scored the best on the distance function.

7.1.3 Results of the ABC procedure

The histograms of the marginal posterior distributions for the two transmission rates are given in Figure 7.1. Here, we see that the posterior of $\bar{\beta}$ (Figure 7.1(b)) is much narrower than the posterior

of $\underline{\beta}$ (7.1(a)) although they were sampled from the same range. This follows from the higher sensitivity of the model output to the former (see Section 6.3.5), which makes this parameter easier to infer [105]. However, it seems that for both transmission rates, the lower values have a higher chance to be retained in the procedure. Since we are inferring two parameters, we also plot their two-dimensional distribution to detect correlations (Figure 7.2).

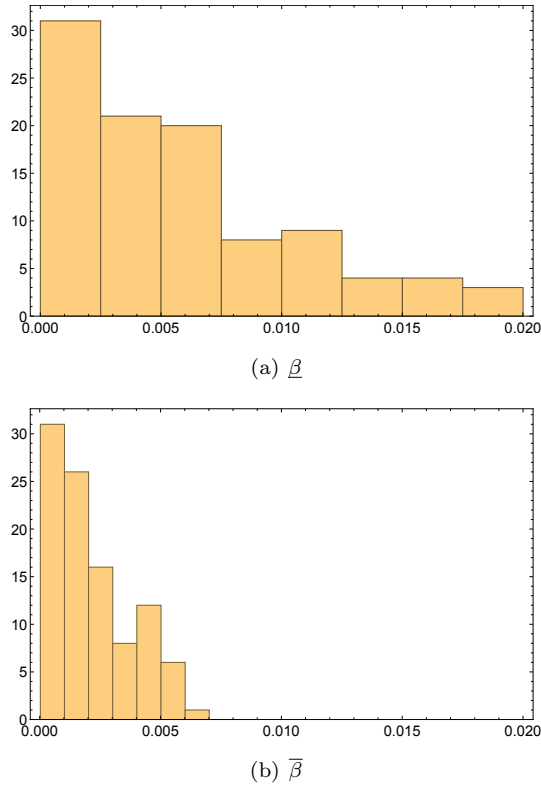


Figure 7.1: Distribution of the values of the 100 retained samples. The range of the plot is the sample range of the prior.

There seems to be some correlation between the two parameters, but the posterior still encompasses a quite wide area for both parameters. Therefore, we repeated the ABC procedure with smaller parameter ranges based on the posterior of Figure 7.2. More precisely, $\underline{\beta}$ was sampled from $[0.01 \times 10^{-4}, 0.01]$, while $\bar{\beta}$ was sampled from $[0.01 \times 10^{-4}, 0.005]$. Again, we chose $N = 1000$ and $\theta = 0.1$, which resulted in the histograms of the marginal posteriors depicted in Figure 7.3.

Again, lower values from the sample ranges have a higher chance at being retained in the procedure. The contour plot of the two-dimensional posterior is given in Figure 7.4.

By examining said posterior and comparing it with the posterior in (Figure 7.2), it is clear that the two parameters are negatively correlated. This is not unexpected, since those parameters govern the same process, meaning a high value in one transmission rate may compensate a low value of the other. The ABC procedure resulted in a two-dimensional posterior, so in the following section, we will validate the model by examining the simulation for different values of the transmission rates in the posterior.

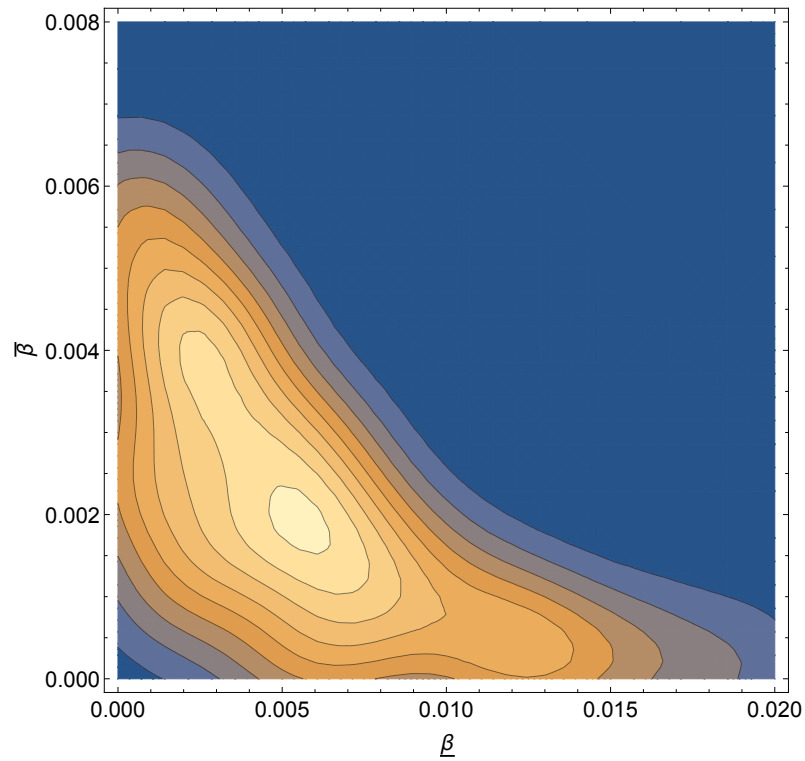


Figure 7.2: Contour plot of the 100 retained samples.

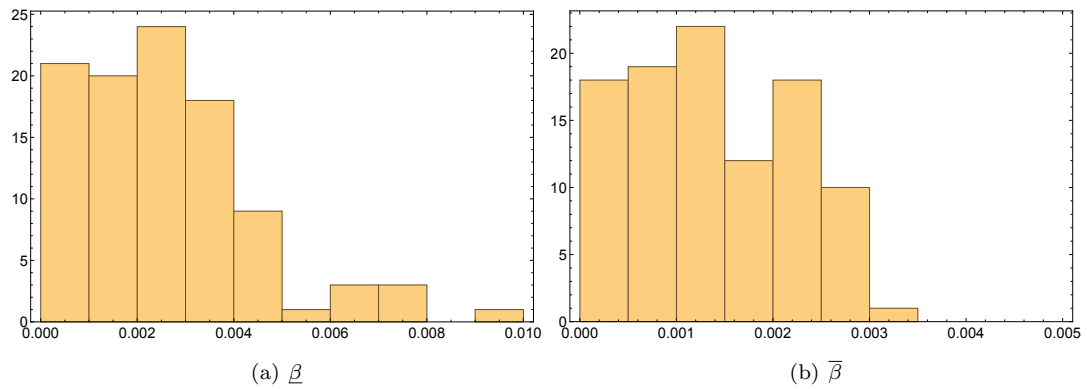


Figure 7.3: Distribution of the values of the 100 retained samples for the second procedure. The range of the plot is the sample range of the prior.

7.1.4 Model validation

From the posterior distribution of the transmission rates ($\underline{\beta}$ and $\bar{\beta}$) we chose three parameter combinations whose locations are given in Figure 7.4, and compared the simulated epidemic wave obtained therewith, and the observed epidemic wave (Section 4.1.3). This was done by comparing their maps for the first four seasons after the epidemic onset as well as their total infected areas (Figure 7.5). It should be noted, however that the model could not be validated with an independent dataset. The values of the three parameter combinations are given in Table 7.2.

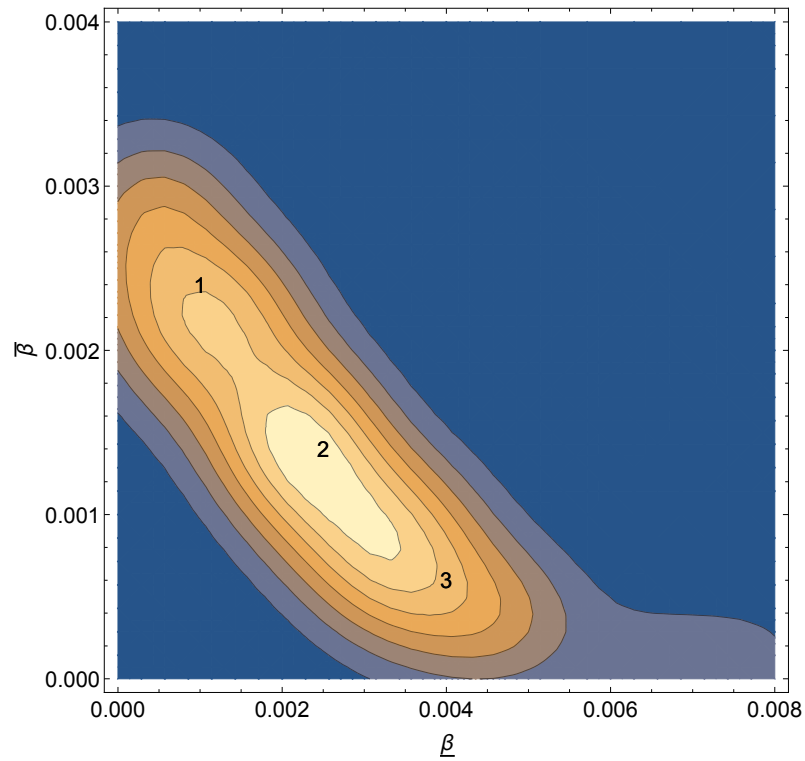


Figure 7.4: Contour plot of the 100 retained samples from the second procedure.

Table 7.2: The parameter values for the simulations.

parameter	Simulation 1	Simulation 2	Simulation 3
$\underline{\beta}$	0.0010	0.0025	0.0040
$\overline{\beta}$	0.0024	0.0014	0.0006

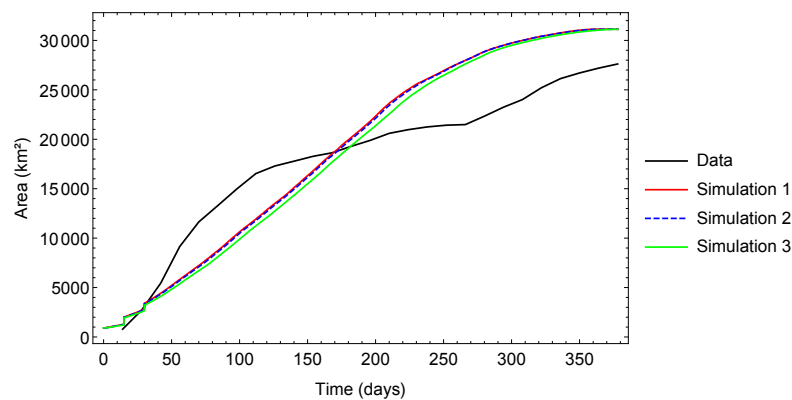


Figure 7.5: Comparison of the simulated infected areas versus the observed infected area.

If we compare the simulated maps for the four seasons (Figure 7.7, 7.8, 7.9 and 7.10), it is clear they are almost visually indistinguishable. Also, the dynamics of the susceptible and infected

rabbits, and rabbits that died due to the disease are very similar among the three simulations (Figure 7.6).

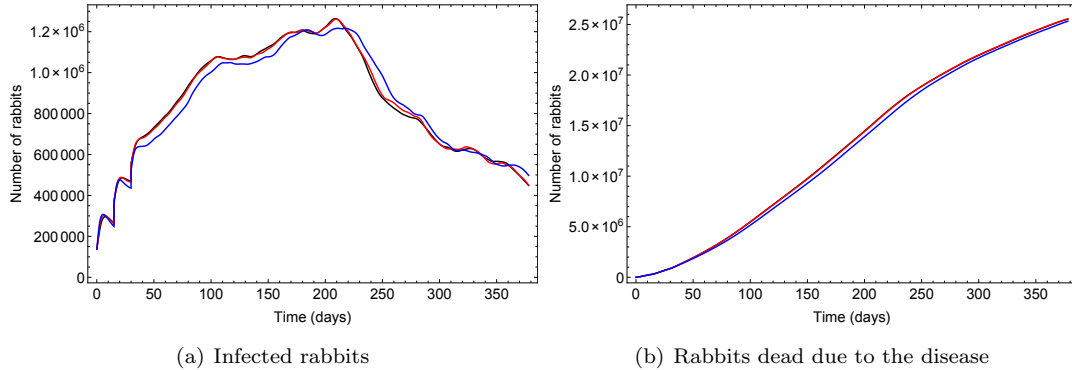


Figure 7.6: Comparison of the disease dynamics between the three simulations of Table 7.2

From this, we may conclude that $\underline{\beta}$ and $\bar{\beta}$ compensate each other, resulting in many possible parameters that yield similar results. There are several remarks to make, however. For the maps of the autumn season of 1953 (Figure 7.7), smaller infected areas are simulated in comparison to the data, contrary to the summer of 1954 (Figure 7.10), when the infected area is overestimated. Figure 7.5 also shows how all three simulations underestimate the infected area at the beginning, but overestimate it at the end. There are also some major differences in how the outbreak of Antwerp fuses with the other outbreaks (Figure 7.8). In reality, the outbreak of Antwerp fused with the other outbreaks in the winter, at a central location in Belgium (Figure 7.8(a)), while in silico this happens around spring, more to the north-west. The location where the in silico fusion happens, is not contained in the epidemic wave up till summer in the data (Figure 7.10(a)). It also seems that the model overestimates the spread in the southern part in Belgium in spring and summer (Figures 7.9 and 7.10).

7.1.5 Conclusions

Now, the crucial question is if this model is able to replicate the spread of the myxomatosis epidemic in Belgium. To answer this, there are several things that should be considered. First, the model is deterministic, while simulating a stochastic process (see Chapter 3). This means that differences between the data and the model simulations are inevitable. Secondly, the data from which we reconstructed the epidemic wave is old, which implies uncertainties. Also, according to the Bulletin Sanitaire, there were several decrees issued with measures to contain the disease [80], especially in the province of West-Flanders, where many nidi were found in domesticated rabbits (see Section 4.1.2). It is possible that those measures impacted the disease spread in that region. Thirdly, the model was calibrated assuming that there was no influence whatsoever of the land cover on the population densities or disease dynamics. Still, the model is capable of simulating an epidemic wave that resembles the data to a certain degree, which shows its potential at modelling the spatial spread of epidemic diseases.

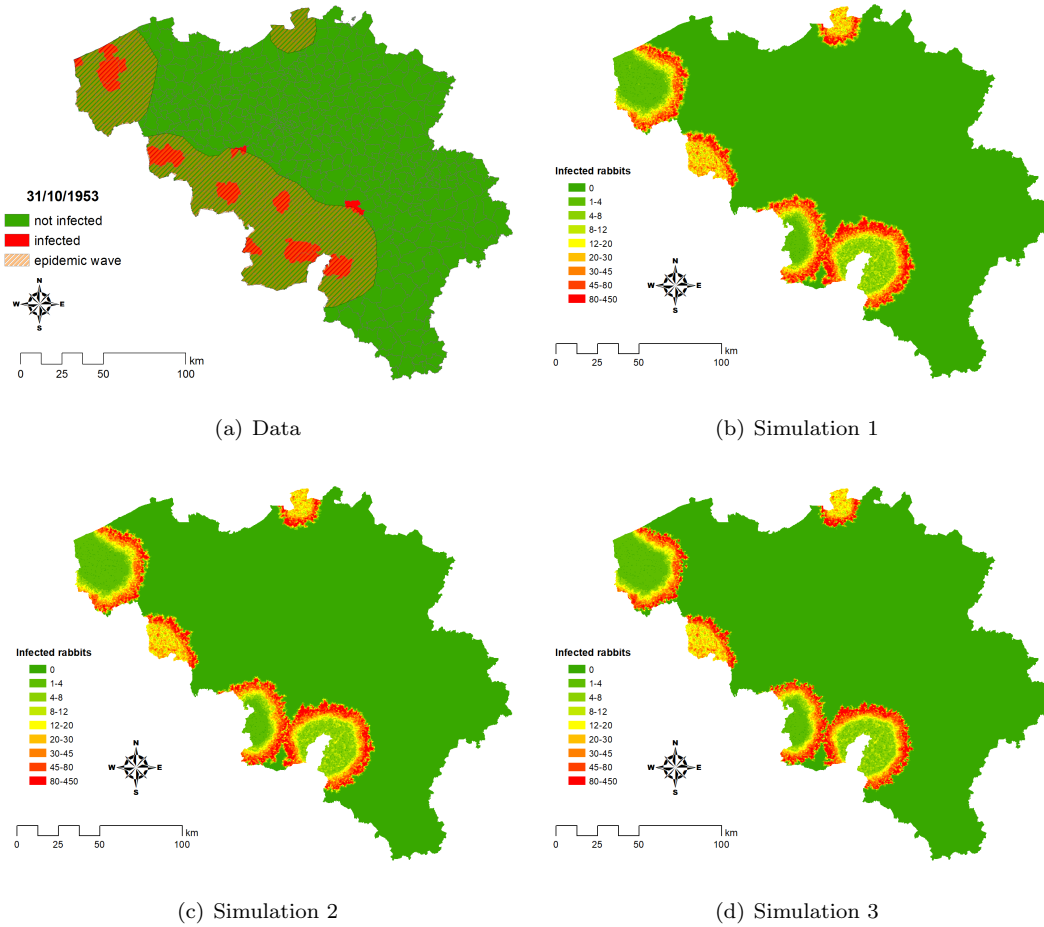


Figure 7.7: Observed and simulated epidemic wave in the autumn of 1953

7.2 Scenario analysis

Using the inferred parameters, we simulated some scenarios to examine if it can be useful for other situations. It should be noted that these scenarios are hypothetical and only serve to illustrate how the model can be improved, or used in alternative contexts.

7.2.1 Revisiting the forest area

From the non-spatial sensitivity analysis of Section 6.3.4, it seemed like the transmission rate of the arable land was globally the most influential. However, from the spatial sensitivity analysis from Section 6.4, we learned that the transmission rate of the forest area was more important in the southern part of Belgium. We also learned that the model overestimates the speed at which the disease spreads in that part of Belgium in Section 7.1.4. For this scenario we will use the values for the transmission rates of Simulation 3 (Table 7.2), except we divide both by 10 for the polygons with forest land cover. The other parameters are those in Table 7.1. The maps of the epidemic wave are shown in Figure 7.11.

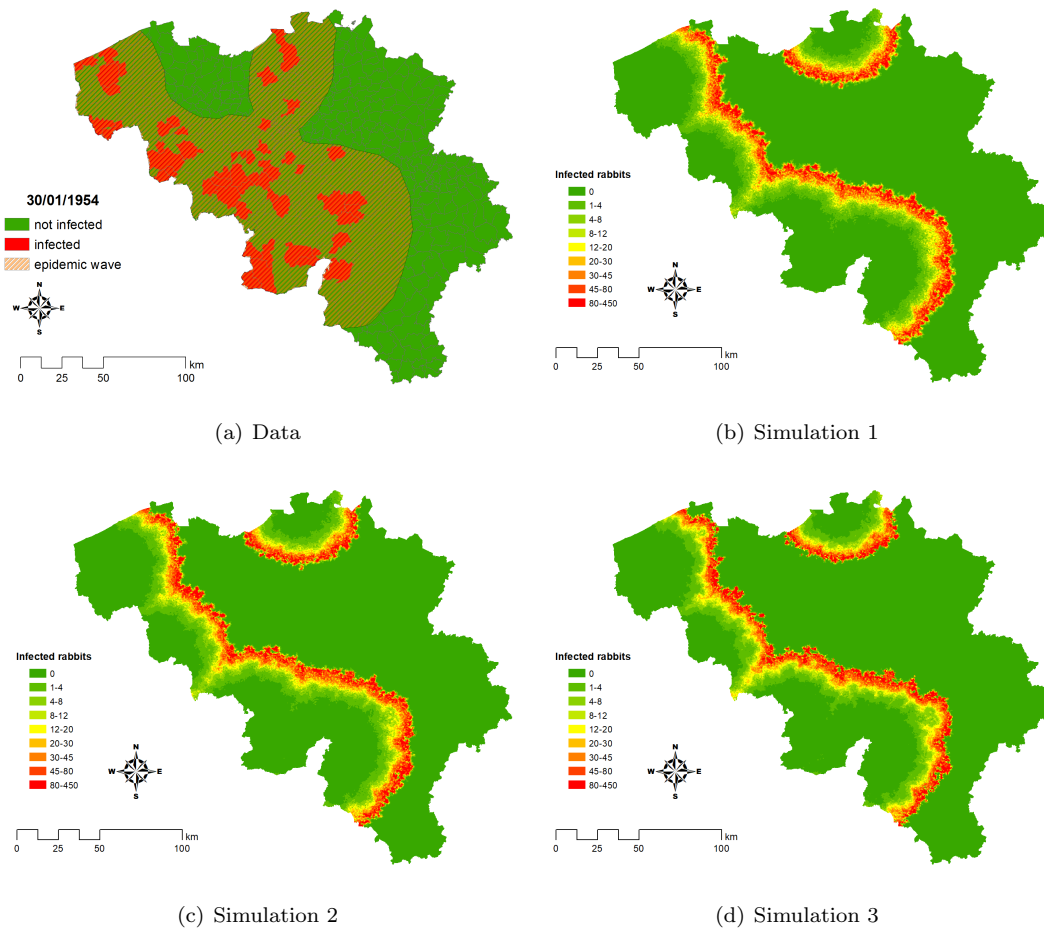


Figure 7.8: Observed and simulated epidemic wave in the winter of 1954

In the autumn of 1953 (Figure 7.11(a)), the differences between this simulation and those of Figure 7.7 do not seem to differ much. However, comparing the maps of the other three seasons (7.8, 7.9 and 7.10 and 7.11(b), 7.11(c), 7.11(d) respectively) clearly shows that lower transmission rates in the forested regions slows down the epidemic wave in general, especially in the south-eastern part of Belgium. This also lowers the amount of infected rabbits and the casualties resulting from it (Figure 7.12). Visually, the maps of the epidemic wave also look more similar to the data. This points out that an additional ABC procedure, where the transmission rates in forest areas are varied relative to the other land covers may yield more accurate simulation results.

7.2.2 Rabbit haemorrhagic disease

RHD is another highly contagious illness that ravaged rabbit populations in Belgium and the rest of the world (Section 2.6). Therefore, it is interesting to adjust the parameters of Table 7.1 to the disease dynamics of RHD and simulate its introduction. As discussed in Section 2.6, the main difference between myxomatosis and RHD is that RHD-infected rabbits survive for much shorter time periods, i.e., only about two to three days. So, we used the transmission rates of Simulation

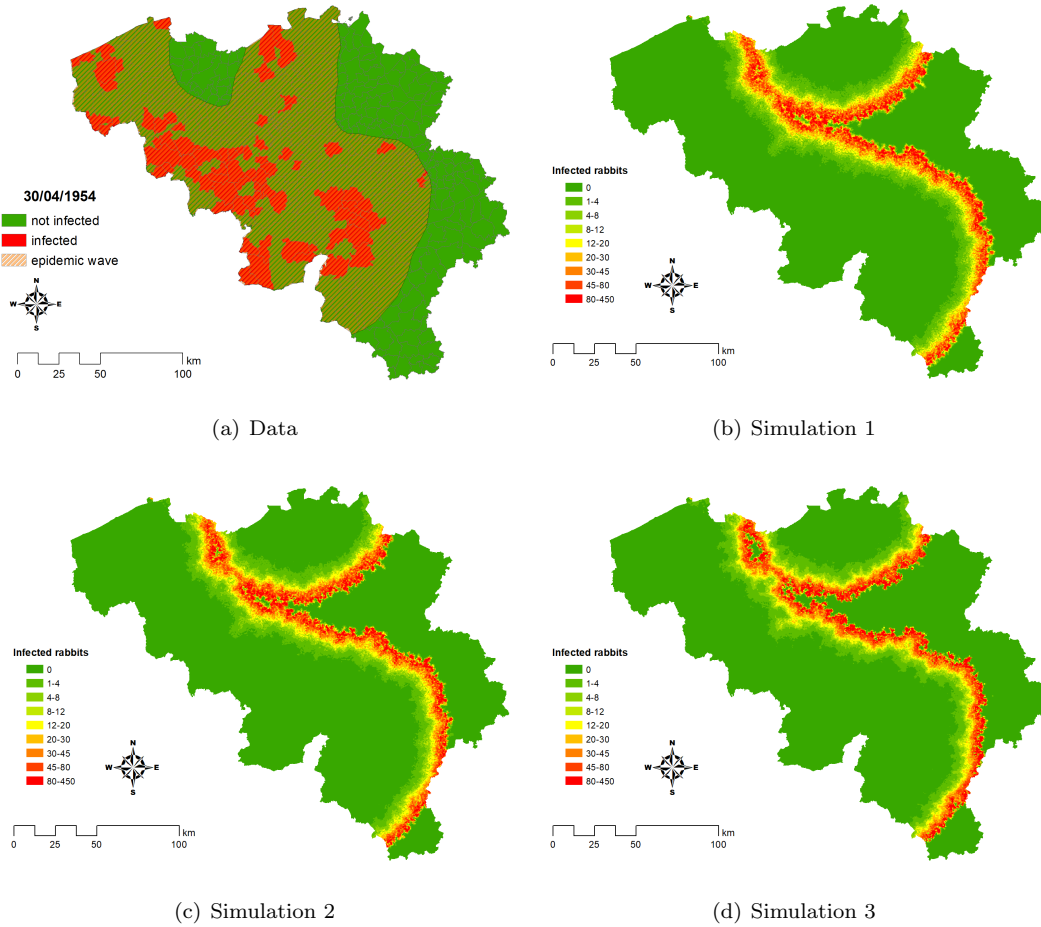


Figure 7.9: Observed and simulated epidemic wave in the spring of 1954

3 and the other parameters from Table 7.1, where we changed ϵ to $1/3$ to reflect the shorter survival time. The simulation results are shown in Figure 7.13.

If we compare those simulations with the corresponding ones of Scenario 3, the visual effect of lowering ϵ seems to be limited to a much thinner epidemic wave. However, if we observe the disease dynamics (Figure 7.12), we see that there are a lot less infected rabbits present at any given time, yet they only result in slightly lower casualties than for the scenario with low transmission rates in the forest.

7.2.3 Chytridiomycosis

In this thesis, the focus up to this point has been on the spread of an epidemic disease in a terrestrial mammal, i.e. the European rabbit (*Oryctolagus cuniculus*). Now, it could be interesting to simulate the spread of a new disease in an animal species that is still quite numerous, but is bound to a specific environment. A disease that satisfies those requirements is chytridiomycosis, a cutaneous disease in amphibians, caused by the chytrid fungus *Batrachochytrium dendrobatidis*, which is an important reason of the decline in global amphibian diversity [36]. To examine whether the model is able to simulate the introduction of this disease, we simulated an introduction of

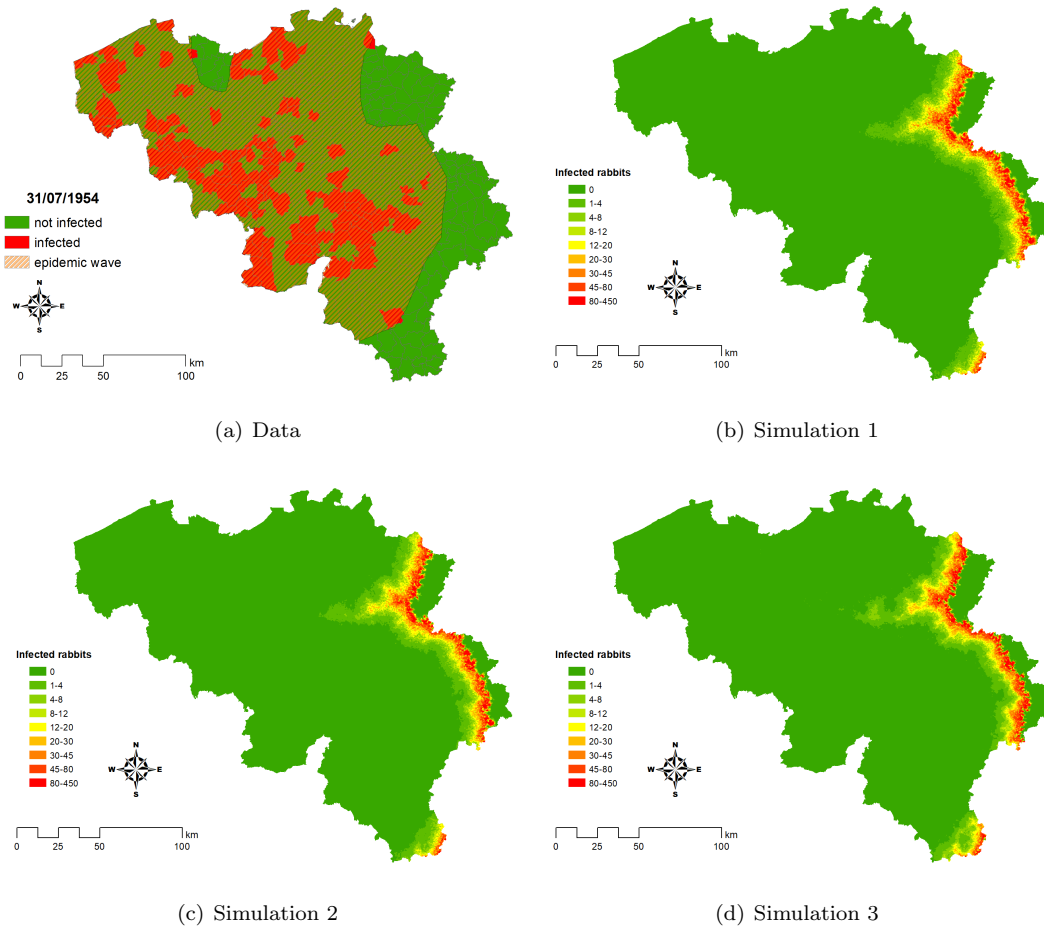


Figure 7.10: Observed and simulated epidemic wave in the summer of 1954

chytridiomycosis in the vicinity of Ghent, Belgium. First, we constructed a map of the suitable amphibian habitat by comparing the map of the water surfaces in Belgium with the map with the Voronoi polygons, so if a polygon clips a water feature, it is marked as a suitable amphibian habitat, and if it does not, it is marked as not suitable. We assumed that population densities of cells marked as unsuitable were $1/50$ th of the population densities of suitable cells. For the transmission rates, we took the values of Simulation 3 (Table 7.2) for the suitable polygons, while we divided them by 100 for the unsuitable ones. The other parameters were those of Table 7.1, except for ϵ . Since amphibians infected with the disease survive in between eight to thirty days, we assumed $\epsilon = 1/18$ [83]. It is also known from literature that the mortality rate (C_M) is about 0.95 [83]. The simulation results are shown in Figure 7.14.

It is clear that the model can simulate the spread of this disease in the sense that it evolves an epidemic wavefront, but the wave seems to spread in a spatially homogeneous way for polygons with strong spatial restrictions. The polygons we used were probably too large given the detail of the water features, so a polygon has a high probability of containing a water feature, and hence marking it entirely as suitable area. Indeed, half of the polygons as suitable. To examine this scenario further, it would be necessary to generate a tessellation in a smaller resolution.

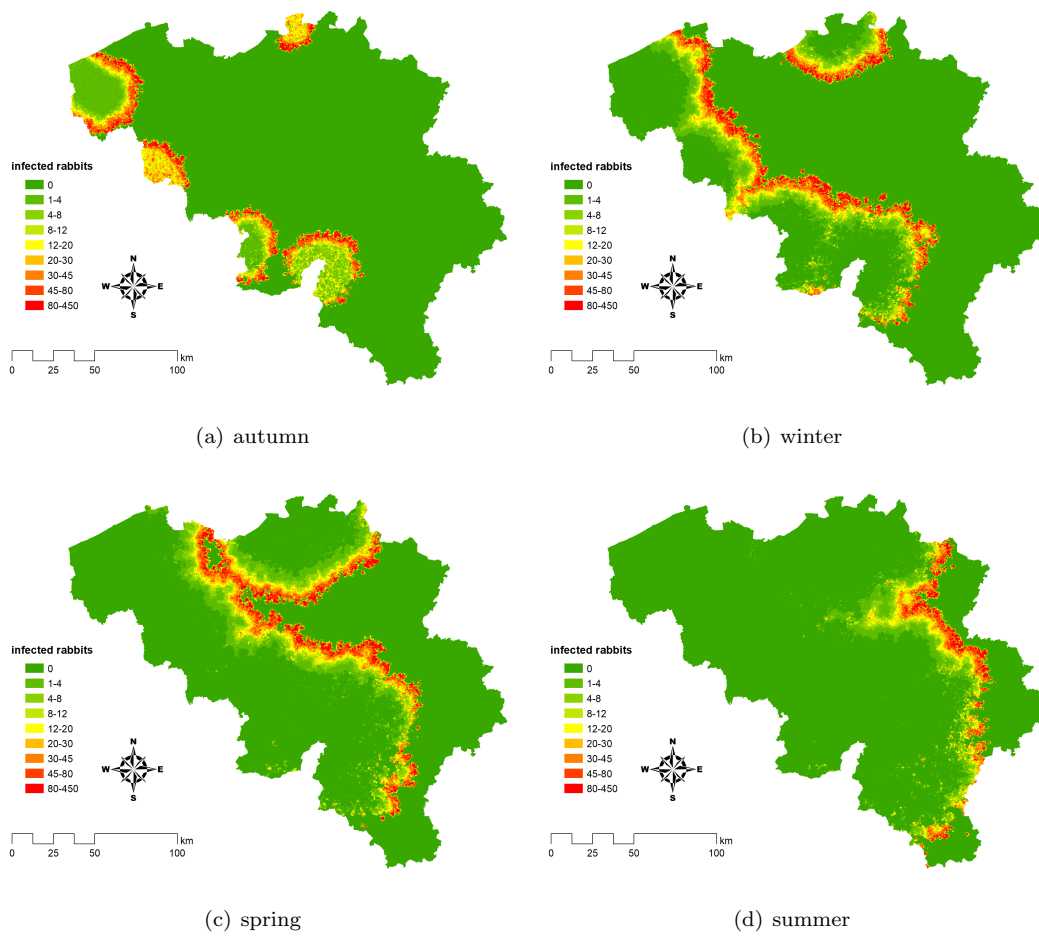
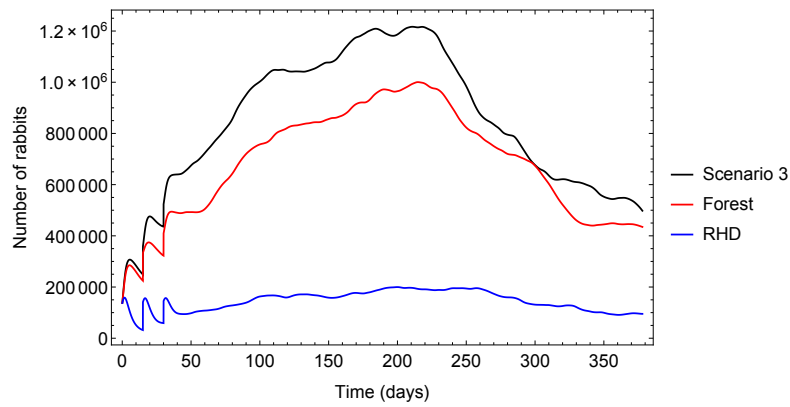
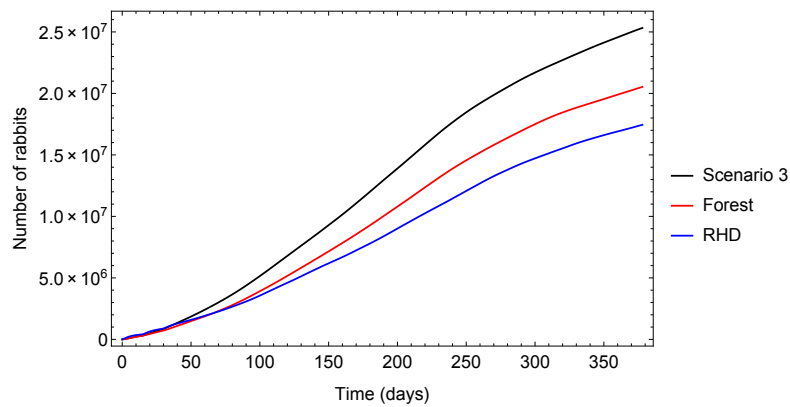


Figure 7.11: Simulation results for the scenario with a slower disease spread in forest areas.



(a) Infected rabbits



(b) Rabbits that died due to the disease

Figure 7.12: Comparison of the disease dynamics between Simulation 3, the scenario with low transmission rates for the forest area, and the scenario of RHD. of Table 7.2

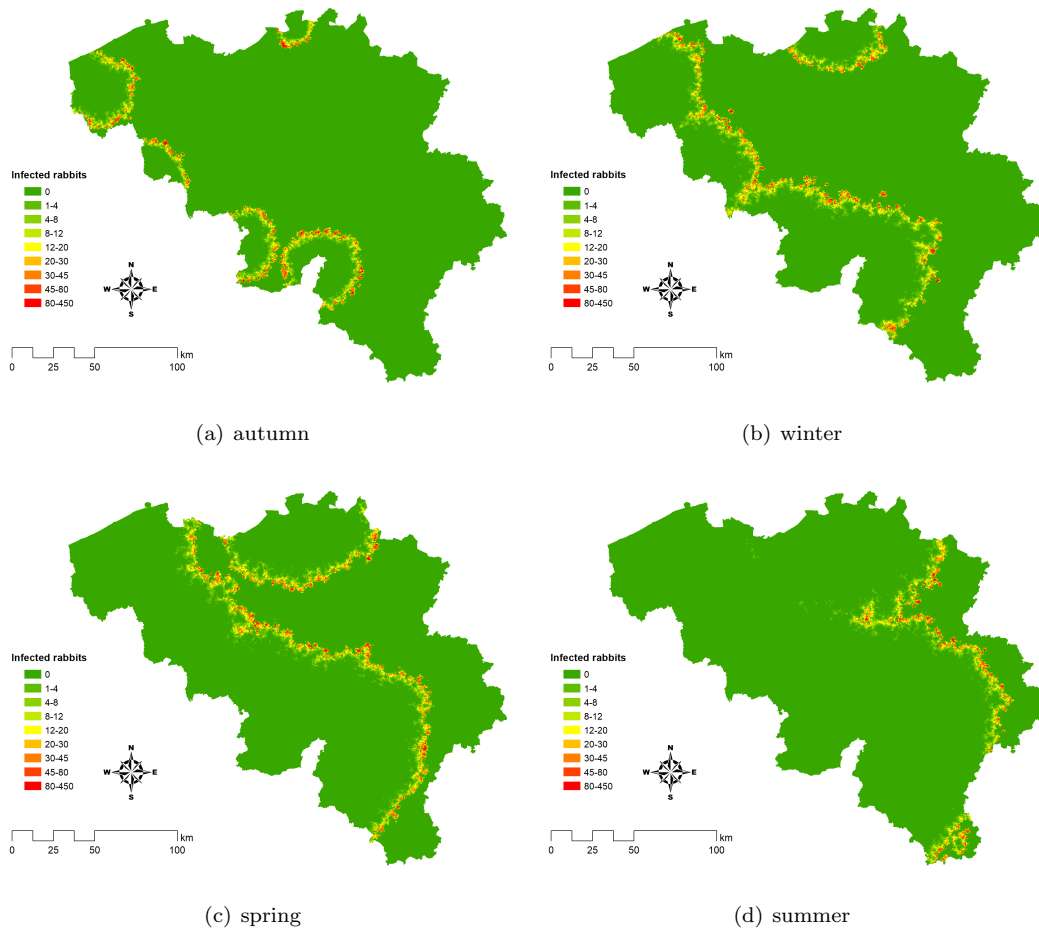


Figure 7.13: Simulation results for the case of an RHD infection.

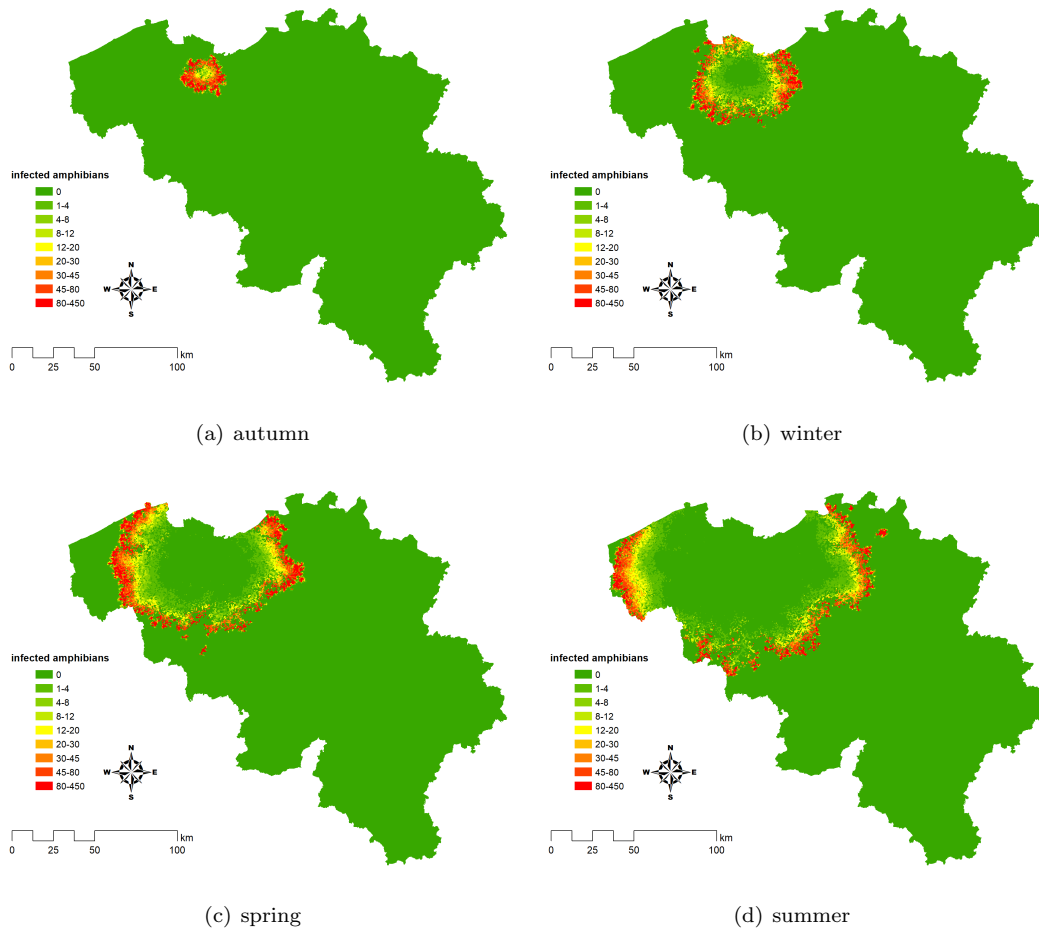


Figure 7.14: Simulation of the epidemic wave for the chytridiomycosis scenario.

CHAPTER 8

Conclusion

There is one main question we addressed in this masters thesis. Is it possible to reconstruct the spatial dynamics of the first myxomatosis epidemic in Belgium with a spatially explicit model? To answer this question, several steps had to be taken.

In Chapter 2 we were derived multiple properties of the myxomatosis dynamics and the reproductive behaviour of the European rabbit from literature. We also provided a thorough review of their respective histories and their importance.

After that, in Chapter 3, we examined the theory behind epidemic modelling, starting from the very basic systems of ordinary differential equations, up to highly complex individual-based models. Supported by this literature review, we interpreted the disease data in Chapter 4. Although the literature asserted that myxomatosis spreads differently under different land covers, the data did not provide sufficient proof to support this claim. This was due to the low quality data, and the fact that a land cover map from the time of introduction is unavailable. Still, we learned that the disease did not enter Belgium gradually along the French border, but instead started from multiple outbreaks. We were also able to reconstruct the progress of the epidemic wave and provided a general idea of the time-frame during which it developed.

In Chapter 5, we showed that the model is able to simulate an epidemic wave, which is a prerequisite for the reconstruction of the myxomatosis epidemic.

Thereafter, in Chapter 6, we performed a sensitivity analysis. We showed that variance-based methods for global sensitivity analyses are able to produce very useful information. Not only did we identify the parameters that are primarily responsible for changes the simulated epidemic wave. We also learned that the parameter values able to reproduce the epidemic wave, were not contained in the parameter space used for the analysis. Furthermore, we also showed that a spatial sensitivity analysis can unveil information that is hidden in non-spatial sensitivity analyses.

In Chapter 7, building on the knowledge gathered in previous chapters. We calibrated the model using approximate Bayesian computation, an inefficient but widely applicable method. Assisted by the knowledge gathered during the sensitivity analyses, we were able to find parameter values with which the model simulated the observed epidemic wave. We also showed that there is still some room for improvement, but due to time constraints were not able to fine-tune the model further.

With that in mind, we can state that we answered the main research question. However, the key part to remember is the importance of a comprehensive sensitivity analysis. Without such an

analysis, we probably could not have determined which parameters to calibrate, and which ones to derive from literature. We also showed the potential of ABC at inferring parameters of complex models, when supported by the knowledge gathered from a sensitivity analysis.

For further research, it could be interesting to expand this type of model to other animal diseases, preferably with a more accurate dataset, to verify if the model performs better results if given more information. We also only calibrated with regard to the speed at which the epidemic wave spreads. This means we did not investigate if the simulated quantities of infected individuals are realistic.

A property that was discussed in Chapter 3, but never investigated for this model is the basic reproductive number, a property that shows whether an epidemic can develop in an entirely susceptible population. The calculation of this property has been investigated in a non-spatial context, but this was not done for this model. Investigating this property may yield further information how an epidemic can develop in a spatial context.

The model structure also is reasonably simple, with few parameters for a spatially explicit model. This means there is still room to include more complexity, like seasonal changes in the reproduction rate for example. This simplicity may also make it suitable to be adapted to other fields.

Bibliography

- [1] Abrantes, J., Van Der Loo, W., Le Pendu, J., and Esteves, P. J. (2012). Rabbit haemorrhagic disease (RHD) and rabbit haemorrhagic disease virus (RHDV): a review. *Veterinary research*, 43(1):12.
- [2] Adamatzky, A. (2010). *Game of Life Cellular Automata*. Springer, London, UK.
- [3] Allen, L., Jones, M., and Martin, C. (1991). A discrete-time model with vaccination for a measles epidemic. *Mathematical biosciences*, 105(1):111–131.
- [4] Anderson, R. M. and May, R. (1982). Coevolution of hosts and parasites. *Parasitology*, 85(02):411–426.
- [5] Anderson, R. M. and May, R. M. (1985). Vaccination and herd immunity. *Nature*, 318:28.
- [6] Andrews, J. R. and Basu, S. (2011). Transmission dynamics and control of cholera in Haiti: an epidemic model. *The Lancet*, 377(9773):1248–1255.
- [7] Aurenhammer, F. (1991). Voronoi diagrams: a survey of a fundamental geometric data structure. *ACM Computing Surveys (CSUR)*, 23(3):345–405.
- [8] Baetens, J. and De Baets, B. (2016). A spatial sensitivity analysis of a spatially explicit model for myxomatosis in belgium. *International Conference of Cellular Automata*, 9863:91–100.
- [9] Bailey, N. T. et al. (1975). *The mathematical theory of infectious diseases and its applications*. Charles Griffin & Company Ltd, High Wycombe, UK.
- [10] Berger, L., Speare, R., and Hyatt, A. (1999). Chytrid fungi and amphibian declines: overview, implications and future directions. *Declines and disappearances of Australian frogs. Environment Australia, Canberra*, 1999:23–33.
- [11] Bergstrom, D. M., Lucieer, A., Kiefer, K., Wasley, J., Belbin, L., Pedersen, T. K., and Chown, S. L. (2009). Indirect effects of invasive species removal devastate world heritage island. *Journal of Applied Ecology*, 46(1):73–81.
- [12] Bolker, B. and Grenfell, B. (1993). Chaos and biological complexity in measles dynamics. *Proceedings of the Royal Society of London B: Biological Sciences*, 251(1330):75–81.
- [13] Bösze, Z. and Houdebine, L. (2006). Application of rabbits in biomedical research: A review. *World Rabbit Science*, 14(1):1–14.

- [14] Box, G. E. and Tiao, G. C. (2011). *Bayesian Inference in Statistical Analysis*, volume 40. John Wiley & Sons, New York, USA.
- [15] Branco, M., Monnerot, M., Ferrand, N., and Templeton, A. R. (2002). Postglacial dispersal of the European rabbit (*oryctolagus cuniculus*) on the Iberian peninsula reconstructed from nested clade and mismatch analyses of mitochondrial dna genetic variation. *Evolution*, 56(4):792–803.
- [16] Brewer, N. R. (2006). Biology of the rabbit. *Journal of the American Association for Laboratory Animal Science*, 45(1):8–24.
- [17] Bull, L. and Mules, M. (1944). An investigation of myxomatosis cuniculi with special reference to the possible use of the disease to control rabbit populations in Australia. *Journal of the Council for Scientific and Industrial Research, Australia*, 17(2).
- [18] Calvete, C., Pelayo, E., and Sampietro, J. (2006). Habitat factors related to wild rabbit population trends after the initial impact of rabbit haemorrhagic disease. *Wildlife Research*, 33(6):467–474.
- [19] Campolongo, F., Cariboni, J., and Saltelli, A. (2007). An effective screening design for sensitivity analysis of large models. *Environmental modelling & software*, 22(10):1509–1518.
- [20] Carley, K. M., Fridsma, D. B., Casman, E., Yahja, A., Altman, N., Chen, L.-C., Kaminsky, B., and Nave, D. (2006). Biowar: scalable agent-based model of bioattacks. *IEEE Transactions on Systems, Man, and Cybernetics-Part A: Systems and Humans*, 36(2):252–265.
- [21] Centers for Disease Control and Prevention (CDC and others) (2003). Severe acute respiratory syndrome—Singapore, 2003. *MMWR. Morbidity and mortality weekly report*, 52(18):405.
- [22] Cooke, B. (2002). Rabbit haemorrhagic disease: field epidemiology and the management of wild rabbit populations. *Revue Scientifique et Technique-Office International des Epizooties*, 21(1):347–358.
- [23] Cowan, D. (1987). Group living in the european rabbit (*oryctolagus cuniculus*): mutual benefit or resource localization? *The Journal of Animal Ecology*, 56(3):779–795.
- [24] Csilléry, K., Blum, M. G., Gaggiotti, O. E., and François, O. (2010). Approximate Bayesian computation (ABC) in practice. *Trends in ecology & evolution*, 25(7):410–418.
- [25] Daley, D. J., Gani, J., and Gani, J. M. (2001). *Epidemic modelling: an introduction*, volume 15. Cambridge University Press, Cambridge, UK.
- [26] Davis, S. E. and DeMello, M. (2003). *Stories rabbits tell: A natural and cultural history of a misunderstood creature*. Lantern Books, New York, USA.
- [27] Delibes-Mateos, M., Delibes, M., Ferreras, P., and Villafuerte, R. (2008). Key role of European rabbits in the conservation of the western Mediterranean basin hotspot. *Conservation biology: the journal of the Society for Conservation Biology*, 22(5):1106–1117.
- [28] Doran, R. J. and Laffan, S. W. (2005). Simulating the spatial dynamics of foot and mouth disease outbreaks in feral pigs and livestock in Queensland, Australia, using a susceptible-infected-recovered cellular automata model. *Preventive Veterinary Medicine*, 70(1):133–152.

- [29] Durbin, J. and Knott, M. (1972). Components of Cramer-von Mises statistics. i. *Journal of the Royal Statistical Society: Series B (Methodological)*, 34(2):290–307.
- [30] Durbin, J., Knott, M., and Taylor, C. (1975). Components of cramér-von mises statistics. ii. *Journal of the Royal Statistical Society. Series B (Methodological)*, 37(2):216–237.
- [31] Dwyer, G. (1992). On the spatial spread of insect pathogens: theory and experiment. *Ecology*, 73(2):479–494.
- [32] Dwyer, G., Levin, S. A., and Buttel, L. (1990). A simulation model of the population dynamics and evolution of myxomatosis. *Ecological Monographs*, 60(4):423–447.
- [33] Fenner, F., Fantini, B., et al. (1999). *Biological control of vertebrate pests*. CABI publishing, Wallingford, UK.
- [34] Fenner, F. and Ratcliffe, F. (1965). *Myxomatosis*. Cambridge University Press, Cambridge, UK.
- [35] Fick, A. (1855). Uber diffusion. *Annalen der Physik*, 170(1):59–86.
- [36] Fisher, M. C., Garner, T. W., and Walker, S. F. (2009). Global emergence of batrachochytrium dendrobatidis and amphibian chytridiomycosis in space, time, and host. *Annual review of microbiology*, 63:291–310.
- [37] Fouchet, D., Le Pendu, J., Guitton, J.-S., Guiserix, M., Marchandeu, S., and Pontier, D. (2009). Evolution of microparasites in spatially and genetically structured host populations: the example of rhdv infecting rabbits. *Journal of Theoretical Biology*, 257(2):212–227.
- [38] Fraser, C. (2007). Estimating individual and household reproduction numbers in an emerging epidemic. *PLoS One*, 2(8):e758.
- [39] Fulforda, G., Leea, X., Bermanb, D., and Hamiltona, G. (2011). Interaction of myxomatosis and rabbit haemorrhagic disease in wild rabbit. In *MODSIM2011, 19th International Congress on Modelling and Simulation.*, pages 912–918. Modelling and Simulation Society of Australia and New Zealand.
- [40] Gardner, M. (1970). Mathematical games: The fantastic combinations of john conways new solitaire game life. *Scientific American*, 223(4):120–123.
- [41] Gehrman, B. and Kretzschmar, C. (1991). Ein experimentelleler Beitrag zur Epizootiologie der Viralen Hamorrhagischen Septikamie der Kaninchen (Rabbit haemorrhagic disease, RHD) Ubertragung durch Fliegen. *Berliner und Munchener Tierarztliche Wochenschrift*, 104:192–194.
- [42] Glasstone, S. (1951). *Textbook of physical chemistry*. Macmillan, London, UK.
- [43] Grassly, N. C. and Fraser, C. (2008). Mathematical models of infectious disease transmission. *Nature Reviews. Microbiology*, 6(6):477.
- [44] Grimm, V. and Railsback, S. F. (2005). *Individual-based modeling and ecology*. Princeton University Press, London, UK.

- [45] Grimm, V., Revilla, E., Berger, U., Jeltsch, F., Mooij, W. M., Railsback, S. F., Thulke, H.-H., Weiner, J., Wiegand, T., and DeAngelis, D. L. (2005). Pattern-oriented modeling of agent-based complex systems: lessons from ecology. *science*, 310(5750):987–991.
- [46] Haran, M. (2009). An introduction to models for disease dynamics. *Spatial Epidemiology SAMSI*, 12:19–23.
- [47] Hayward, J. (1961). The ability of the wild rabbit to survive conditions of water restriction. *Wildlife Research*, 6(2):160–175.
- [48] Heesterbeek, J. A. P. (2002). A brief history of R_0 and a recipe for its calculation. *Acta Biotheoretica*, 50(3):189–204.
- [49] Hill, A., Butterworth, R., Joiner, S., Jackson, G., Rossor, M., Thomas, D., Frosh, A., Tolley, N., Bell, J., Spencer, M., et al. (1999). Investigation of variant Creutzfeldt-Jakob disease and other human prion diseases with tonsil biopsy samples. *The Lancet*, 353(9148):183–189.
- [50] Iooss, B. and Lemaître, P. (2015). A review on global sensitivity analysis methods. In *Uncertainty Management in Simulation-Optimization of Complex Systems*, volume 59, pages 101–122. Springer, New York, USA.
- [51] Jeltsch, F., Müller, M., Grimm, V., Wissel, C., and Brandl, R. (1997). Pattern formation triggered by rare events: lessons from the spread of rabies. *Proceedings of the Royal Society of London B: Biological Sciences*, 264(1381):495–503.
- [52] John, F. (1982). *Partial differential equations, volume 1 of Applied Mathematical Sciences*. Springer, New York, USA.
- [53] Kaneko, K. (1992). Overview of coupled map lattices. *Chaos: An Interdisciplinary Journal of Nonlinear Science*, 2(3):279–282.
- [54] Keogh, E. and Mueen, A. (2011). Curse of dimensionality. In *Encyclopedia of Machine Learning*, pages 257–258. Springer, New York, USA.
- [55] Kermack, W. and McKendrick, A. (1927). A contribution to the mathematical theory of epidemics. *Proceedings of the Royal Society of London. Series A, Containing Papers of a Mathematical and Physical Character*, 115(772):700–721.
- [56] Kerr, P. J. (2012). Myxomatosis in Australia and Europe: a model for emerging infectious diseases. *Antiviral research*, 93(3):387–415.
- [57] Kim, K. I., Lin, Z., and Zhang, L. (2010). Avian-human influenza epidemic model with diffusion. *Nonlinear Analysis: Real World Applications*, 11(1):313–322.
- [58] Krauss, H., Schieffer, H., and Slenczka, W. (2003). *Zoonoses: infectious diseases transmissible from animals to humans*. ASM press, Washington DC, USA.
- [59] Langer, W. L. (1964). The black death. *Scientific American*, 210(2):114–121.
- [60] Le Gall-Reculé, G., Lavazza, A., Marchandean, S., Bertagnoli, S., Zwingelstein, F., Cavadini, P., Martinelli, N., Lombardi, G., Guérin, J.-L., and Lemaitre, E. (2013). Emergence of a new lagovirus related to rabbit haemorrhagic disease virus. *Veterinary research*, 44(1):81.

- [61] Le Gall-Reculé, G., Zwingelstein, F., Boucher, S., Le Normand, B., Plassiart, G., Portejoie, Y., Decors, A., Bertagnoli, S., Guérin, J., and Marchandeu, S. (2011). Detection of a new variant of rabbit haemorrhagic disease virus in france. *The Veterinary record*, 168(5):137–138.
- [62] Lees, A. C. and Bell, D. J. (2008). A conservation paradox for the 21st century: the European wild rabbit *oryctolagus cuniculus*, an invasive alien and an endangered native species. *Mammal Review*, 38(4):304–320.
- [63] Lenghaus, C., Westbury, H., Collins, B., Ratnamohan, N., and Morrissy, C. (1994). Overview of the RHD project in Australia. pages 104–129. Bureau of Resource Sciences, Canberra, Australia.
- [64] Li, G., Rosenthal, C., and Rabitz, H. (2001). High dimensional model representations. *The Journal of Physical Chemistry A*, 105(33):7765–7777.
- [65] Lilburne, L. and Tarantola, S. (2009). Sensitivity analysis of spatial models. *International Journal of Geographical Information Science*, 23(2):151–168.
- [66] Lintusaari, J., Gutmann, M., Dutta, R., Kaski, S., and Corander, J. (2016). Fundamentals and recent developments in approximate bayesian computation. *Syst. Biol*, 66(1):66–82.
- [67] Lipsitch, M., Cohen, T., Cooper, B., Robins, J. M., Ma, S., James, L., Gopalakrishna, G., Chew, S. K., Tan, C. C., Samore, M. H., et al. (2003). Transmission dynamics and control of severe acute respiratory syndrome. *Science*, 300(5627):1966–1970.
- [68] Lockley, R. (1961). Social structure and stress in the rabbit warren. *The Journal of Animal Ecology*, 30(2):385–423.
- [69] Lombardi, L., Fernández, N., and Moreno, S. (2007). Habitat use and spatial behaviour in the European rabbit in three Mediterranean environments. *Basic and Applied Ecology*, 8(5):453–463.
- [70] Lombardi, L., Fernández, N., Moreno, S., and Villafuerte, R. (2003). Habitat-related differences in rabbit (*oryctolagus cuniculus*) abundance, distribution, and activity. *Journal of Mammalogy*, 84(1):26–36.
- [71] Lumpkin, S. and Seidensticker, J. (2011). *Rabbits : The Animal Answer Guide*. Johns Hopkins University Press, Baltimore, US.
- [72] Macal, C. M. and North, M. J. (2010). Tutorial on agent-based modelling and simulation. *Journal of simulation*, 4(3):151–162.
- [73] Macdonald, D. W. (1980). *Rabies and wildlife. A biologist’s perspective*. Oxford University Press, Oxford, UK.
- [74] Macdonald, G. (1973). *Dynamics of tropical diseases*. Oxford University Press, London, UK.
- [75] Mann, H. B. and Whitney, D. R. (1947). On a test of whether one of two random variables is stochastically larger than the other. *The Annals of Mathematical Statistics*, 18(1):50–60.
- [76] Marin, J.-M., Pudlo, P., and Sedki, M. (2012). Optimal parallelization of a sequential approximate Bayesian computation algorithm. In *Simulation Conference (WSC), Proceedings of the 2012 Winter*, pages 1–7.

- [77] Marlier, D., Mainil, J., Boucraut-Baralon, C., Linden, A., and Vindevogel, H. (2000). The efficacy of two vaccination schemes against experimental infection with a virulent myxomatous or a virulent nodular myxoma virus strain. *Journal of comparative pathology*, 122(2):115–122.
- [78] May, R. M. and Anderson, R. M. (1979). Population biology of infectious diseases: Part i. *Nature*, 280(5722):361–367.
- [79] McKay, M. D., Beckman, R. J., and Conover, W. J. (1979). Comparison of three methods for selecting values of input variables in the analysis of output from a computer code. *Technometrics*, 21(2):239–245.
- [80] Ministry of agriculture: Veterinary service (1953-1956). *Bulletin Sanitaire*. Brussels, Belgium.
- [81] Morris, M. D. (1991). Factorial sampling plans for preliminary computational experiments. *Technometrics*, 33(2):161–174.
- [82] Murray, J., Stanley, E., and Brown, D. (1986). On the spatial spread of rabies among foxes. *Proceedings of the Royal Society of London B: Biological Sciences*, 229(1255):111–150.
- [83] Nichols, D. K., Lamirande, E. W., Pessier, A. P., and Longcore, J. E. (2001). Experimental transmission of cutaneous chytridiomycosis in dendrobatid frogs. *Journal of Wildlife Diseases*, 37(1):1–11.
- [84] Okubo, A., Maini, P., Williamson, M., and Murray, J. (1989). On the spatial spread of the grey squirrel in Britain. *Proceedings of the Royal Society of London B: Biological Sciences*, 238(1291):113–125.
- [85] Overmars, M., De Berg, M., van Kreveld, M., and Schwarzkopf, O. (1997). *Computational Geometry: Algorithms and Applications*. Springer, Berlin, Germany.
- [86] Pacala, S. W. and Deutschman, D. H. (1995). Details that matter: the spatial distribution of individual trees maintains forest ecosystem function. *Oikos*, 74(3):357.
- [87] Palomares, F. and Delibes, M. (1997). Predation upon European rabbits and their use of open and closed patches in Mediterranean habitats. *Oikos*, 80(2):407–410.
- [88] Pizzitutti, F., Pan, W., Barbieri, A., Miranda, J. J., Feingold, B., Guedes, G. R., Alarcon-Valenzuela, J., and Mena, C. F. (2015). A validated agent-based model to study the spatial and temporal heterogeneities of malaria incidence in the rainforest environment. *Malaria Journal*, 14(1):514.
- [89] Pritchard, J. K., Seielstad, M. T., Perez-Lezaun, A., and Feldman, M. W. (1999). Population growth of human Y chromosomes: a study of Y chromosome microsatellites. *Molecular Biology and Evolution*, 16(12):1791–1798.
- [90] Ratcliffe, F., Myers, K., Fennessy, B., and Calaby, J. (1952). Myxomatosis in Australia; a step towards the biological control of the rabbit. *Nature*, 170(4314):7–11.
- [91] Reynolds, C. W. (1987). Flocks, herds and schools: A distributed behavioral model. *Computer Graphics*, 21(4):25–34.

- [92] Roche, B., Drake, J. M., and Rohani, P. (2011). An agent-based model to study the epidemiological and evolutionary dynamics of influenza viruses. *BMC bioinformatics*, 12(1):87.
- [93] Saltelli, A., Ratto, M., Andres, T., Campolongo, F., Cariboni, J., Gatelli, D., Saisana, M., and Tarantola, S. (2008). *Global sensitivity analysis: the primer*. John Wiley & Sons, Chichester, UK.
- [94] Saltelli, A., Tarantola, S., Campolongo, F., and Ratto, M. (2004). *Sensitivity Analysis in Practice: a Guide to Assessing Scientific Models*. John Wiley & Sons, Chichester, UK.
- [95] Samsuzzoha, M., Singh, M., and Lucy, D. (2010). Numerical study of an influenza epidemic model with diffusion. *Applied Mathematics and Computation*, 217(7):3461–3479.
- [96] Saunders, G., Cooke, B., McColl, K., Shine, R., and Peacock, T. (2010). Modern approaches for the biological control of vertebrate pests: an australian perspective. *Biological Control*, 52(3):288–295.
- [97] Saunders, I. (1980). A model for myxomatosis. *Mathematical Biosciences*, 48(1):1–15.
- [98] Smith, J., O’Nions, R., Schilling, J., Unni, C., and Bender, M. (1981). Population dynamics of fox rabies in Europe. *Nature*, 289:765.
- [99] Sobol, I. M. (1993). Sensitivity estimates for nonlinear mathematical models. *Mathematical Modelling and Computational Experiments*, 1(4):407–414.
- [100] Sobol, I. M. (2001). Global sensitivity indices for nonlinear mathematical models and their monte carlo estimates. *Mathematics and Computers in Simulation*, 55(1-3):271–280.
- [101] Sobol, I. M. and Myshetskaya, E. (2008). Monte carlo estimators for small sensitivity indices. *Monte Carlo Methods and Applications*, 13(5-6):455–465.
- [102] Taylor, L. H., Latham, S. M., and Mark, E. (2001). Risk factors for human disease emergence. *Philosophical Transactions of the Royal Society of London B: Biological Sciences*, 356(1411):983–989.
- [103] Teweldemedhin, E., Marwala, T., and Mueller, C. (2004). Agent-based modelling: a case study in hiv epidemic. In *Hybrid Intelligent Systems, 2004. HIS’04. Fourth International Conference on*, pages 154–159.
- [104] Thompson, H. (1994). *The European rabbit : the history and biology of a successful colonizer*. Oxford University Press, Oxford, England.
- [105] Toni, T., Welch, D., Strelkowa, N., Ipsen, A., and Stumpf, M. P. (2009). Approximate Bayesian computation scheme for parameter inference and model selection in dynamical systems. *Journal of the Royal Society Interface*, 6(31):187–202.
- [106] Velascohernandez, J. X. (1994). A model for chagas disease involving transmission by vectors and blood transfusion. *Theoretical population biology*, 46(1):1–31.
- [107] Villafuerte, R., Calvete, C., Blanco, J., and Lucientes, J. (1995). Incidence of viral hemorrhagic disease in wild rabbit populations in Spain. *Mammalia*, 59(4):651–660.

- [108] Virgós, E., Cabezas-Díaz, S., Malo, A., Lozano, J., and López-Huertas, D. (2003). Factors shaping European rabbit abundance. *Acta Theriologica*, 48(1):113–122.
- [109] von Holst, D., Hutzelmeyer, H., Kaetzke, P., Khaschei, M., and Schönheiter, R. (1999). Social rank, stress, fitness, and life expectancy in wild rabbits. *Naturwissenschaften*, 86(8):388–393.
- [110] Williams, K., Parer, I., Coman, B., Burley, J., Braysher, M., et al. (1995). *Managing vertebrate pests: rabbits*. Australian Government Publishing Service, Canberra, Australia.
- [111] Wobeser, G. A. (2007). *Disease in wild animals*. Springer, Berlin, Germany.
- [112] Wolfram, S. (2002). *A New Kind of Science*. Wolfram Media, Champaign, USA.
- [113] Wu, J., Dhingra, R., Gambhir, M., and Remais, J. V. (2013). Sensitivity analysis of infectious disease models: methods, advances and their application. *Journal of The Royal Society Interface*, 10(86):20121018.
- [114] Xu, W. (1991). Viral haemorrhagic disease of rabbits in the People’s Republic of China: epidemiology and virus characterisation. *Revue Scientifique et Technique (International Office of Epizootics)*, 10(2):393–408.
- [115] Zhou, Y., Ma, Z., and Brauer, F. (2004). A discrete epidemic model for SARS transmission and control in china. *Mathematical and Computer Modelling*, 40(13):1491–1506.